NASA Reference Publication 1064

Two-Dimensional Model Studies of the Effect of Supersonic Aircraft Operations on the Stratospheric Ozone Content

R. C. Whitten, W. J. Borucki, I. G. Poppoff,
L. Glatt, G. F. Widhopf, L. A. Capone,
and C. A. Reigel

FEBRUARY 1981

NASA

NASA Reference Publication 1064

Two-Dimensional Model Studies of the Effect of Supersonic Aircraft Operations on the Stratospheric Ozone Content

R. C. Whitten and W. J. Borucki
Ames Research Center
Moffett Field, California

I. G. Poppoff
Flick Point Associates
Carnelian Bay, California

L. Glatt and G. F. Widhopf
Aerospace Corporation
El Segundo, California

L. A. Capone and C. A. Reigel
San Jose State University
San Jose, California

TWO-DIMENSIONAL MODEL STUDIES OF THE EFFECT OF SUPERSONIC AIRCRAFT

OPERATIONS ON THE STRATOSPHERIC OZONE CONTENT

R. C. Whitten, W. J. Borucki, I. G. Poppoff,* L. Glatt,† G. F. Widhopf,† L. A. Capone,‡ and C. A. Reigel‡

Ames Research Center

An earlier assessment (NASA Reference Publication 1026) of potential effects of advanced supersonic aircraft on stratospheric ozone employed one-dimensional photochemical models to obtain estimates of globally averaged changes in ozone. The study reported here, an extension of the earlier work, was undertaken to estimate the latitudinal dependence of the ozone perturbation; two two-dimensional photochemical models were used for the purpose. Two SST design concepts assumed in the previous work were also employed for the work reported here.

As predicted in an earlier study, it appears that realistic SST fleet sizes should not cause concern with respect to the reduction of the total ozone overburden. For a fleet of 250 aircraft, the change in the ozone column is predicted to be very close to zero; in fact, the ozone overburden may actually increase as a result of nitrogen oxides deposited at altitudes of 17.5 or 20 km. The calculations performed, using the chemical system described herein (ca. 1978), show that above 25 to 30 km the ozone abundance decreases via catalytic destruction, but at lower heights it increases, mainly as a result of coupling with odd-hydrogen species. Water vapor released in the engine exhaust is predicted to cause ozone decreases; for the hypothetical engines used in the study, the total column ozone changes due to water-vapor emission largely offset the predicted ozone increases due to NO_x emission. The actual effect of water vapor may be less than calculated because present models do not include thermal feedback. "Feedback" refers to the cooling effect of additional water vapor that would tend to slow the HO_x reactions which destroy ozone.

Because it is also appropriate to the study reported here, the reader is referred to the last paragraph of the "Summary" of the earlier work.

I. INTRODUCTION

In a previous publication (Poppoff et al., 1978, hereinafter referred to as "Part I") the results of an assessment of the potential effect of future aircraft operations on the abundance and distribution of ozone in the stratosphere was reported. The assessment was made with a one-dimensional photochemical model (Turco and Whitten, 1977). It was found that in contrast to the earlier predictions in the Report of Findings of the DOT's Climatic Impact Assessment Program (Grobecker et al., 1974) and the National Academy of Science report, "Environmental Impact of Stratospheric Flight" (1975), nitrogen oxide emissions by aircraft cruising in the stratosphere could, for some cases of injection, cause *increases* in the ozone column density.[1] The situation appears to be reversed with respect to water vapor

---

[1] Ozone depletions are still found at higher altitudes in the stratosphere; however, ozone increases in the lower stratosphere are greater than the upper stratosphere depletions.

emissions by aircraft engines: the older work predicted a negligible effect of water vapor on stratospheric ozone whereas the recent assessment in Part I led to predictions of small ozone losses. Still, the assessment of the water-vapor effect is in some doubt because of the neglect of thermal-photochemical feedback (e.g., Luther and Duewer, 1977), which tends to diminish the water-vapor effect. Injection of water vapor in the stratosphere may also cause a "greenhouse" increase in surface temperature and a decrease in stratospheric temperature. Based on the computations of Manabe and Wetherald (1967), we estimate these temperature changes to be $\approx0.04°$ C and $1.0°$ C, respectively.

These changes in our ideas about potential effects on the ozone layer of aircraft cruising in the stratosphere are due largely to relatively recent direct measurements (Howard and Evenson, 1977; Burrows et al., 1977) of the rate coefficient for the reaction

$$NO + HO_2 \rightarrow NO_2 + OH \qquad (1)$$
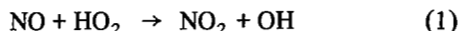
The newly measured value is about 30-40 times larger than the older one obtained by indirect means and has altered many of our ideas of stratospheric aeronomy. The aeronomical effects of a large rate for reaction (1), discussed in detail in Part I, are summarized later in this report. It is worth mentioning at this point that a recent direct measurement (Zahniser and Howard, 1978) of the rate coefficient of the reaction

$$HO_2 + O_3 \rightarrow OH + 2O_2 \qquad (2)$$
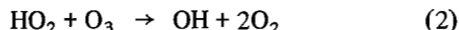
leads to predictions of even larger ozone increases due to NO_X emissions. The work of Zahniser and Howard (reaction (2)) was reported too late to be used in Part I and for most of the computations reported here; however, some computations were made with the new value of the rate coefficient and are presented for comparison.

Assessments using two- and three-dimensional models of the latitudinal variation of the effect of aircraft operations on ozone have been reported (Alyea et al., 1975; Borucki et al., 1976; Cunnold et al., 1977; Widhopf et al., 1977; and Hidalgo and Crutzen, 1977). They all used values of the rate coefficient for reaction (1) that were considerably smaller than those of Howard and Evenson (1977) and Burrows et al. (1977). As would be expected, all of these calculations predicted ozone *losses* due to supersonic transport operations, although

Widhopf et al. (1977) and Hidalgo and Crutzen (1977) did predict that ozone increases would be caused by aircraft operating below about 14 km. Using the new value of the rate coefficient for reaction (1), Widhopf and Glatt (1979a) and Glatt and Widhopf (1978) predicted ozone increases in the stratosphere due to combined NO_X and H_2O emission. It should be noted that these differences in the results reported from the earlier studies and those reported here are due almost entirely to the use of the earlier, smaller values for the rate coefficient (1) and not to any basic lack in the models or the theory used by the groups making the assessments; however, there have been refinements in both theory and models since the earlier studies. In section V we will return to the results of the earlier studies.

A new study of potential aircraft effects on the ozone layer, using multidimensional models, is thus needed in order to bring the assessments up to date. It is the purpose of this report to try to meet this requirement with the aid of two two-dimensional models, one developed at Ames Research Center (Borucki et al., 1976; Whitten et al., 1977) and the other developed at the Aerospace Corporation (Widhopf et al., 1977).[2] The models used the same reaction rate coefficients and similar photolytic cross sections, but different numerical techniques and different transport parameterizations; although the new value of the rate coefficient for reaction (2) was reported too late for incorporation into the Aerospace calculations for this particular study, we have been able to include it for a few of the Ames computations. A detailed comparison of the model results and a determination of the specific reasons for model differences leads to added confidence in the results of both models.

In the following sections, we discuss our model of aircraft emissions (sec. II), the two photochemical models used in the study (sec. III), predictions of trace constituent ambient distributions (sec. IV), and the results of the assessments (for which the calculations were performed mainly in 1978 and completed in January 1979), a comparison with earlier work, and discussion of the assessments in terms of stratospheric aeronomy (sec. V). Finally, our results are summarized in section VI.

II. EMISSIONS MODEL

In section II of Part I (Poppoff et al., 1978) we discussed the potential emissions of nitrogen oxides from two suggested SST design concepts (denoted types A and B). Type A, documented in a report by Baber and Swanson (1976), is based on the AST-100 airframe and on a single-spool turbojet with variable turbine geometry. The flight conditions assumed in the document include a speed of Mach 2.7 and a cruise profile varying from 19 to 21 km, nominally centered at an altitude of 20 km. The initial fuel consumption rate for this particular case is 44,100 kg/hr and the average consumption rate over the cruise portion of the flight is 37,800 kg/hr. For the type B aircraft, a set of conditions that are representative of design concepts using the Pratt and Whitney VSCE 502B variable-cycle study engine and more advanced airframes was used. For these conditions, the cruise speed is Mach 2.3, the cruise profile is centered at an altitude of 17.5 km, the initial fuel consumption rate is 41,050 kg/hr, and the average fuel consumption rate is estimated to be 35,200 kg/hr. The essential difference between the two design concepts (insofar as potential effect on stratospheric constituents is concerned) is the flight altitude. In the studies reported here, far-term engine emission technology for both type A and type B aircraft was assumed (6 and 7 g NO_2/kg fuel, respectively; see table 1 of Part I). Water vapor is also emitted by aircraft engines; the amount is determined stoichiometrically in well-burned fuel and is equivalent to an emission index of about 1.3 kg H_2O/kg fuel.

In modeling the latitudinal distribution of aircraft emissions, zonal symmetry was assumed, that is, that the effluents undergo zonal spreading rapidly and uniformly. This approximation is a reasonable one because of the strong zonal wind fields (Belmont et al., 1975). A hypothetical route structure was then constructed by selecting from the April 1977 Official Airline Guide (Worldwide edition) those long-range ($\gtrsim$ 2000 n. mi.) over-water routes that were then (1977) flown by Boeing 747's (including 747-SP). Such B-747 traffic was selected because it was believed to be representative of the type of traffic that might be partially transferred to large (250–300-passenger) supersonic transports in the future. In constructing our traffic model the magnitude of future Southern Hemisphere operations may have been underestimated, since they may grow faster than the Northern Hemisphere counterpart; unfortunately, there are no quantitative estimates of such asymmetric growth.

Having established a route structure, the appropriate great circle routes and the emissions in each latitude increment (5° for the Ames model, 10° for the Aerospace model) were computed. The aircraft were assumed to rise in altitude linearly as fuel was consumed, with nominal midcruise altitudes of 20 and 17.5 km for types A and B aircraft, respectively (i.e., the altitude spread for a 4000-n. mi. flight by type A aircraft is 19 to 21 km and 16 to 18 km for the type B aircraft). Fuel burned in reaching cruise altitude was not included because the "flight envelope" of the consumption, that is, the rate of consumption as a function of altitude, was not known. From the design data reported by Baber and Swanson (1976), the amount of fuel so consumed *in the stratosphere* appears to be rather small compared with fuel burned at cruise altitude. The NO_X emission rates for each altitude and latitude increment were then adjusted such that the simulated global emission rate was that characteristic of 250 type A or type B aircraft flying 7 hr/day in the cruise mode. The NO_X emission data for type A aircraft with an NO_X emission index of 6 g NO_2/kg fuel are shown in figure 1. The same distribution was used for the type B aircraft simulation by lowering the altitude regime accordingly.

The effect on stratospheric ozone of the combined engine emissions of supersonic (type A far-term technology) and subsonic aircraft is also considered in this report. For the subsonic aircraft emission model, the NO_X emission rates suggested by Oliver et al. (1977) were used; the subsonic emission estimates are presented in table 1.

III. THE PHOTOCHEMICAL MODELS

It is difficult to model the atmosphere, especially the troposphere. Atmospheric models necessarily use a finite grid spacing (or a finite number of waves in spectral representation) and thus ignore the coupling of subgrid scale motions with the large-scale motions that can be modeled. Two-dimensional models are more restricted than three-dimensional models because they can simulate only zonally-averaged atmospheric conditions and thus cannot follow the development of planetary wave systems. Instead, it

is customary to specify empirically a set of transport parameters composed of those that specify a large-scale meridional bulk motion (usually by a stream function) and those that specify smaller-scale processes that lead to mixing (by "eddy transport" coefficients). The bulk motion can be calculated by zonally averaging the wind fields predicted by three-dimensional models or by computing the meridional wind field from the energy and momentum equations (e.g., Vupputuri, 1975; Harwood and Pyle, 1977). Eddy coefficients are then obtained indirectly from measurements and adjusted if necessary until the computed distributions match the observed distributions of atmospheric tracers, such as those discussed in section IV. Two-dimensional models are thus highly empirical in nature, and they are incapable of simulating the observed variability of atmospheric constituents.

Because the two photochemical models employed for the current study have been described in detail in the literature (Borucki et al., 1976; Whitten et al., 1977; Widhopf et al., 1977), they are only briefly described here. Both models are based on the governing equations for trace constituents in a meridional plane

$$\frac{\partial n_i}{\partial t} + \nabla \cdot \left(n_i v + \Phi_i \right) = P_i - L_i \qquad (3)$$

where P_i and L_i are production and loss rates, respectively, for the ith constituent, v is meridional bulk velocity, Φ is the "eddy flux" which represents large-scale eddy motions, and n_i is the number density of the ith constituent where the Ames model solves directly for n_i and the Aerospace model computes the corresponding mixing ratio; P_i and L_i will, of course, have different forms, depending on whether equation (3) is written in terms of the number density or mixing ratio. For example, the "eddy" fluxes in each model are expressed as

$$\Phi_i = \begin{cases} -K_e \cdot \left[\nabla n_i + \left(\frac{1}{H} + \frac{1}{T}\frac{dT}{dz} \right) \hat{e}_z n_i \right] \text{(Ames model)} \\ \\ -K_e \cdot \left[\nabla \left(\rho n_i \right) \right] \qquad \text{(Aerospace model)} \end{cases} \qquad (4)$$

in which K_e represents the eddy-diffusivity tensor (vertical, meridional, and "off-diagonal" terms); ρ, H, and T are the atmospheric density, scale height, and temperature, respectively; and $\hat{e}_z$ is a vertical unit vector.

Ames Model

Spherical geometry is employed in equations (3) and (4) with the horizontal coordinate extending along a meridian from lat. 80° S to lat. 80° N in 5° intervals and the vertical coordinate extending from the ground to an altitude of 60 km in 2.5-km intervals. The end boundary conditions assume zero flux of all constituents across the vertical boundaries. The upper boundary conditions are specified by zero vertical flux for all species, and the lower boundary conditions are either (1) chemical equilibrium or (2) fixed concentration that is usually representative of measured values. Species having very rapid loss mechanisms (e.g., O, OH, HO_2) were assumed to be in photochemical equilibrium at the lower boundary. Long-lived species were held fixed at the ground (e.g., N_2O at 7.5×10^{12} cm^{-3}, O_3 at 4.5×10^{11} cm^{-3}). For the computations reported here, we fixed the concentrations of the water soluble species HNO_3, HCl, and H_2O_2 equal to zero at the lower boundary. The mixing fractions of CO_2 were fixed at all grid points at 367 ppmv.

The chemical rate equations are solved using an implicit technique. Omitting the transport term from equation (3) yields the finite difference form (with $Q = P - L$)

$$\frac{n_i^{j+1} - n_i^j}{\Delta t} = Q_i^{j+1} \qquad (5)$$

which can be linearized by taking the first term in a Taylor series expansion about Q_i^j:

$$\frac{n_i^{j+1} - n_i^j}{\Delta t} = Q_i^j + \sum_k \frac{\partial Q_i^j}{\partial n_k} \left(n_k^{j+1} - n_k^j \right) \qquad (6)$$

The members of the set of equations are coupled and require solution by matrix methods; the "families" approach was not used for the computation reported here. Diurnal averaging of photodissociation rates and reaction rate coefficients is performed, using, respectively, the techniques reported by Cogley and Borucki (1976) and Turco and Whitten (1978). The transport computations are time-split into those for vertical and horizontal advection and diffusion. Solutions for the transport processes are obtained from a mass-conserving, forward-time, space-centered finite difference formulation of the equations. An

implicit formulation is used for the horizontal diffusion, and an explicit formulation is used for all other transport processes.

The atmospheric meridional bulk velocity and eddy transport fields are derived in the manner discussed by Borucki et al. (1976) and Whitten et al. (1977). The eddy coefficients, originally derived by the method of Reed and German (1965), have been modified so as to simulate observed tracer distributions (agreement with tracer data is discussed in the following section). The stream functions from which the bulk velocities were calculated were based partly on the meridional circulation field computed by Cunnold et al. (1975) and partly on mean observed meridional winds.

The model currently contains constituents in the oxygen-nitrogen-hydrogen-carbon-chlorine families and generally uses the rate coefficients recommended in the NASA Chlorofluoromethane Workshop Report (Hudson, 1977) or in the work of Turco and Whitten (1975) on the effect of chlorofluoromethanes on ozone. Exceptions to the rule are discussed later.

Aerospace Corporation Model

The Aerospace model (Widhopf, 1975; Widhopf et al., 1977) employs spherical geometry, as does the Ames model, but it extends from pole to pole in $10°$ intervals; the vertical coordinate extends from the surface to an altitude of 50 km with a 1-km grid spacing from the surface to 35 km and with a 2.5-km grid spacing at higher altitudes. The lateral boundary conditions for all constituents are zero flux across the polar regions. The species $O(^3P)$, $O(^1D)$, O_3, OH, HO_2, N, and H are taken to be in photochemical equilibrium at the upper boundary; the mass mixing ratios of NO_2, N_2O, CH_4, CO, and HNO_3 were analytically continued to the upper boundary by a second-order extrapolation in space and time (Widhopf, 1975; Widhopf and Taylor, 1974). At the lower boundary the concentrations of O_3, N_2O, and CH_4 were held fixed (6×10^{11} parts/cm^3, 0.31 ppmv, and 1.35 ppmv, respectively), while removal of H_2O, HNO_3, NO_2, NO, and H_2O_2 from the troposphere was simulated by rainout-washout (Glatt and Widhopf, 1978; Widhopf and Glatt, 1979a); H_2O and HNO_3 were removed at average rates defined by Junge (1963) and NO_2, NO, and H_2O_2 were assumed to be removed at one-tenth that rate. Other species [$O(^3P)$, $O(^1D)$, OH, HO_2, N,

and H] were taken to be in photochemical equilibrium at the lower boundary because of their relatively short lifetimes. Anthropogenic emissions of NO_X are included in the model, and the lower boundary condition for CO is interpreted from the measurements of Seiler (1974).

The chemical rate equations were solved using a second-order implicit technique (Widhopf and Victoria, 1973). The chemical production-loss term Q_i is approximated by the expansion

$$Q_i^j = \frac{1}{2}\left(Q_i^{j+1} + Q_i^{j-1}\right) \quad (7)$$

where

$$Q_i^{j+1} = Q_i^j + \sum_k \frac{\partial Q_i^j}{\partial C_k}\left(C_k^{j+1} - C_k^j\right)$$
$$+ \frac{\partial Q_i^j}{\partial \rho}\left(\rho_i^{j+1} - \rho_i^j\right)$$
$$+ \frac{\partial Q_i^j}{\partial T}\left(T_i^{j+1} - T_i^j\right) \quad (8)$$

In equation (8) c represents the mass mixing ratio, ρ is the air density, and T is the air temperature. Note that equations (7) and (8) are similar to (5) and (6), except that (6) does not contain the density and temperature terms and is a first-order approximation, whereas (7) is a second-order approximation in time. Diurnal averaged local photolysis rates are computed at every third time step using a technique developed by Kramer and Widhopf (1978), and diurnal averaging of reaction rate coefficients is carried out using a technique similar to that of Turco and Whitten (1978). Advective and diffusive terms that are important in determining the time-dependent distributions of the species are treated using a leap-frog and Dufort-Frankel second-order accurate finite-difference scheme, respectively. The longer lived species (time constant >2 days) are treated in an explicit manner.

The atmospheric meridional bulk velocity and eddy transport fields are derived in the manner discussed in Widhopf et al. (1977). Briefly stated, the mean meridional circulation was obtained from the work of Louis (1973) and Louis et al. (1974), and the eddy coefficients were based principally on the work of Luther (1973), Hunten (1975), and

Newell et al. (1966). In testing these coefficients against dispersion of inert tracers in the atmosphere, they were found not to be totally adequate (Widhopf, 1975) and were improved by numerical experimentation described by Widhopf et al. (1977).

The important features of the Ames and Aerospace models are compared in table 2.

Reaction Rate Coefficients

The reaction rate coefficients used in the work reported here are essentially those reported in Part I with some exceptions; the values are listed in tables 3-7. As indicated in those tables, the Aerospace model contained no chlorine constituents for this particular investigation; although it has since been modified to include chlorine, the changes were not made in time for this study. Finally, we mention the recent measurement (Zahniser and Howard, 1978) of the rate coefficient for the very important reaction (2), the temperature-dependent value of which is given as

$$k = (1.4 \pm 0.4) \times 10^{-14}$$
$$\times \exp(-580 \pm 100/T)\, cm^3 \, sec^{-1}$$

Although this measurement was announced too late for most of our assessments, we were able to make several calculations with the Ames model using the new data for reaction (2). The results are discussed in section V.

IV. AMBIENT ATMOSPHERE

Before discussing the application of our models to impact assessments, it is important to demonstrate their capabilities for predicting ambient stratospheric characteristics. First, however, we will make a few remarks about photochemical "time constants."[3] If the characteristic time constants are very small, a few days or less, the constituent in question is nearly in a photochemical steady state (in daytime at least); therefore, it is not directly influenced by transport, although transport may be indirectly important through its influence on the distribution

---

[3]By "time constants," we mean the time required for the constituent concentration to decrease to e^{-1} of its value at the time the source strength is set equal to zero.

of the parent gas from which the species is formed. On the other hand, if the time constants are large, abundances and distributions are governed largely by transport, and photochemistry may be relatively unimportant. An extreme example is carbon 14 — it is chemically inert, but does decay radioactively with a lifetime in excess of 5,000 yr. Other, less extreme examples are the total concentration of odd nitrogen (NO_y), which is formed within the stratosphere and removed, mainly by downward transport, into the troposphere, where it can be removed by rainout-washout. Other examples are the chlorofluoro-methanes (CFM), which are transported from the troposphere into the stratosphere where they are photolyzed. Because constituents with large time constants (of the order of months to years) act as tracers, they are especially valuable in studying transport in the upper atmosphere; we will now consider them in some detail.

Tracers

During large thermonuclear explosions, vast quantities of carbon 14, formed by neutron bombardment of nitrogen 14, are injected into the stratosphere over a range of altitudes. One can estimate the rates of vertical transport by measuring the temporal change in the distribution of the (excess) carbon 14 over a period of several years (Johnston et al., 1976). In fact, substantial use has been made of the data from the large (57 MT) Soviet high-latitude (75° N) test. However, there may be limitations to the use of these data for transport studies: Chang (1975) has conjectured that an unsampled reservoir of excess carbon 14 was feeding the region at lat. 30° N, and Mahlman (1975) showed that lack of a tropospheric sink does influence the apparent vertical transport, leading to an underestimate of the eddy diffusivity. Therefore, one can interpret these simulations as does Oliver et al. (1977) as an estimate of the lower bound to the rate of vertical transport in the stratosphere.

Figure 2 shows the predictions of excess carbon 14 for the two models at lat. 30° N 9 months after injection together with the corresponding measured number density distributions. The Aerospace model is in quite good agreement with observation, but the Ames model shows somewhat faster removal of the carbon 14 than measurements seem to indicate. Here it should be remarked that the Aerospace model used the carbon-14 data to refine the eddy transport parameterization at higher latitudes. Since the

measurements are not extensive enough to provide a definitive test of model transport and could be interpreted as yielding a lower bound to the rate of vertical transport, neither model is inconsistent with observation.

Bauer et al. (1978) have suggested the use of zirconium-95 data from recent Chinese atmospheric thermonuclear explosions as a tracer of vertical transport. However, as they point out, the particulate nature of that isotope requires the proper treatment of sedimentation velocities. Since neither model is able to satisfactorily treat the size distribution of such aerosol particles, we do not employ the zirconium-95 data in the studies described in this report.

A potentially more definitive set of transport tracers (because sources and sinks are known or can be determined) is composed of those constituents that are transported upward from the troposphere into the stratosphere and decomposed there. These constituents include N_2O, CH_4, and chlorofluoromethanes. For example, nitrous oxide is a good tracer because it has a stratospheric lifetime against chemical attack that is very much larger than its lifetime against photolysis by sunlight. Hence, using knowledge of the photoabsorption cross sections and solar radiation intensity to compute the chemical loss rates, one can employ such tracers to make useful estimates of transport rates in the lower stratosphere. Their usefulness as tracers is complicated somewhat by uncertainty as to the location of the principal ports of entry into the stratosphere (i.e., are they injected primarily in the intertropical convergence zone (ITCZ) or at other latitudes as well?) and lack of adequate data above 30 km. The use of methane data as a check of transport parameterization is further complicated by the dominant loss mechanism, reaction with OH, because the OH abundance is itself dependent on the methane abundance (see Part I for a complete discussion) and is very uncertain.

Predictions of the vertical distributions of N_2O are compared with measurements in figure 3. Although neither model is inconsistent with observations, there are insufficient data for a definitive evaluation of the transport simulation. The considerable scatter in the high-latitude data of Schmeltekopf et al. (1977) probably reflects variable conditions of transport. Similar considerations hold for the predicted and measured methane profiles shown in figure 4. This kind of comparison is further complicated by adoption of a lower boundary condition for methane. The tropospheric mixing ratio adopted as the lower boundary condition for the Aerospace model was 1.35 ppbv, based on early measurements, whereas the Ames model employed mixing ratios of ≈1.8 to 2 ppbv, based on fits to the tropospheric and lower stratospheric measurements. More recent measurements (Fabian et al. 1979) yield an average mixing ratio of approximately 1.65 ppbv.

To evaluate the simulation of the horizontal as well as vertical transport, we turn our attention to the predicted distributions of some of the species that are formed in whole or in part within the stratosphere: ozone, nitric acid, and water vapor. Ozone is formed mainly at altitudes above 30 km due to the photodissociation of molecular oxygen in the Herzberg continuum (e.g., Whitten and Poppoff, 1971) and subsequent attachment of the oxygen atoms to O_2. After formation it can, of course, be destroyed by the various processes discussed in Part I or it can be transported downward and poleward by atmospheric motions of varying scales. The horizontal gradients in the ozone concentration, which are associated with the poleward transport, are believed to be caused by eddies in the lower stratosphere; the eddies, according to Newell (1963), cause the mixing surfaces to slope more steeply toward the pole than do the surfaces of equal potential temperature. That is, parcels of ozone moving poleward in the lower stratosphere tend also to move downward in the transport region to altitudes where their destruction becomes less efficient. Figure 5 shows some isopleths of ozone concentration for the two models obtained using the older value (see Hudson, 1977, for reaction (2)). Note that the ozone abundances in the lower stratosphere increase toward the poles and that the altitude of peak concentration slopes downward as one goes toward the pole. The agreement between the two models is quite good except at altitudes below ~17 km and at high latitudes; the differences below 17 km may result, in part, from different choices of lower boundary conditions for ozone, and those at high latitude may reflect different values of the transport parameters.

Figure 6 shows computed and observed ozone profiles for three latitudes for the older value of the rate coefficient for reaction (2). The ozone abundances are overestimated by both models at all latitudes. However, figure 7 shows that when the newer value for the rate constant (Zahniser and Howard, 1978) is used, the agreement between observation and theory is greatly improved. The

7

principal reason for the improvement is the substantially increased ozone loss rate below 25 km (see Whitten et al., 1978; Turco et al., 1978). Figure 8 shows the corresponding computed and observed column densities for the summer and fall seasons; obviously, the agreement with observation is much improved. Similar results are obtained in other studies by Widhopf and Glatt (1979b). Here it should be remarked that neither model contained chlorine when the computations with the older value of the rate coefficient for reaction (2) was used. However, the Ames model was altered to simulate the effect of 2.5 ppbv of Cl_X (the sum of HCl, Cl, ClO, and $ClONO_2$). The absence in the simulation of observed abundances of chlorine compounds could not account for the overestimate of stratospheric ozone abundance.

A second tracer that is formed within the stratosphere is "odd-nitrogen," composed of NO, NO_2, NO_3, N_2O_5, HNO_3, HNO_2, and $ClONO_2$ and sometimes called "NO_y" (the sum of NO and NO_2 concentrations is usually called "NO_x"). Although odd-nitrogen is not a directly measured quantity, its principal components, NO, NO_2, and HNO_3, have been measured individually. Total NO_y is important for an intercomparison of the two models because (1) the comparison of its predicted distribution shows the effects of the two different transport parameterizations, and (2) the predicted amount and distribution of NO_y in the atmosphere is related to the predicted change in ozone. Figure 9 shows profiles of computed NO_y at low, mid-, and high latitudes and some (mostly midlatitude) data representative of a compilation by Ackerman (1975) of numerous measurements of NO, NO_2, and HNO_3. At altitudes between 17 and 40 km, the predictions obtained from the two models agree with each other quite well. However, at low altitudes the Aerospace model predicts substantially less NO_y than does the Ames model, except in the lower 4-5 km where anthropogenic NO_x injection is simulated in the Aerospace model. At high altitudes, the Aerospace model predicts more NO_y than does the Ames model because the former assumes a small source of mesospheric NO_y that is absent from the latter. Such a source may be characteristic of auroral latitudes where electron bombardment dissociation of N_2 is expected to yield a net production of NO. At lower latitudes (i.e., equatorward of $\sim 60°$) there probably exists a net NO sink through the reaction

$$N + NO \rightarrow N_2 + O \qquad (9)$$
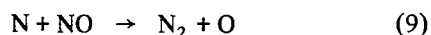
This difference in upper boundary conditions effects the distributions appreciably only above ~ 35 km (Duewer et al., 1977). The differences at altitudes between 14 and 17 km are due, in part, to the simulations of washout-rainout in the Aerospace model; washout-rainout is not simulated in the Ames model. We believe these differences to be useful in exploring the model dependence of ozone destruction discussed in section V because they provide limiting cases for natural sources and sinks.

The principal NO_y species in the lower stratosphere is nitric acid; since many observations of this constituent have been made (Lazrus and Ganrud, 1974; Murcray et al., 1975), it is useful to compare predictions with the observations. However, column densities show much less variability due to small-scale variations in transport than do local concentrations. Therefore, the column densities that cover a range of altitudes and show much less variability are most useful for comparisons with model predictions. Such comparisons are shown in figure 10. Obviously the predicted and measured column densities for the two models greatly exceed the measurements, although the predicted latitudinal gradients agree rather well with the measured gradients.

In order to understand the discrepancy, it is useful to examine another related parameter, the HNO_3/NO_2 ratio, and to compare the calculated and observed values. The usefulness of the comparison is apparent from considerations of the NO_y budget. If the nitric acid abundance is high compared with observation, one would expect the HNO_3/NO_2 ratio to be large. Estimates of the ratio as a function of altitude obtained by several investigators are shown in figure 11 together with predictions obtained with the Ames model for lat. $45°$ N and with the Aerospace model at lat. $40°$ N. Although the model predictions strongly disagree with the data of Evans et al. (1976), they do not disagree nearly as strongly with the other data. In any case, the high predicted HNO_3 levels shown in figure 10 are roughly consistent with the apparently high predicted HNO_3/NO_2 ratios shown in figure 11. The Aerospace values are higher than the Ames ratios, which is consistent with the larger HNO_3 column densities obtained in the Aerospace model. Schiff et al. (1978) and Evans et al. (1978) have suggested that the discrepancy between measurement and theory can be resolved by assigning a pressure dependence to reaction (1) such that the rate coefficient is substantially reduced; however, at present it is not clear

that such a pressure dependence exists.[4] The relation of the HNO_3/NO_2 ratio to predicted effects on stratospheric ozone of SST-emitted NO_X will be discussed in section V.

A third species which has many of the attributes of a tracer is stratospheric water vapor. Unfortunately, the sources of water vapor are poorly understood. Many years ago Dobson et al. (1946) proposed that water vapor enters the stratosphere almost entirely through the tropical tropopause, which forms a cold trap; the cold trap then determines the water-vapor mixing ratio. Since then, it has become generally accepted that methane oxidation yields an additional source, largely in the middle stratosphere. Harries (1976) has summarized the various measurements made up to 1976; the range of mass mixing ratio values, obtained by averaging the measurements, is shown in figure 12. Comparison with the predicted mixing ratios, also shown in figure 12, indicates that the agreement is reasonable; however, the wide spread of the measured values should be noted. Note that the Aerospace model calculates the distribution of water vapor everywhere and that the Ames model prescribes the tropospheric distribution using standard atmosphere data.

Reactive Species

There are several highly reactive species that are important to our studies: OH, HO_2, NO, NO_2, and CH_3O_2. We will begin our discussion with the odd-hydrogen radicals OH and HO_2.

The hydroxyl radical is formed in the stratosphere by the reaction of excited oxygen atoms with water vapor:

$$O(^1D) + H_2O \rightarrow 2OH \qquad (10)$$

and by methane oxidation. The latter process, which is initiated by the OH destruction reaction

$$OH + CH_4 \rightarrow H_2O + CH_3 \qquad (11)$$
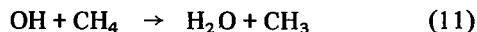
is believed to yield a net production of nearly two OH molecules for each methane decomposition reaction (see Part I for a complete discussion). In the upper stratosphere the methane oxidation

---

[4] If this reaction of OH with HNO3 should prove to be substantially faster than indicated in table 2, the HNO3/NO2 ratio could be significantly lowered.

sequence is a small contributor to OH formation, but in the lower stratosphere, as our studies have shown, it is nearly as important as the water-vapor source of OH. The hydrogen radicals are lost primarily by reaction with each other,

$$OH + HO_2 \rightarrow H_2O + O_2 \qquad (12)$$
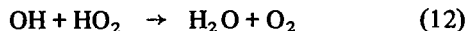
We have plotted the predictions of OH concentration in figure 13, which also shows Anderson's observed values obtained at a solar zenith angle of $\sim 86°$ (at Palestine, Texas, lat. 32° N, in July and January). Because of the large solar zenith angle, the observed values should be multiplied by a factor of about 1.5 to 2 when compared with the mean daytime predicted concentrations shown in figure 13(a). Hence, they appear to be somewhat larger than our predictions would indicate for large solar zenith angles, at least for heights above 30 km. Furthermore, we note that Anderson's January 1976 values were obtained a little later in the year than were the corresponding predicted values (mid-November) and at a slightly lower latitude; in mid-February at lat. 35° N, the predicted concentrations of OH are about 20% lower than those shown for lat. 40° N in mid-November. Thus, the agreement between measured and predicted hydroxyl concentrations can be regarded only as fair for altitudes above 30 km, although the difference between observation and calculation is much less than it was prior to the measurement of the rate coefficient for reaction (1) by Howard and Evenson (1977).

So far, no stratospheric measurements of OH abundance have been made below 30 km. At altitudes below 20 km, there are substantial differences between the predictions of the two models relative to OH, which we attribute largely to the differences in predicted ozone concentrations and rainout-washout of HO_X and HNO_3. Smaller ozone abundances, as obtained with the Aerospace model, lead to less predicted $O(^1D)$ and thus a small rate of formation of OH. The absence of rainout-washout in the Ames model results in higher HO_X, NO_X, and HNO_3 abundances. Comparison with HNO_3 measurements and NO_X estimates due to Fishman and Crutzen, obtained by balancing the CO budget, show good agreement with Aerospace model predictions in the troposphere (Widhopf and Glatt, 1979a). Smaller OH concentrations also mean that the rate of OH conversion to HO_2 via the reaction
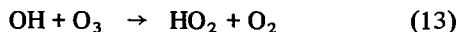
$$OH + O_3 \rightarrow HO_2 + O_2 \qquad (13)$$

is slowed, thus decreasing the effect on OH of the smaller ozone abundance. The larger OH concentrations predicted by the Ames model at altitudes below 20 km have an important bearing on the differences in the SST effects on ozone predicted by the two models. This aspect is discussed in section V.

Figure 14 compares predictions of HO_2 for the two models. Although no measurements of HO_2 have yet been made, we show these results as a further useful comparison of the HO_X chemistry contained in the models. We attribute the substantial difference at high latitudes in autumn to differences in computed mean solar zenith angles near lat. 70° N. The radical CH_3O_2, which has not yet been observed in the stratosphere, can also be classed as an HO_X radical because of the similar chemical behavior of H and CH_3. The predicted profiles of CH_3O_2 are substantially different above 30 km, as shown in figure 15; however, it is not important to the chemical cycle above that altitude. The reason for this divergence is the dependence of CH_3O_2 production on the distribution of its methane source (cf. fig. 4). Because it is less abundant and probably somewhat less reactive, the radical CH_3O_2 is probably of much less direct importance to ozone chemistry than is HO_2. Its main role is as an intermediary in the methane oxidation sequence.

As has been discussed many times (see Part I for references) the odd-nitrogen species NO and NO_2 strongly influence ambient ozone as well as ozone loss due to supersonic transport emissions. Figure 16 compares the distributions predicted by the two models with each other and with the results of a simultaneous measurement of NO and NO_2 by Ackerman et al. (1975). It is seen that the predictions of both models are slightly smaller than the measured values, but the disagreement is not serious (see the HNO_3/NO_2 data in fig. 11). The principal reasons for the differences between the two sets of predictions are the effects of the tropospheric conditions (discussed earlier with respect to NO_y) and slightly different partitioning of NO_X between NO and NO_2. Partitioning is determined approximately by the relation

$$\frac{[NO]}{[NO_2]} \approx \frac{J}{k[O_3]} \qquad (14)$$

where J is the photolysis rate of NO_2, $[O_3]$ is the local ozone number density, and k is the rate coefficient of the reaction

$$NO + O_3 \;\rightarrow\; NO_2 + O_2 \qquad (15)$$
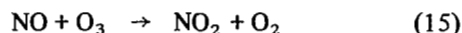
If partitioning favors NO_2, more of the NO_X will be converted to nitric acid and total NO_X will decrease slightly. The partitioning of NO_X predicted by the two models is very close at altitudes above 20 km; at lower altitudes, the Aerospace model predicts less NO_2 and more NO than the Ames model because of the smaller ozone abundance computed by the former.

Conclusions

We can summarize the principal points made in the preceding discussion of the ambient (unperturbed) atmosphere as follows:

1. Insufficient data are available on the distributions of excess carbon 14 from atmospheric nuclear tests and on the ambient distributions of nitrous oxide and methane to permit the transport parameters of one model to be chosen over those of the other. Although the ozone and NO_y data appear to be in reasonable agreement with observations, we must nevertheless conclude that insufficient tracer data are available for a satisfactory definition of the transport parameters.

2. The predicted ozone abundance computed by both models is in reasonable agreement with observation when the new rate coefficients for reactions (1) and (2) are used.

3. The NO_y computed by the two models agrees quite well between 18 and 40 km altitude. The differences below 18 km and above 40 km are due to different boundary conditions and rainout-washout.

4. The predicted OH abundance at altitudes above 30 km appears to be low in light of Anderson's (1976) measured values. On the other hand, it may be too high at lower altitudes, which is suggested by the apparently excessive computed nitric acid concentrations (fig. 10) and HNO_3/NO_2 ratios (fig. 11). The latter characteristics are important because they are closely related to the magnitudes of the predicted ozone changes induced by NO_X emissions from SST's.

V. RESULTS AND DISCUSSION

In this section we present and discuss the results obtained for operation of types A and B aircraft (20-km and 17.5-km nominal flight altitudes, respectively), using the emissions model shown in figure 1; one scenario for the type A aircraft includes emissions by subsonic aircraft as well. These results take the form of plots of relative ozone column change as a function of latitude and the vertical distributions of the absolute ozone and NO_y changes at various latitudes. We then compare the results from the Ames and Aerospace models with each other and with the results of previous multidimensional model calculations (e.g., Alyea et al., 1975; Borucki et al., 1976; Widhopf et al., 1977; and Hidalgo and Crutzen, 1977). Finally, we briefly discuss the uncertainties associated with the calculations.

Flight Scenarios

To arrive at reasonable estimates of the possible effects on stratospheric ozone of supersonic aircraft operations as described in section II, we constructed the following scenarios:

1. Five years of operation of type A aircraft (nominal cruising altitude of 20 km), using the NO_x injection rate given in figure 1 and the corresponding water-vapor injection rate ($\sim$200 g H_2O/g NO_2). In the Ames model, the simulation of NO_x and water-vapor emission was performed at an altitude of 20 km because of the 2.5-km vertical grid spacing. For the Aerospace model, injection at 19, 20, and 21 km was simulated, as shown in figure 1. No chlorine constituents were included in the models and the older value of the rate coefficient for reaction (2) was used. We note here that when the new value for that rate coefficient was announced by Zahniser and Howard (1978), the 5-yr runs had already been completed.

2. Five years of operation of type B aircraft (nominal cruising altitude of 17.5 km). The altitudes at which injection was simulated were lowered: to 17.5 km for the Ames model, and to 16, 17, and 18 km for the Aerospace model. Otherwise, the NO_x emission rates shown in figure 1, along with the corresponding water-vapor emission rates, were used. The same chemical model used to perform the case of injection at an altitude of 20 km was

also used here because these runs were also completed prior to the announcement of the new rate for reaction (2).

3. Five years of operation of type A aircraft together with a nominal fleet of subsonic aircraft, using the emission rates shown in figure 1 and table 1. To simulate the removal of NO_x in the troposphere, the increase in HNO_3 was set equal to zero at an altitude of 5 km in the Ames model. A comparison of our results for the increase of NO_y (ΔNO_y) with results from a variant of the Ames model which contained "rainout" boundary conditions showed that causing ΔNO_y to vanish at an altitude of 5 km gave a good approximation to the "rainout" conditions. The Aerospace model simulated rainout-washout directly in the same manner discussed for the calculation of the natural atmosphere.

In order to then simulate steady-state conditions in an atmosphere containing chlorine constituents, we employed two additional scenarios, using the Ames model only:

4. Fifteen years of operation of type A aircraft using the NO_x injection rate given in figure 1; to minimize computer usage, the NO_y injection, without any chemistry, was simulated for 13 yr; this simplification is justified because stratospheric NO_y is a nearly-conserved quantity. The full model, which contained 2.5 ppbv of ozone-active chlorine (at an altitude of 60 km), was then run until the seasonal changes in ozone abundance became repetitive ($\sim$2 yr); the last two seasons (summer and autumn) were then very close to a steady-state cyclic variation. The new value of the rate coefficient of reaction (2) was used.

5. Same as (4), but with type B aircraft.

Changes in NO_y

Figures 17 through 21 show the changes in NO_y (ΔNO_y) that are predicted by the models for scenarios (1) to (5), respectively, at latitudes of 0°, 40°, and 70° N. We present results for only the Northern Hemisphere because nearly all of the simulated aircraft emissions occur there; the eventual buildup of ΔNO_y in the Northern Hemisphere would be nearly twice as large as in the Southern Hemisphere. Plots of ΔNO_y are useful because the distribution is influenced only by transport and the mesospheric and tropospheric sinks; stratospheric

photochemistry does not affect it. The predicted spatial distributions of the increase in water vapor (ΔH_2O) due to SST emissions was found to be very similar to those of ΔNO_y (except for a multiplicative factor of about 550); hence, we do not show them here.

Comparison of the vertical profiles obtained by the Ames and Aerospace models for scenario (1), shown in figure 17, and scenario (2), presented in figure 18, suggest that the Aerospace model predicts that ΔNO_y is concentrated in a narrow altitude range. This is a result of at least three effects. First, the vertical resolution is quite different (1 km vs 2.5 km), which will tend to maintain a sharper profile in the Aerospace model. Second, the Aerospace model includes rainout-washout, which tends to decrease the concentration in the troposphere faster. Finally, the faster vertical diffusion in the Ames model accounts for some of the difference. Such relative behavior of the predicted ΔNO_y is consistent with the predicted temporal behavior of excess carbon 14 shown in figure 2. In addition to the differences in vertical diffusion, differences in resolution and transport evidently cause the maxima in the predicted ΔNO_y profiles to occur at an altitude that is about 2 km lower at lat. 70° N in the Aerospace model than in the Ames model. As we noted previously, neither model is inconsistent with available tracer observations; hence, the results from each model should be regarded as reasonable simulations of the distribution of the ΔNO_y.

The distribution of the ΔNO_y is rather strongly dependent on the flight altitude. For the case of NO_y injection at 20 km, more of the simulated NO_y is retained in the stratosphere near the injection altitude by the Aerospace model than by the Ames model (fig. 17). However, the Ames model predicts faster upward transport to higher altitudes for injection at 17.5 km. At high latitudes the Aerospace model tends to retain more of the ΔNO_y at lower altitudes than does the Ames model, and this has a significant bearing on the ozone change resulting from stratospheric injection. This is probably affected by washout-rainout, which would decrease ΔNO_y proportionately faster for the 17.5-km case than for the 20-km case, and by the effect of faster vertical diffusion in the Ames model. In the 17.5-km-injection-height case more total ΔNO_y is retained by the Ames model than by the Aerospace model, which is the opposite of the carbon-14 result. This indicates that rainout-washout accounts for the differences, because such processes are not important

to carbon-14 distributions. As we shall see later (also see Part I), the increase of NO_y at relatively low altitudes (i.e., below ~20 km) leads to ozone increases, and enhanced NO_y at higher altitudes leads to ozone decreases. One should also note in both models the downward trend of the ΔNO_y as it is moved poleward. Such an effect is, of course, expected because it is closely related to two high-latitude phenomena: (1) the increase in ambient ozone and (2) the lower altitudes at which peak ozone concentrations occur. That is, some of its sources and sinks are similar to those of ozone in that NO_y is formed in the upper stratosphere (via reaction of $O(^1D)$ with N_2O) and lost by transport into the troposphere.

In scenario (3) the Aerospace model, as we might expect from our foregoing comments concerning vertical diffusion, resolution, and rainout-washout, shows retention of the vertical distribution of injected NO_x (see table 1) and less vertical diffusion than the Ames model. In this the former predicts a deeper minimum between the stratospheric and tropospheric contributions at mid-latitudes than does the Ames model.
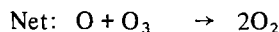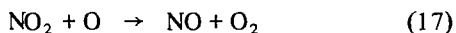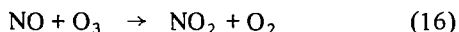
We cannot, of course, compare results from both models for scenarios (4) and (5) (figs. 20 and 21); however, it is worth noting that the vertical distribution of the injected NO_y is more dispersed in the steady-state case than after 5 yr of operations. The spreading is asymmetric; that is, the ΔNO_y increase is greater above the peak than below it. From our comments above, such behavior has an important bearing on predicted ozone changes since the more NO_y that is transported to higher altitudes, the greater the likelihood that ozone will decrease.
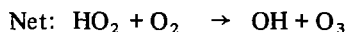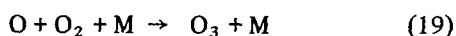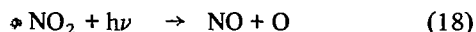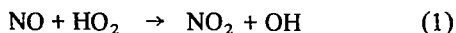
Changes in Ozone

Predicted changes in the vertical distribution of ozone (ΔO_3) as a consequence of stratospheric emissions of NO_y and water vapor are presented in figures 22 through 27. The most striking features of the profiles of ΔO_3 are the changes from ozone gains to ozone losses at altitudes between 18 and 22 km. In general, calculations using the Ames model showed smaller ozone gains at low altitudes and larger ozone losses at high altitudes than did the Aerospace model. Such behavior of the stratospheric ozone is in part a consequence of the predicted vertical distributions of ΔNO_y shown in figures 17 through 21 and in part a consequence of the vertical distributions

of OH and HO_2. Note that at altitudes between 10 and 20 km the Ames model contains more OH than the Aerospace model, and between 20 and 30 km, less HO_2 than the Aerospace model (except at high latitudes in autumn). The overall effect of these differences is a prediction by the Aerospace model of more ozone gain between 10 and 30 km. Figure 24 includes a simulated fleet of subsonic aircraft (see table 1) along with a nominal fleet of type A SST's. In this case the ozone gains, which occur in the troposphere, greatly exceed the losses, which occur above ~20 km, and thus yield a net increase in ozone. For scenarios (1) and (2) the changes in total ozone column are very close to zero for the Aerospace model, but are negative and of the order of tenths of a percent for the Ames model. Discussion of the Ames predictions of ozone column change is deferred until we discuss the steady-state results.
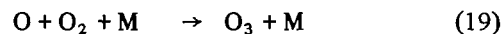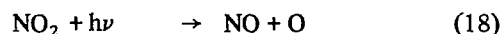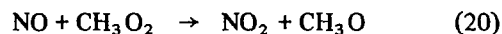
The catalytic chain of reactions responsible for ozone destruction by nitrogen oxides has been known for a long time (Crutzen, 1970; Johnston, 1971):

$$NO + O_3 \quad \to \quad NO_2 + O_2 \qquad (16)$$

$$NO_2 + O \quad \to \quad NO + O_2 \qquad (17)$$

$$\text{Net:} \quad O + O_3 \quad \to \quad 2O_2$$

and is not discussed further here (see Part I). In writing the catalytic sequence composed of reactions (16) and (17), one must keep in mind that the quantity of NO_2 participating in reaction (17) is exactly that produced in reaction (16). Other sources of NO_2 must be excluded when evaluating the net rate of the cycle. Similar arguments hold for the other cycles discussed below. Because of reactions (16) and (17), increases of NO_y at higher stratospheric altitudes lead to decreases in ozone. On the other hand, increases of NO_y at lower altitudes lead to increases in ozone because of reactions that have only recently been recognized; they are reactions that catalytically form ozone (see Part I; also Widhopf et al., 1977; Hidalgo and Crutzen, 1977; Crutzen and Howard, 1978; Turco et al., 1978):

$$NO + HO_2 \quad \to \quad NO_2 + OH \qquad (1)$$

$$NO_2 + h\nu \quad \to \quad NO + O \qquad (18)$$

$$O + O_2 + M \quad \to \quad O_3 + M \qquad (19)$$

$$\text{Net:} \quad HO_2 + O_2 \quad \to \quad OH + O_3$$

and to a lesser extent

$$NO + CH_3O_2 \quad \to \quad NO_2 + CH_3O \qquad (20)$$

$$NO_2 + h\nu \quad \to \quad NO + O \qquad (18)$$

$$O + O_2 + M \quad \to \quad O_3 + M \qquad (19)$$

$$\text{Net:} \quad CH_3O_2 + O_2 \quad \to \quad CH_3O + O_3$$
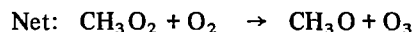
in which CH_3O_2 is an intermediate product in the methane oxidation chain. Although reaction (20) provides a direct link between methane oxidation and ozone generation, a more important, but indirect, influence results from the copious formation of HO_2 during the methane oxidation process. In fact, methane decomposition may be the largest source of HO_2 in the lower stratosphere. In addition to ozone formation through the sequences listed above, NO introduced into the lower stratosphere converts HO_2 normally present into OH. Such conversion has two effects: (1) it shifts the reactive NO component of NO_y into the relatively inert nitric acid and (2) it amplifies the oxidation rate of methane and CO, thereby generating HO_2 and ozone more rapidly.

As discussed elsewhere (Part I; Crutzen and Howard, 1978; Turco et al., 1978) the earlier failure to recognize the significance of reactions (1) and (2) was not recognized due to the low values ascribed to the rate coefficients (see Hudson, 1977, for a discussion relative to reaction (1), and Whitten et al., 1978, for a discussion relative to reaction (2)). The larger, and now generally accepted, values (see table 2) were first reported by Howard and co-workers (Howard and Evenson, 1977; Zahniser and Howard, 1978).

In computing the ozone changes shown in figures 25 and 26 (i.e., steady-state conditions), an ozone-active chlorine mixing ratio of 2.5 ppbv at an altitude of 60 km was included in the Ames model because such a chlorine abundance is probably a reasonable extrapolation to the years 1990-2000. Chlorine is important in the present context because it is closely coupled to NO_x through the reactions
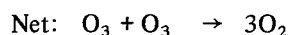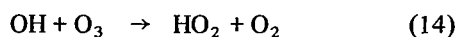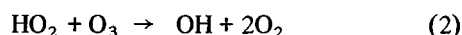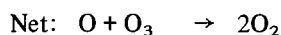
$$ClO + NO_2 + M \quad \to \quad ClONO_2 + M \qquad (21)$$

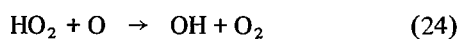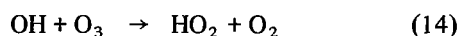$$ClO + NO \quad \to \quad Cl + NO_2 \qquad (22)$$
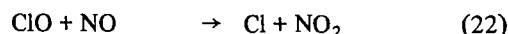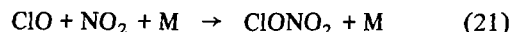
Thus, if stratospheric NO_x is increased, the rates of reactions (21) and (22) will be increased. Since reaction (21) tends to shift Cl_x away from the active forms, Cl and ClO, increasing its rate will decrease

ozone loss due to chlorine catalysis. Reaction (22) competes with the rate-controlling odd-oxygen loss process

$$ClO + O \rightarrow Cl + O_2 \qquad (23)$$
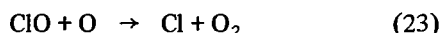
Hence, increasing the rate of reaction (22) will decrease the effectiveness of reaction (23). As we discussed in Part I, the emission of NO_X at SST flight altitudes can therefore be expected to lead to greater ozone increases (or smaller ozone losses) when substantial abundances of chlorine are present.

As noted before, our studies also included the simulation of water-vapor emission by aircraft flying in the stratosphere. Added water vapor is important because, through its oxidation by $O(^1D)$, it leads to enhanced HO_2 and OH abundances. Although increased HO_2 does have a tendency to increase ozone via reaction (1), such an effect is overwhelmed by direct destruction by the HO_X:

$$OH + O_3 \rightarrow HO_2 + O_2 \qquad (14)$$

$$\underline{HO_2 + O \rightarrow OH + O_2} \qquad (24)$$

Net: $\quad O + O_3 \rightarrow 2O_2$

$$HO_2 + O_3 \rightarrow OH + 2O_2 \qquad (2)$$

$$\underline{OH + O_3 \rightarrow HO_2 + O_2} \qquad (14)$$

Net: $\quad O_3 + O_3 \rightarrow 3O_2$

Thus, a large value for the rate coefficient for reaction (2) can be expected to lead to non-negligible ozone decreases (Turco et al., 1978). Because OH attacks the dominant stratospheric chlorine reservoir, HCl, to release the ozone-active Cl,

$$OH + HCl \rightarrow H_2O + Cl \qquad (25)$$
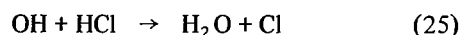
an increased stratospheric OH abundance can be expected to lead to *greater* ozone destruction by chlorine catalysis. In fact, we showed in Part I, that in a globally averaged sense and for the aircraft-emission indices considered, $HO_X - Cl_X$ coupling is expected to result in an ozone loss that nearly balances the ozone gain resulting from $NO_X - Cl_X$ coupling.

It is important to point out here that our model calculations did not take account of the thermal feedback effect: an ozone decrease will lead to lower upper stratospheric temperatures; because

of substantial positive activation energies of the reactions that govern the catalytic destruction of ozone, such temperature changes will tend to limit ozone loss. For the case of water-vapor injection, increased stratospheric water-vapor loading causes the cooling rates to increase because of increased emission of thermal infrared radiation by H_2O. Stratospheric temperatures are thus lowered, causing the catalytic reactions that destroy ozone to slow. Luther and Duewer (1977) carried out such computations for a case in which they assumed the water-vapor mixing ratio increase to be constant with altitude, and found that thermal feedback nearly canceled the destruction that would have occurred if such feedback were absent. Of course, as figures 17 through 21 suggest, the ΔH_2O can be expected to be much larger below 30 km than above. Since thermal feedback is probably significant only above 30 km, we expect it to be of less importance than was proposed by Luther and Duewer. However, Glatt and Widhopf (1979a) studied the temperature coupling using a two-dimensional steady-state model for a similar combined supersonic and subsonic fleet and found heating below the injection region, whereas cooling occurred in and above the injection region. Thus, temperature feedback may be important in the lower stratosphere.

To investigate the limiting situation in which ozone destruction due to water-vapor emission is absent, we simulated a variant of scenario (5) in which we omitted the ΔH_2O from the calculations. The results are shown in figure 27. As expected, the ozone gains below ~25 km are much greater than those shown in figure 25 (in which water-vapor emission is included), and the ozone losses above 25 km are less than indicated in figure 25 (cf. fig. 13(a) of Part I).

Figures 28 through 32 show the computed relative ozone column changes using the Ames model (scenarios (4) and (5)); we assumed steady-state conditions in an atmosphere containing a mixing ratio of 2.5 ppbv of ozone-active chlorine at an altitude of 60 km. For the scenario (4), shown in figure 28, we assumed operation of type A aircraft (20-km nominal cruising altitude) and the old value of the rate coefficient for reaction (2). Small ozone decreases due to NO_X and H_2O emission are predicted at all latitudes and seasons, but their magnitudes are somewhat larger in the Northern than in the Southern Hemisphere. We can qualitatively account for the results shown in figure 28 by referring to figure 20, which shows that in summer

and autumn ΔNO_y in the catalytically destructive region above 20 km is larger at high latitudes (Northern Hemisphere) than at lower latitudes. Because catalytic destruction dominates ozone production under the conditions of figure 28, we find that the latitudinal behavior of the change in ozone column shown is quite reasonable. To clarify our simulation of the interaction of added NO_x with ozone when the new large value of the rate coefficient for reaction (2) is used, the results for scenario (4) are presented in figure 29. The results shown in figure 29 are for the addition of NO_x only by a fleet of supersonic aircraft operating at a nominal cruise altitude of 20 km; there is a small increase in the ozone column at all latitudes. Furthermore, the ozone increase is nearly independent of season and is also nearly symmetric about the equator. Figure 30 shows the expected increase as a function of latitude when water-vapor emission only is included in the computations. Ozone depletion caused by water-vapor emission is a minimum near the equator ($\sim0.7\%$) rising to larger values at high latitudes ($\sim1.4\%$ above lat. $60°$ N, $\sim1.1\%$ below lat. $60°$ S. The difference between the corresponding abscissas of figures 29 and 30 gives (approximately) the predicted ozone change due to NO_x and water-vapor emissions, which is presented in figure 31. The corresponding ozone change for scenario (5) is presented in figure 32. The slight hemispherical asymmetry in ozone loss due to water-vapor emission is largely responsible for the rather strong asymmetry shown in figure 31. Both the structure in the percentage ozone loss and the latitude-dependence portrayed in figures 31 and 32 are quite uncertain; the total column loss, which is very close to zero, is the remnant of the near-cancellation of ozone loss at high altitude and gain at low altitude.

Comparison with Results of Earlier Studies

Many one-dimensional model studies using the older values of the rate coefficients for reactions (1) have been carried out (see Grobecker et al., 1974, and Part I for a review of the results). However, to our knowledge, the only one-dimensional model calculations using the new, larger values of the rate coefficients for *both* reactions (1) and (2) are those reported by Turco et al. (1978). It is instructive to compare the globally averaged ozone change for scenario (4) with and without water-vapor emission

(figs. 30, 31) to the corresponding one-dimensional model predictions (fig. 2 of Turco et al., 1978). The globally averaged equivalent NO_y injection rate is 0.58×10^9 kg NO_2 per year; the predicted ozone increase for the Chang-Dickinson eddy-diffusivity profile and no water-vapor emission is $\sim1.5\%$, which is very close to the value $\sim1.25\%$ given in figure 30. For the case that includes the effects of water-vapor emission, Turco et al. gave results only for the Wofsy-type eddy diffusivity, $\sim0.2\%$ of ozone gain which is to be compared with the 0.21% given in figure 28.

All of the earlier multidimensional studies (Alyea et al., 1975; Borucki et al., 1976; Widhopf et al., 1977; and Hidalgo and Crutzen, 1977) used the old (pre-1977) values of the rate coefficients of reactions (1) and (2); they also neglected the effects of water-vapor emissions, which was justifiable in the light of the pre-1977 knowledge of stratospheric chemistry. As a result, simulations of supersonic aircraft operations led to predictions of ozone loss, globally averaged relative reductions being roughly consistent with predictions from one-dimensional models. However, the last two papers reported results obtained for subsonic aircraft flying in the troposphere and in the low stratosphere (below ~14 km). The low altitudes of injection of NO_x from subsonic aircraft generally was shown to yield predictions of ozone increase because most of the NO_x was retained in the lower atmosphere where it generated ozone via the methane oxidation sequence and reaction (20); because little of the NO_x emitted at low altitude rises to the region of catalytic destruction of ozone, the net result is an ozone increase. However, Widhopf and Glatt (1979a) did include water-vapor modeling and found that with the use of the new rate coefficient for reaction (1) a predicted increase in both stratospheric and tropospheric ozone resulted. In all of the studies of NO_x emissions from supersonic aircraft in which it was assumed that most of the emission occurred in northern midlatitudes, much larger effects were predicted in the Northern than in the Southern Hemisphere. Furthermore, the predicted relative ozone decrease increased with increasing latitudes (e.g., see fig. 14 of Borucki et al., 1976, for a comparison of three model results). This latitudinal dependence was also obtained in the current studies in which the Ames model was used when the old value of the rate coefficient for reaction (2) was used and a nominal cruise altitude (type A aircraft) was assumed (see fig. 28), although the latitudinal gradient is not nearly so pronounced

as when the old value for the rate coefficient for reaction (1) was used. The reason for that characteristic of figure 28 is that catalytic destruction of ozone outweighs low-altitude ozone generation. As shown in figures 29 to 32, the latitudinal dependence of the ozone decrease is quite different when the new values of the rate coefficients for reactions (1) and (2) are used. The differences occur because the model then predicts that more ozone is generated at low altitudes by the NO_y addition and destroyed at high altitudes by the water-vapor addition. Ozone at lower altitudes is largely controlled by transport; hence, the greater the percentage of total ozone at lower altitudes, the greater the influence of meridional transport. Including the effect of washout-rainout on NO_x may reduce the effects seen in the Southern Hemisphere, since the lower altitude NO_y would then be taken out of the troposphere faster than it could be transported to the Southern Hemisphere.

Sensitivities and Uncertainties

Because of the large computer times required for two-dimensional model simulations, it is not practical to use them for sensitivity studies. However, a number of sensitivity tests using a one-dimensional model were reported in Part I (table 7); our estimates of sensitivity are expected to apply to our two-dimensional models (in a globally averaged sense) as well. We note here the sensitivity study carried out with the rate coefficient for reaction (2) (varying its value by a factor of 3); the actual increase of the rate coefficient value by a factor of ~4.5 as a consequence of its measurement by Zahniser and Howard (1978) leads to changes in predicted ozone perturbation that are qualitatively consistent with the ozone change *differences* between figures 28 and 31.

Table 8 of Part I summarizes most of the sources of uncertainty in our SST ozone perturbation estimates. However, it is necessary to qualify our discussion of transport uncertainty because we are dealing here with horizontal as well as vertical transport. In our earlier discussion of the distributions of trace species and their prediction, we showed that although the transport parameters of the Ames and Aerospace models are not inconsistent with observation, neither are they firmly supported by observation. In fact, the substantial differences between the transport models, indicated in section IV and in figures 17 through 21, show that they cannot both be accurate simulations of nature. These differences are mainly responsible for the differences in predicted ozone perturbations that were obtained from the two models: After 5 yr of simulated type A SST operations (and using the old value of the rate coefficient for reaction (2) the Ames model predicted small ozone decreases, and the Aerospace model predicted very small ozone increases. In assessing the significance of the uncertainty associated with transport, one should bear in mind the small magnitudes of ozone change that are involved and that they result from the near-cancellation effect of large values of catalytic destruction of ozone at high altitudes pitted against large values of ozone generation at low altitudes. Thus, small changes in the transport parameters can have large relative effects on predicted ozone gain or loss.

VI. CONCLUDING REMARKS

From the foregoing discussion we see that not only have supersonic transport assessments changed since the Climatic Impact Assessment Program, but they have even undergone modifications since the publication of Part I of the present work (Poppoff et al., 1978). Although figure 16 in Part I pertains to the history of one-dimensional model predictions, it is appropriate to update the figure by remarking that the estimate of 0.2 to 0.3% ozone gain opposite the "no H_2O" should be increased. With the new, larger rate coefficient for reaction (2) the estimates of ozone gain should be increased to 1.2 to 2%. If the details of the stratospheric chemistry outlined in this report are correct, we predict substantial ozone gains from NO_x emissions in the stratosphere. This prediction differs radically from those reported before 1977, all of which suggested that substantial ozone losses would be caused by the operation of supersonic aircraft, but ozone increases would occur when subsonic emissions were considered. Conversely, water-vapor emission, which was once believed to have negligible effect on stratospheric ozone, may cause the destruction of a substantial amount of ozone with no NO_x emission; perhaps an ozone loss of as much as 1% could result from a fleet of 250 SST's, although the true value would probably be less, depending on the magnitude of the thermal feedback effect. A combination of NO_x and

H_2O emission results in a small net ozone increase. Finally, and most important in the current context, the predicted latitudinal variation of the ozone changes using the Ames model has undergone marked modification. Determination of the meridional variation of ozone change is important because the amount of solar UBV that penetrates the ozone shield is dependent on the local optical depth of the ozone on the slant path to the Sun. We no longer predict the largest effect in the Northern Hemisphere. For aircraft operating at a nominal cruise altitude of 20 km, we find only a variation between equator and pole of ~50% if water vapor is not effective in destroying ozone (fig. 29), even though most of the NO_x is injected at latitudes between 30° and 60° N. The small interhemispherical asymmetries shown in figure 29 are due to differences in transport. If water vapor is effective, we find that ozone gains may be smaller in the Northern Hemisphere than in the Southern Hemisphere. However, if the operating altitude is lowered to 17.5 km, the meridional variation is very small. Of course, for an SST fleet of about 250 aircraft, the ozone gain due to existing fleets of subsonic aircraft would far outweigh the supersonic aircraft effects (cf. fig. 24, 25). Inclusion of washout-rainout effects may also alter the results of scenarios (4) and (5).

Despite the recent advances in stratospheric aeronomy discussed in this report, some significant uncertainties remain. Because of the predictions of HNO_3/NO_2 ratios that are apparently too large (compared with measurements — see fig. 11), we may have overestimated the low-altitude ozone increase due to reaction (1); it is thus conceivable that aircraft operations in the stratosphere could still lead to small ozone losses. The importance of thermal feedback from the water-vapor injection into the ozone chemistry is very uncertain. This thermal coupling, which is due to infrared cooling by the water vapor deposited in the stratosphere, has the effect of slowing some of the reactions that destroy ozone. As we have emphasized several times in our discussion, large uncertainties in the transport rates of trace substances in the stratosphere cause considerable uncertainty in computed ozone change because of the cancellation effect of low-altitude ozone production and high-altitude ozone destruction. Finally, the effects of ozone redistribution (increase below ~25 km and decrease above) especially on stratospheric thermal structure, have never been assessed. All of these uncertainties apply not only to the globally averaged ozone change, but to meridional variations as well.

Ames Research Center
National Aeronautics and Space Administration
Moffett Field, California 94035,
August 22, 1980

REFERENCES

Ackerman, M.: NO, NO_2 and HNO_3 Below 35 km in the Atmosphere. J. Atmos. Sci., vol. 32, no. 9, 1975, pp. 1649-1657.

Ackerman, M.; Fontanella, J. C.; Frimout, D.; Girard, A.; and Louisnard, N.: Simultaneous Measurements of NO and NO_2 in the Stratosphere. Planet. Space Sci., vol. 23, no. 4, 1975, pp. 651-660.

Ackerman, M.; Frimout, D.; and Muller, C.: Stratospheric CH_4, HCl and ClO and the Chlorine-Ozone Cycle. Nature, vol. 269, no. 5625, 1977, pp. 226-227.

Alyea, F. N.; Cunnold, D. M.; and Prinn, R. G.: Stratospheric Ozone Destruction by Aircraft-Induced Nitrogen Oxides. Science, vol. 188, no. 4184, 1975, pp. 117-121.

Anderson, J. G.: The Absolute Concentration of $OH(X^2\Pi)$ in the Earth's Stratosphere. Geophys. Res. Lett., vol. 3, no. 3, 1976, pp. 165-168.

Baber, H. T.; and Swanson, E. E.: Advanced Supersonic Technology Concept AST-100 Characteristics Developed in a Baseline-Update Study. NASA TM X-72,815, 1976.

Bauer, E.; Oliver, R. C.; and Wasylkiwskyj, W.: On the Use of Zirconium 95 Data from Chinese Atmospheric Thermonuclear Explosions to Study Stratospheric Transport in a One-Dimensional Parameterization. J. Geophys. Res., vol. 83, no. C8, 1978, pp. 4019-4028.

Belmont, A. D.; Dartt, D. G.; and Nastrom, G. D.: Variations of Stratospheric Zonal Winds, 20-65 km, 1961-1971. J. Appl. Meterol., vol. 14, no. 4, 1975, pp. 585-594.

Borucki, W. J.; Whitten, R. C.; Watson, V. R.; Woodward, H. T.; Riegel, C. A.; Capone, L. A.; and Becker, T.: Model Predictions of Latitude-Dependent Ozone Depletion due to Supersonic Transport Operations. AIAA J., vol. 14, no. 12, 1976, pp. 1738-1745.

Burrows, J. P.; Harris, G. W.; and Thrush, B. A.: Rates of Reaction of HO_2 with HO and O Studied by Laser Magnetic Resonance. Nature, vol. 267, no. 5608, 1977, pp. 223-234.

Bush, Y. A.; Schmeltekopf, A. L.; Fehsenfeld, F. C.; Albritton, D. L.; McAfee, J. R.; Goldan, P. D.; and Ferguson, E. E.: Stratospheric Measurements of Methane at Several Latitudes. Geophys. Res. Lett., vol. 5, no. 12, 1978, pp. 1027-1029.

Chang, J. S.: Uncertainties in the Validation of Parameterized Transport in 1-D Models of the Stratosphere. Proceedings of the 4th Conference of the Climatic Impact Assessment Program, U.S. Department of Transportation, DOT-TSC-OST-75-38, UCRL-77419, NTIS, Springfield, Va., 4-7 Feb. 1975, pp. 175-182.

Cogley, A. C.; and Borucki, W. J.: Exponential Approximation for Daily Average Solar Heating or Photolysis. J. Atmos. Sci., vol. 33, no. 7, 1976, pp. 1347-1356.

Cox, R. A.: Current Status of Some Kinetics Data Required for Modeling Tropospheric Photochemistry. IAGA/IAMAP Joint Assembly, Seattle, Wash., 22 Aug.-3 Sept. 1977.

Crutzen, P. J.: The Influence of Nitrogen Oxides on the Atmospheric Ozone Content. Quart. J. Roy. Meteorol. Soc., vol. 96, no. 48, 1970. pp. 320-325.

Crutzen, P. J.; and Howard, C. J.: The Effect of HO_2 + NO Reaction-Rate Constant on One-Dimensional Model Calculations of Stratospheric Ozone Perturbations. PAGEOPH, vol. 116, 1978, pp. 497-510.

Cunnold, D. M.; Alyea, F. N.; Phillips, N. A.; and Prinn, R. G.: A Three-Dimensional Dynamical-Chemical Model of Atmospheric Ozone. J. Atmos. Sci., vol. 32, no. 1, 1975, pp. 170-194.

Cunnold, D. M.; Alyea, F. N.; and Prinn, R. G.: Relative Effects on Atmospheric Ozone of Latitude and Altitude of Supersonic Flight. AIAA J., vol. 15, no. 3, 1977, pp. 337-345.

Dobson, G. M. B.; Brewer, A. W.; and Cwilong, B. M.: Meteorology of the Lower Stratosphere. Proc. Roy. Soc., London, A, vol. 185, no. 1001, 1946, pp. 144-175.

Duewer, W. H.; Wuebbles, D. J.; Ellsaesser, H. W.; and Chang, J. S.: NO_X Catalytic Ozone Destruction: Sensitivity to Rate Coefficients. J. Geophys. Res., vol. 82, no. 6, 1977, pp. 935-942.

Ehhalt, D. H.: Sampling of Stratospheric Trace Constituents. Can. J. Chem., vol. 52, no. 8, 1974, pp. 1510-1518.

Ehhalt, D. H.: In Situ Measurements of Stratospheric Trace Constituents. Rev. Geophys. Space Phys., vol. 16, no. 2, 1978, pp. 217-224.

Evans, W. F. J.; Kerr, J. B.; Wardle, D. I.; McConnell, J. C.; Ridley, B. A.; and Schiff, H. I.: Intercomparison of NO, NO_2, and HNO_3 Measurements with Photochemical Theory. Atmosphere, vol. 14, no. 3, 1976, pp. 189-198.

Evans, W. F. J.; McElroy, C. T.; Kerr, J. B.; McConnell, J. C.; and Ridley, B. A.: Simulation of Stratoprobe Nitrogen Constituent Measurements with Current Stratospheric Photochemistry. EOS Trans. Am. Geophys. Union, vol. 59, no. 12, 1978, p. 1078.

Fabian, P.; Borchers, R.; Weiler, K. H.; Schmidt, U.; Volz, A.; Ehhalt, D. H.; Seiler, W.; and Müller, F.: Simultaneously Measured Vertical Profiles of H_2, CH_4, CO, N_2O, $CFCl_2$, and CF_2Cl_2 at the Mid-Latitude Stratosphere and Troposphere. J. Geophys. Res., vol. 84, no. C6, 1978, pp. 3149-3154.

Fontanella, J. C.; Girard, A.; Gramont, L.; and Louisnard, N.: Vertical Distribution of NO, NO_2, and HNO_3 as Derived from Stratospheric Absorption Infrared Spectra. Appl. Opt., vol. 14, no. 4, 1975, pp. 825-839.

Glatt, L.; and Widhopf, G. F.: Aircraft HO_X and NO_X Emission Effects on Stratospheric Ozone and Temperature. NASA CR-158945, 1978.

Grobecker, A. J.; Coroniti, S. C.; and Carron, R. H.: Report of Findings: The Effects of Stratospheric Pollution by Aircraft. U.S. Department of Transportation Report DOT-TSC-75-50, NTIS, Springfield, Va., Dec. 1974.

Harries, J. E.: The Distribution of Water Vapor in the Stratosphere. Rev. Geophys. Space Phys., vol. 14, no. 4, 1976, pp. 565-575.

Harries, J. E.: Ratio of HNO_3 to NO_2 Concentrations in the Daytime Stratosphere. Nature, vol. 274, no. 5668, 1978, p. 235.

Harries, J. E.; Moss, D. G.; Swann, N. R. W.; Neill, G. F.; and Gildwarg, P.: Simultaneous Measurements of H_2O, NO_2 and HNO_3 in the Daytime Stratosphere from 15 to 35 km. Nature, vol. 259, no. 5541, 1976, pp. 300-302.

Harwood, R. S.; and Pyle, J. A.: Studies of the Ozone Budget Using a Zonal Mean Circulation Model and Linearized Photochemistry. Quart. J. Roy. Meteorol. Soc., vol. 103, no. 436, 1977, pp. 319-343.

Heath, D. F.; Mateer, C. L.; and Krueger, A. J.: The Nimbus 4 Backscatter Ultraviolet (BUV) Atmospheric Ozone Experiment — Two Years Operation. PAGEOPH, vol. 106-108, no. V-VII, 1973, pp. 1238-1263.

Hidalgo, H.; and Crutzen, P. J.: The Tropospheric and Stratospheric Composition Perturbed by NO_X Emissions of High-Altitude Aircraft. J. Geophys. Res., vol. 82, no. 37, 1977, pp. 5833-5866.

Howard, C. J.; and Evenson, K. M.: Kinetics of the Reaction of HO_2 with NO. Geophys. Res. Lett., vol. 4, no. 10, 1977, pp. 437-440.

Hudson, R. D., ed.: Chlorofluoromethanes and the Stratosphere. NASA RP-1010, 1977.

Hunten, D. M.: Residence Times of Aerosols and Gases in the Stratosphere. Geophys. Res. Lett., vol. 2, no. 1, 1975, pp. 26-28.

Johnston, H. S.: Reduction of Stratospheric Ozone by Nitrogen Oxide Catalysts from Supersonic Transport Exhaust. Science, vol. 173, no. 3996, 1971, pp. 517-522.

Johnston, H. S.; Kattenhorn, D.; and Whitten, G.: Use of Excess Carbon 14 Data to Calibrate Models of Stratospheric Ozone Depletion by Supersonic Transports. J. Geophys. Res., vol. 81, no. 3, 1976, pp. 368-380.

Junge, C. E.: Air Chemistry and Radioactivity. Academic Press, New York and London, 1963, p. 10.

Kramer, R. F.; and Widhopf, G. F.: Evaluation of Daylight or Diurnally Averaged Photolytic Rate Coefficients in Atmospheric Photochemical Models. J. Atmos. Sci., vol. 35, no. 9, 1978, pp. 1726-1734.

Lazrus, A. L.; and Gandrud, B. W.: Distribution of Stratospheric Nitric Acid Vapor. J. Atmos. Sci., vol. 31, no. 4, 1974, pp. 1102-1108.

Loewenstein, M.; Starr, W. L.; and Murcray, D. G.: Stratospheric NO and HNO_3 Observations in the Northern Hemisphere for Three Seasons. Geophys. Res. Lett., vol. 5, no. 6, 1978, pp. 531-534.

Louis, J. F.; London, J.; and Danielsen, E.: The Interaction of Radiation and the Meridional Circulation of the Stratosphere. IAMAP First Special Assembly, Melbourne, Australia, Jan. 1974.

Luther, F. M.: Monthly Mean Values of Eddy Diffusion Coefficients in the Lower Stratosphere. AIAA Paper 73-498, June 1973.

Luther, F. M.; and Duewer, W. H.: Effect of Changes in Stratospheric Water Vapor and Abundance on Predicted Ozone Reductions. IAGA/IAMAP Joint Assembly, Seattle, Wash., Aug. 22-Sept. 3, 1977.

Mahlman, J. D.: Some Fundamental Limitations of Simplified-Transport Models as Implied by Results from a Three-Dimensional General Circulation/Tracer Model. Proceedings of the 4th Conference on the Climatic Impact Assessment Program, U.S. Department of Transportation, DOT-TSC-OST-75-38, NTIS, Springfield, Va., Feb. 1975, pp. 132-146.

Manabe, S.; and Wetherald, R. T.: Thermal Equilibrium of the Atmosphere with a Given Distribution of Relative Humidity. J. Atmos. Sci., vol. 24, no. 3, 1967, pp. 241-259.

Murcray, D. G.; Barker, D. B.; Brooks, J. N.; Goldman, A.; and Williams, W. J.: Seasonal and Latitudinal Variation of the Stratospheric Concentration of HNO_3. Geophys. Res. Lett., vol. 2, no. 6, 1975, pp. 223-226.

National Academy of Sciences: Environmental Impact of Stratospheric Flight: Biological and Climatic Effects of Aircraft Emissions in the Stratosphere. Washington, D.C., 1975.

Newell, R. E.: Transfer through the Tropopause and Within the Stratosphere. Quart. J. Roy. Meteorol. Soc., vol. 89, no. 380, 1963, pp. 167-204.

Newell, R. E.; Wallace, J. M.; and Mahoney, J. R.: The General Circulation of the Atmosphere and Its Effects on the Movement of Trace Substances. Part 2. Tellus, vol. 18, no. 2/3, 1966, pp. 363-380.

Oliver, R. C.; Bauer, E.; Hidalgo, H.; Gardner, K. A.; and Wasylkiwskyj, W.: Aircraft Emissions: Potential Effects on Ozone and Climate — A Review and Progress Report. Part 1. U.S. Department of Transportation, FAA EQ 77-3, DOT-FA76 WA-3757, NTIS, Springfield, Va., Mar. 1977.

Poppoff, I. G.; Whitten, R. C.; Turco, R. P.; and Capone, L. A.: An Assessment of the Effect of Supersonic Aircraft Operations on the Stratospheric Ozone Content. NASA RP-1026, 1978.

Reed, R. J.; and German, K. E.: A Contribution to the Problem of Stratospheric Diffusion by Large-Scale Mixing. Mon. Weather Rev., vol. 93, no. 5, 1965, pp. 313-321.

Schiff, H. I.; Ridley, B. A.; McConnell, J. C.; and Evans, W. P. J.: Some Considerations Regarding the Possible Pressure Dependence of the $NO + HO_2$ and $OH + HO_2$ Reaction Rates. EOS, Trans. Am. Geophys. Union, vol. 59, no. 12, 1978, p. 1075.

Schmeltekopf, A. L.; Albritton, D. L.; Crutzen, P. J.; Goldman, P. D.; Harrop, W. J.; Henderson, W. R.; McAfee, J. R.; McFarland, M.; Schiff, H. I.; Thompson, T. L.; Hofmann, D. J.; and Kjome, N. T.: Stratospheric Nitrous Oxide Altitude Profiles at Various Latitudes. J. Atmos. Sci., vol. 34, no. 5, 1977, pp. 729-736.

Seiler, W.: The Cycle of Atmospheric CO. Tellus, vol. 26, no. , 1974, pp. 110-135.

Telegadas, K.: The Seasonal Stratospheric Distribution and Inventories of Excess Carbon-14 from March 1955 to July 1969. U.S. Atomic Energy Commission Health and Safety Laboratory, Report 243, NTIS, Springfield, Va., 1971, pp. 3-86.

Turco, R. P.: Photodissociation Rates in the Atmosphere Below 100 km. Geophys. Surveys, vol. 2, no. 2, 1975, pp. 153-192.

Turco, R. P.; and Whitten, R. C.: Chlorofluoromethanes in the Stratosphere and Some Possible Consequences for Ozone. Atmos. Env., vol. 9, no. 12, 1975, pp. 1045-1061.

Turco, R. P.; and Whitten, R. C.: The NASA-Ames Research Center One- and Two-Dimensional Stratospheric Models. I. The One-Dimensional Model. NASA TP-1002, 1977.

Turco, R. P.; and Whitten, R. C.: A Note on the Diurnal Averaging of Aeronomic Models. J. Atmos. Terr. Phys., vol. 40, no. 1, 1978, pp. 13-20.

Turco, R. P.; Whitten, R. C.; Poppoff, I. G.; and Capone, L. A.: SST's, Nitrogen Fertilizer, and Stratospheric Ozone: A New Appraisal. Nature, vol. 276, no. 5690, 1978, pp. 805-807.

Vedder, J. F.; Tyson, B. J.; Brewer, R. B.; Boitnott, C. A.; and Inn, E. C. Y.: Lower Stratosphere Measurements of Variation with Latitude of CF_2Cl_2, $CFCl_3$, CCl_4, and N_2O Profiles in the Northern Hemisphere. Geophys. Res. Lett., vol. 5, no. 1, 1978, pp. 33-36.

Vupputuri, R. K. R.: Seasonal and Latitudinal Variations of N_2O and NO_X in the Stratosphere. J. Geophys. Res., vol. 80, no. 9, 1975, pp. 1125-1132.

Whitten, R. C.; and Poppoff, I. G.: Fundamentals of Aeronomy. John Wiley and Sons, New York and London, 1971, pp. 125-128.

Whitten, R. C.; Borucki, W. J.; Watson, V. R.; Shimazaki, T.; Woodward, H. T.; Riegel, C. A.; Capone, L. A.; and Becker, T.: The NASA Ames Research Center One- and Two-Dimensional Stratospheric Models. II. The Two-Dimensional Model. NASA TP-1003, 1977.

Whitten, R. C.; Borucki, W. J.; Capone, L. A.; and Turco, R. P.: The Effect of the Reaction $HO_2 + O_3 \rightarrow OH + 2O_2$ on Stratospheric Ozone. Nature, vol. 275, no. 5680, 1978, pp. 523-524.

Widhopf, G. F.: A Two-Dimensional Photochemical Model of the Stratosphere Including Initial Results of Inert Tracer Studies. Proceedings of the 4th Conference on the Climatic Impact Assessment Program, T. M. Hard and A. J. Broderick, eds., U.S. Department of Transportation, DOT-TSC-OST-75-38, NTIS, Springfield, Va., Feb. 1975, pp. 316-331.

Widhopf, G. F.; and Taylor, T. D.: Numerical Experiments on Stratospheric Meridional Ozone Distributions Using a Parameterized Two-Dimensional Model. Proceedings of the 3rd Conference of the Climatic Impact Assessment Program, U.S. Department of Transportation, DOT-TSC-OST-75-38, NTIS, Springfield, Va., 26 Feb.-1 Mar. 1974, pp. 376-389.

Widhopf, G. F.; and Victoria, K. J.: On the Solution of the Unsteady Navier-Stokes Equations Including Multicomponent Finite Rate Chemistry. Computers and Fluids, vol. 1, no. 2, 1973, pp. 159-184.

Widhopf, G. F.; and Glatt, L.: Two-Dimensional Description of the Natural Atmosphere Including Active Water Vapor Modeling and Potential Perturbations due to NO_x and HO_x Aircraft Emissions. Aerospace Corp., Los Angeles, Calif., Report ATR-79(4858)-IND, U.S. Department of Transportation Report FAA-AEE-79-07, 15 Apr. 1979a.

Widhopf, G. F.; and Glatt, L.: Numerical Modeling of Atmospheric Pollution. Proceedings of the 6th International Conference on Numerical Methods in Fluid Dynamics, Tbilsii, USSR, 20-25 June 1978, Springer-Verlag, New York, Lecture Notes in Physics, vol. 90, 1979b.

Widhopf, G. F.; Glatt, L.; and Kramer, R. F.: Potential Ozone Column Increase Resulting from Subsonic and Supersonic Aircraft NO_x Emissions. AIAA J., vol. 15, no. 9, 1977, pp. 1322-1330.

Wilcox, R. W.; Nastrom, G. D.; and Belmont, A. D.: Periodic Variations of Total Ozone and of its Vertical Distribution. J. Appl. Meteorol., vol. 16, no. 3, 1977, pp. 290-298.

Zahniser, M. S.; and Howard, C. J.: Direct Measurement of the Temperature Dependence of the Rate Constant for the Reaction $HO_2 + O_3 \rightarrow OH + 2O_2$. Fourth Biennial Rocky Mountain Regional Meeting of the American Chemical Society, Boulder, Colo., 5-7 June 1978.

TABLE 1.— 1990 WORLDWIDE AIRCRAFT NO$_x$ EMISSIONS,
HIGH ESTIMATES, kg/yr[a]

Latitude	NO$_x$ emissions, kg/yr							
	6-8 km	8-9 km	9-10 km	10-11 km	11-12 km	12-13 km	13-14 km	14-15 km
N 60+	3.35E6	3.03E6	1.43E7	1.31E7	1.46E7	1.31E6	9.99E5	2.03E5
50-60	2.15E7	2.59E7	9.44E7	1.06E8	9.09E7	8.26E6	3.72E6	1.06E6
40-50	7.60E7	8.70E7	1.79E8	2.79E8	1.62E8	2.48E7	4.59E6	1.04E6
30-40	7.74E7	9.20E7	1.67E8	3.09E8	1.72E8	2.97E7	3.11E6	8.70E5
20-30	2.61E7	2.83E7	6.74E7	1.02E8	6.92E7	8.73E6	1.55E6	6.00E5
10-20	1.11E7	1.18E7	2.65E7	4.28E7	3.99E7	3.67E6	4.74E5	7.70E4
0-10	4.80E6	5.14E6	1.50E7	1.82E7	1.36E7	1.26E6	1.73E5	0
10-0	3.31E6	3.77E6	1.22E7	1.38E7	1.09E7	8.65E5	1.38E5	0
20-10	2.74E6	3.21E6	1.14E7	1.52E7	1.15E7	1.11E6	3.15E5	6.60E4
30-20	3.67E6	4.01E6	9.47E6	1.37E7	8.66E6	9.31E5	5.10E4	0
40-30	4.01E6	4.63E6	6.62E6	1.18E7	6.14E6	1.21E6	8.64E4	2.58E4
50-40	2.36E5	3.05E5	3.19E5	8.28E5	4.46E5	9.29E4	1.5 E1	0
60-50	4.77E4	3.79E4	2.99E4	2.52E4	1.04E4	1.45E3	0.97	0
S 60+	0	0	0	0	0	0	0	0
Total	2.343E8	2.691E8	6.036E8	9.255E8	5.999E8	8.197E7	1.521E7	3.94E6

[a]Oliver et al. (1977)
[b]2.343E8 ≡ 2.343 × 10^8

TABLE 2.– COMPARISON OF THE AMES AND AEROSPACE TWO-DIMENSIONAL MODELS

Characteristic	Ames model	Aerospace model
Vertical dimensions	0 to 60 km	0 to 50 km
Horizontal dimensions	80° S to 80° N	90° S to 90° N
Vertical resolution	2.5 km	1 km from 0 to 35 km, 2.5 km from 35 to 50 km
Horizontal resolution	5°	10°
Transport, advective	Parameterized	Parameterized
Transport, eddy	Parameterized	Parameterized
Transport, temporal changes	Seasonal	Monthly
Upper boundary conditions	Diffusive equilibrium	Photochemical equilibrium $(O, O(^1D), O_3, OH, HO_2, N, H)$ flux condition (other species)
Lower boundary conditions	Chemical equilibrium $(O, OH, HO_2,$ and other reactive species)	Chemical equilibrium $(O, OH, HO_2,$ and other reactive species)
Includes rainout-washout	No	Yes (for $NO_X, H_2O, H_2O_2, HNO_3$)
Includes methane oxidation sequences	Yes	Yes
Includes chlorine	Yes	No
Transports water vapor	Yes	Yes
Reaction rates	See tables 3-7	See tables 3-7
Diurnal averaging		
Photo rates	Yes	Yes
Rate coefficients	Yes	Yes
Temperature feedback	No	No
Time step	1 day	2 day

TABLE 3.– REACTION-RATE CONSTANTS FOR THE O-N-H SYSTEM

Reaction	Rate constant[a]	Note	Reaction	Rate constant[a]	Note
$O + O_2 + M \rightarrow O_3 + M$	$1.1 \times 10^{-34} e^{520/T}$ $1.07 \times 10^{-34} e^{510/T}$	b, c	$N + O_3 \rightarrow NO + O_2$	$2.0 \times 10^{-11} e^{-1070/T}$ $5.0 \times 10^{-12} e^{-650/T}$	c
$O + O + M \rightarrow O_2 + M$	$3.0 \times 10^{-33} (300/T)^3$	b	$N + NO \rightarrow O + N_2$	$8.2 \times 10^{-11} e^{-410/T}$	
$O + O_3 \rightarrow O_2 + O_2(^1\Sigma_g^+)$	$1.9 \times 10^{-11} e^{-2330/T}$	b	$N + O_2 \rightarrow NO + O$	$5.5 \times 10^{-12} e^{-3220/T}$	
$O + OH \rightarrow H + O_2$	4.2×10^{-11}		$N + NO_2 \rightarrow N_2O + O$	$2.0 \times 10^{-11} e^{-800/T}$	d
$O_3 + H \rightarrow OH + O_2$	$1.2 \times 10^{-10} e^{-560/T}$				
			$NO_2 + O_3 \rightarrow NO_3 + O_2$	$1.2 \times 10^{-13} e^{-2450/T}$	
$O + HO_2 \rightarrow OH + O_2$	3.5×10^{-11}		$NO_2 + O + M \rightarrow NO_3 + M$	1.0×10^{-31}	b, e
$O_3 + OH \rightarrow HO_2 + O_2$	$1.5 \times 10^{-12} e^{-1000/T}$		$NO + NO_3 \rightarrow NO_2 + NO_2$	8.7×10^{-12}	b
$H + O_2 + M \rightarrow HO_2 + M$	$2.1 \times 10^{-32} e^{290/T}$		$NO_2 + NO_3 + M \rightarrow N_2O_5 + M$		b, e
$NO + O_3 \rightarrow NO_2 + O_2$	$2.1 \times 10^{-12} e^{-1450/T}$		$N_2O_5 + M \rightarrow NO_2 + NO_3 + M$		b, e
$O + NO_2 \rightarrow NO + O_2$	9.1×10^{-12}				
			$NO + HO_2 \rightarrow NO_2 + OH$	8.0×10^{-12}	
$NO + O + M \rightarrow NO_2 + M$	$1.6 \times 10^{-32} e^{584/T}$		$NO_2 + OH + M \rightarrow HNO_3 + M$		f
$OH + OH \rightarrow H_2O + O$	$1.0 \times 10^{-11} e^{-550/T}$		$HNO_3 + O \rightarrow OH + NO_3$	1.0×10^{-14}	b, g
$OH + HO_2 \rightarrow H_2O + O_2$	3.0×10^{-11}		$HNO_3 + OH \rightarrow H_2O + NO_3$	8.0×10^{-14}	
$HO_2 + HO_2 \rightarrow H_2O_2 + O_2$	2.5×10^{-12}				
$H_2O_2 + OH \rightarrow H_2O + HO_2$	$1.0 \times 10^{-11} e^{-750/T}$		$NO + OH + M \rightarrow HNO_2 + M$	$1.8 \times 10^{-32} e^{1135/T}$	b, g
$H_2O_2 + O \rightarrow OH + HO_2$	$2.8 \times 10^{-12} e^{-2125/T}$ $2.75 \times 10^{-12} e^{-2125/T}$	c	$HNO_2 + O \rightarrow OH + NO_2$	1.0×10^{-14}	b, g
			$HNO_2 + OH \rightarrow H_2O + NO_2$	8.0×10^{-14}	
$O_3 + HO_2 \rightarrow OH + O_2 + O_2$	$7.3 \times 10^{-14} e^{-1275/T}$				
$OH + OH + M \rightarrow H_2O_2 + M$	$1.26 \times 10^{-32} e^{900/T}$ $1.3 \times 10^{-32} e^{900/T}$	c			

[a]Rate constants are in molecule·cm·sec units; unless otherwise noted, the rate constants are taken from Hudson (1977). [b]For detailed data reference see the reaction tabulation in Turco and Whitten (1975). [c]The upper expression was used by Ames investigators, the lower one by Aerospace Corporation workers. [d]This reaction was included in the Aerospace model only. [e]For the complete pressure-dependent rate expression, see Turco and Whitten (1975). [f]The expression adopted for this rate constant is given in Hudson (1977). [g]These reactions were included in the Ames model only.

TABLE 4.– REACTION-RATE CONSTANTS FOR
EXCITED OXYGEN SPECIES

Reaction	Rate constant[a]	Note
$O(^1D) + N_2 \rightarrow O + N_2$	$2.0 \times 10^{-11} e^{107/T}$	b
$O(^1D) + O_2 \rightarrow O + O_2(^1\Sigma_g^+)$	$2.9 \times 10^{-11} e^{67/T}$	b
$O(^1D) + H_2O \rightarrow OH + OH$	2.3×10^{-10}	
$O(^1D) + N_2O \rightarrow NO + NO$	5.5×10^{-11}	
$O(^1D) + N_2O \rightarrow N_2 + O_2$	5.5×10^{-11}	
$O(^1D) + H_2 \rightarrow OH + H$	9.9×10^{-11}	
$O(^1D) + N_2 + M \rightarrow N_2O + M$	3.5×10^{-37}	

[a] Rate constants are in molecule·cm·sec units. Unless otherwise noted, the rate constants are taken from Hudson (1977).

[b] These reactions were included in the Ames model only.

TABLE 5.— REACTION-RATE CONSTANTS FOR
CARBON COMPOUNDS

Reaction	Rate constant[a]	Note
$CO + OH \rightarrow CO_2 + H$	1.4×10^{-13}	b
$CH_4 + OH \rightarrow CH_3 + H_2O$	$2.4 \times 10^{-12} e^{-1720/T}$	
	$2.36 \times 10^{-12} e^{-1710/T}$	
$CH_4 + O \rightarrow CH_3 + OH$	$2.8 \times 10^{-11} e^{-4350/T}$	c
	$3.5 \times 10^{-11} e^{-4550/T}$	
$CH_4 + O(^1D) \rightarrow CH_3 + OH$	1.3×10^{-10}	
$CH_4 + O(^1D) \rightarrow CH_2O + H_2$	1.4×10^{-11}	b
$CH_3 + O_2 + M \rightarrow CH_3O_2 + M$		d, e
$CH_3 + O \rightarrow CH_2O + H$	1.2×10^{-10}	d, e
$CH_2O + O \rightarrow CHO + OH$	$2.0 \times 10^{-11} e^{-1450/T}$	
$CH_2O + OH \rightarrow CHO + H_2O$	$3.0 \times 10^{-11} e^{-250/T}$	
	1.4×10^{-11}	
$CHO + O_2 \rightarrow CO + HO_2$	6.0×10^{-12}	
$CHO + O \rightarrow CO + OH$	1.0×10^{-10}	d, e
$CHO + O \rightarrow CO_2 + H$	7.3×10^{-11}	d, e
$CH_3O_2 + NO \rightarrow CH_3O + NO_2$	2.0×10^{-12}	b, f
	1.5×10^{-12}	
$CH_3O_2 + CH_3O_2 \rightarrow 2CH_3O + O_2$	2.0×10^{-15}	d, e
$CH_3O + O_2 \rightarrow CH_2O + HO_2$	$1.6 \times 10^{-13} e^{-3300/T}$	
$CH_3O_2 + HO_2 \rightarrow CH_4O_2 + O_2$	2.5×10^{-12}	d
$CH_4O_2 + OH \rightarrow CH_3O_2 + H_2O$	$1.0 \times 10^{-11} e^{-750/T}$	d, e

[a]Rate constants are in molecule·cm·sec units; unless otherwise noted, the rate constants are taken from Hudson (1977). [b]The upper expression was used by Ames investigators, the lower one by Aerospace Corporation workers. [c]These reactions were included in the Aerospace model only. [d]For detailed data references, see the reaction tabulation in Turco and Whitten (1975). [e]These reactions were used in the Ames model only. [f]Based on a lower limit measurement of Cox (1977).

TABLE 6.— PHOTODISSOCIATION RATES FOR O-N-H-C CONSTITUENTS

Photodissociation process[a]	Dissociation rate,[b] $\sec^{-1}$
$O_2 + h\nu \xrightarrow{\lambda < 176 \text{ nm}} O(^1D) + O$	6.6×10^{-7}
$O_2 + h\nu \xrightarrow{176 \leq \lambda < 242 \text{ nm}} O + O$	5.9×10^{-8}
$O_3 + h\nu \xrightarrow{\lambda < 267 \text{ nm}} O_2(^1\Sigma_g^+) + O(^1D)$	2.1×10^{-4}
$O_3 + h\nu \xrightarrow{\lambda < 310 \text{ nm}} O_2(^1\Delta_g) + O(^1D)$	3.9×10^{-3}
$O_3 + h\nu \xrightarrow{310 < \lambda < 350 \text{ nm}} O_2(^1\Delta_g) + O$	8.1×10^{-4}
$O_3 + h\nu \xrightarrow{450 < \lambda < 750 \text{ nm}} O_2 + O$	2.3×10^{-4}
$NO + h\nu \rightarrow N + O$	6.1×10^{-6}
$NO_2 + h\nu \rightarrow NO + O$	6.4×10^{-3}
$NO_3 + h\nu \rightarrow NO + O$	2.0×10^{-2}
$\rightarrow NO_2 + O$	5.0×10^{-2}
$N_2O + h\nu \rightarrow N_2 + O(^1D)$	9.8×10^{-7}
$N_2O_5 + h\nu \rightarrow NO_2 + NO_2 + O$	3.1×10^{-4}
$HNO_2 + h\nu \rightarrow OH + NO$	4.8×10^{-4}
$HNO_3 + h\nu \rightarrow OH + NO_2$	9.0×10^{-5}
$H_2O + h\nu \rightarrow OH + H$	4.4×10^{-6}
$H_2O_2 + h\nu \rightarrow OH + OH$	7.1×10^{-5}
$HO_2 + h\nu \rightarrow OH + O$	4.4×10^{-4}
$CO_2 + h\nu \xrightarrow{167 \leq \lambda \leq 216 \text{ nm}} CO + O$	6.4×10^{-9}, (c)
$CH_2O + h\nu \rightarrow CHO + H$	6.6×10^{-5}
$CH_2O + h\nu \rightarrow CO + H_2$	8.9×10^{-5}
$CH_4O_2 + h\nu \rightarrow CH_3O + OH$	7.1×10^{-5}

[a] For detailed data references and discussion, see Turco (1975) and Turco and Whitten (1975).

[b] Twenty-four hour average photodissociation rates at 120 km altitude are given.

[c] This process was included in the Aerospace model only.

TABLE 7.– PHOTOCHEMICAL REACTIONS AND RATE COEFFICIENTS FOR CHLORINE COMPOUNDS

Reaction	Rate constant[a]	Note
$Cl + O_3 \rightarrow ClO + O_2$	$2.7 \times 10^{-11} e^{-257/T}$	
$Cl + CH_4 \rightarrow HCl + CH_3$	$7.3 \times 10^{-12} e^{-1260/T}$	
$Cl + H_2 \rightarrow HCl + H$	$3.5 \times 10^{-11} e^{-2290/T}$	
$Cl + HO_2 \rightarrow HCl + O_2$	3.0×10^{-11}	
$ClO + O \rightarrow Cl + O_2$	$7.7 \times 10^{-11} e^{-130/T}$	
$ClO + NO \rightarrow Cl + NO_2$	$1.0 \times 10^{-11} e^{200/T}$	
$ClO + NO_2 + M \rightarrow ClONO_2 + M$		b
$ClONO_2 + O \rightarrow ClO + NO_3$	$3.0 \times 10^{-12} e^{-808/T}$	
$Cl + ClO_2 \rightarrow ClO + ClO$	5.9×10^{-11}	
$HCl + OH \rightarrow Cl + H_2O$	$3.0 \times 10^{-12} e^{-425/T}$	
$HCl + O \rightarrow Cl + OH$	$1.1 \times 10^{-11} e^{-3370/T}$	
$ClO + h\nu \rightarrow Cl + O$	2.8×10^{-3}	c
$ClONO_2 + h\nu \rightarrow ClO + NO_2$	5.6×10^{-4}	c
$HCl + h\nu \rightarrow Cl + H$	1.6×10^{-6}	c
$CF_2Cl_2 + h\nu \rightarrow Cl + Cl$	1.3×10^{-6}	c
$CFCl_3 + h\nu \rightarrow Cl + Cl + Cl$	7.1×10^{-6}	c

[a] Rate constants are in molecule·cm·sec units; unless otherwise noted, the rate constants are taken from Hudson (1977).

[b] The expression adopted for this rate constant is given in Hudson (1977) as computed by Ames workers.

[c] Twenty-four hour average photodissociation rates at 120 km altitude are given.
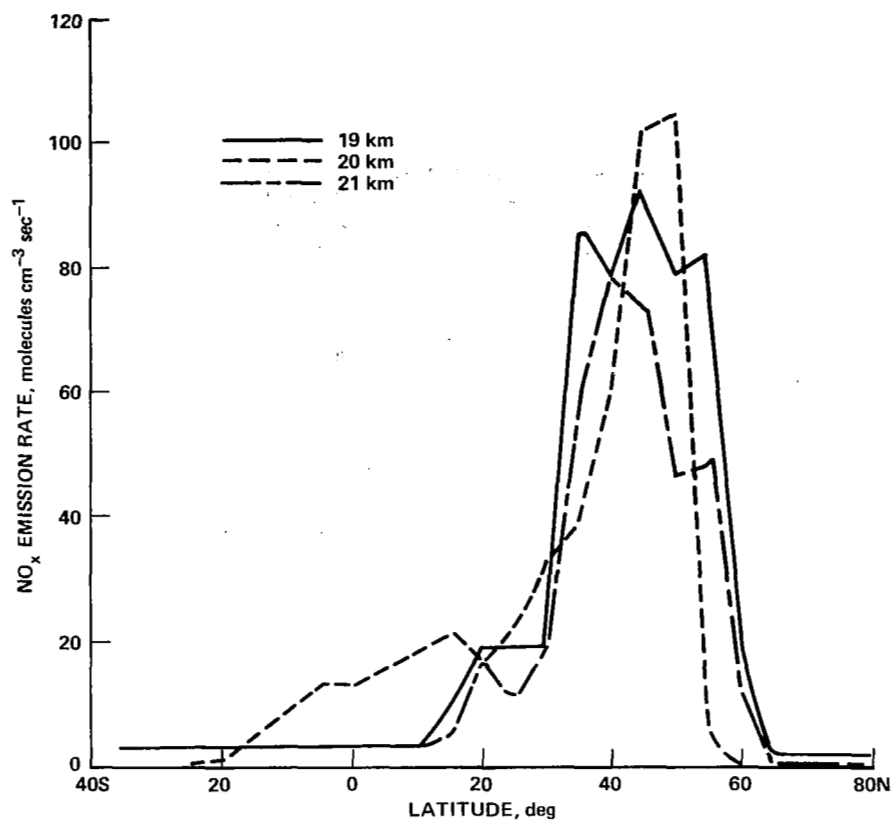
Figure 1. — Nitrogen oxide emission rate in molecules of NO cm^{-3} sec^{-1} which represents the SST emissions model discussed in the text; the mismatches among the three curves occur because of the complex nature of the modeled air route structure and the increase in flight altitudes as fuel is consumed.
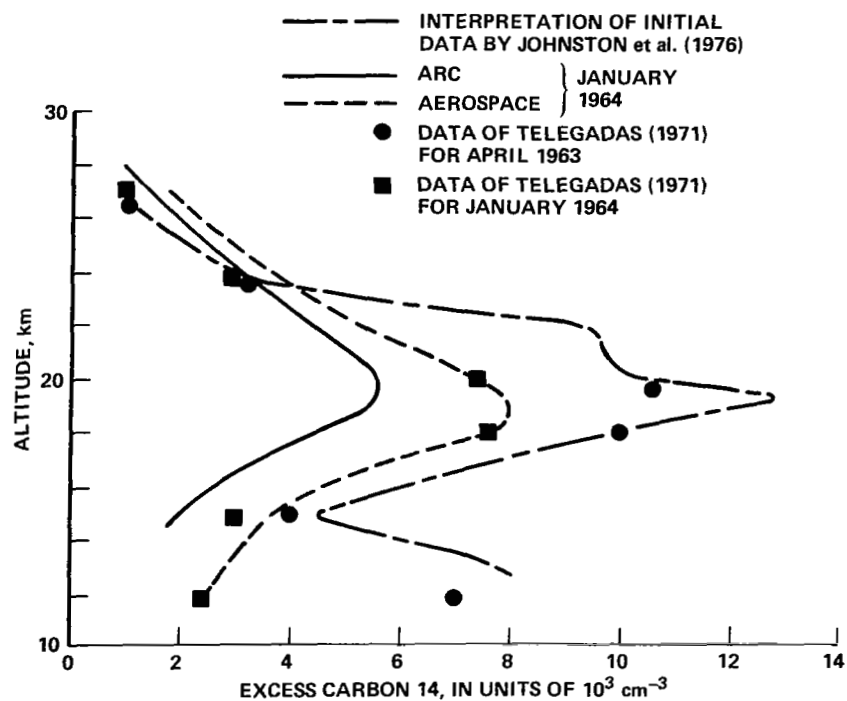
Figure 2. — Comparison of calculated and observed carbon-14 profiles at lat. 30° N 9 months after an atmospheric nuclear test explosion; observational data are from Telegadas (1971).
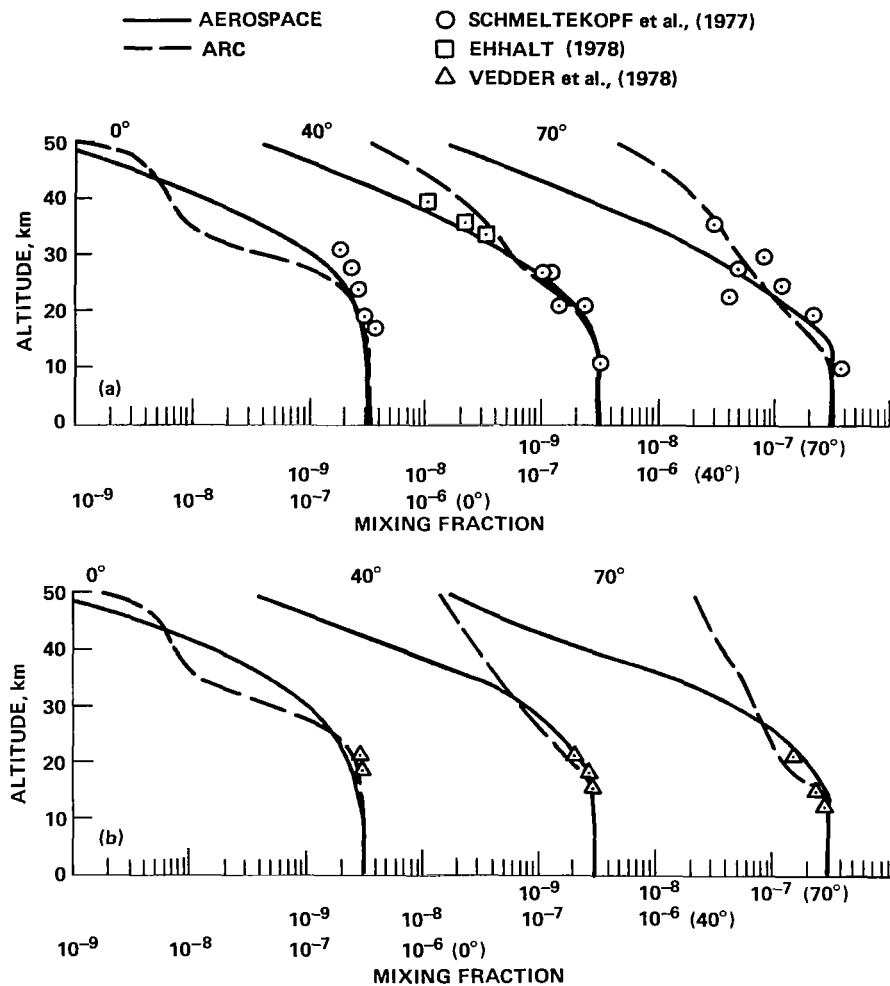
Figure 3. — Comparison of calculated and measured profiles of nitrous oxide (N_2O) at three latitudes in the Northern Hemisphere. (a) Summer. (b) Autumn.
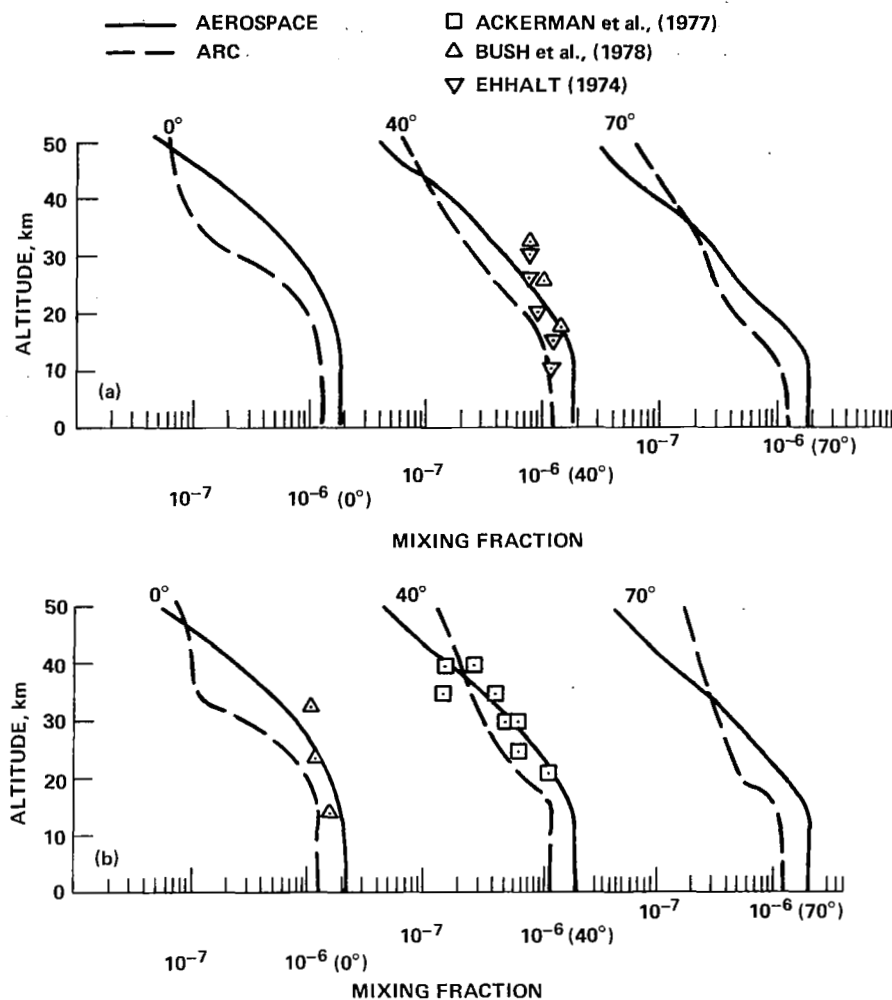
Figure 4. — Comparison of calculated and measured profiles of methane (CH$_4$) at three latitudes in the Northern Hemisphere. (a) Summer. (b) Autumn.
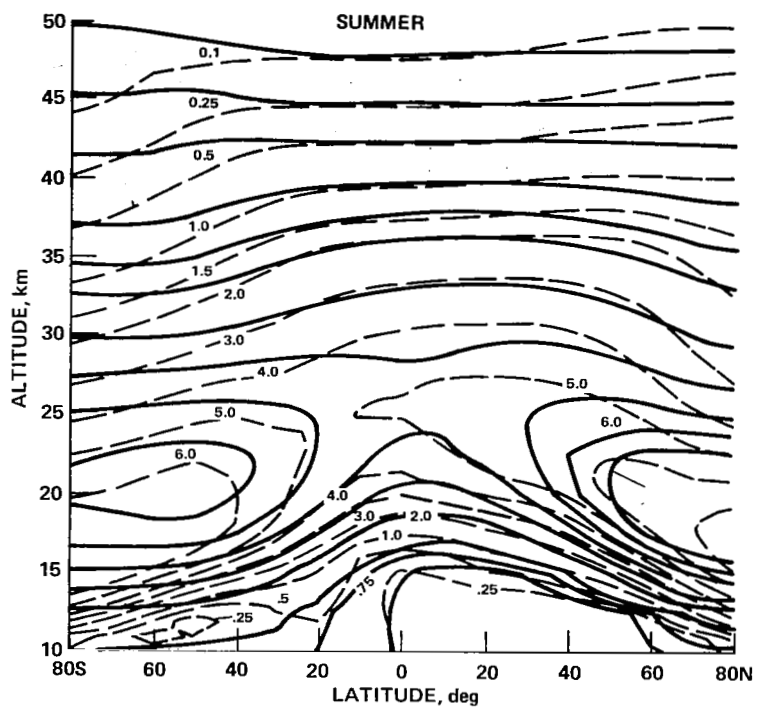
(a) Summer.

Figure 5.— Computed isopleths of ozone concentration in units of 10^{12} cm^{-3}; the solid lines represent the Ames model, the broken lines the Aerospace model.
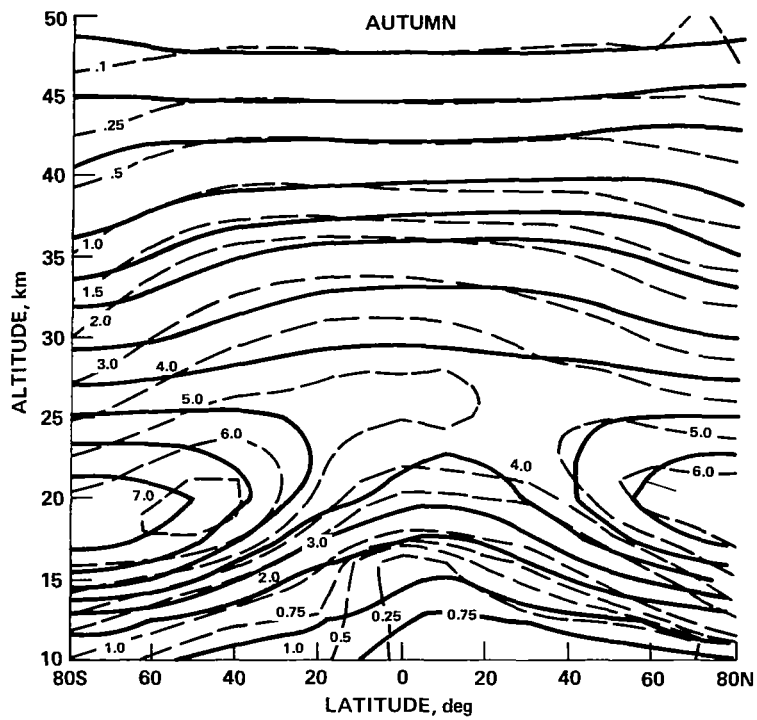
(b) Autumn.

Figure 5.— Concluded.
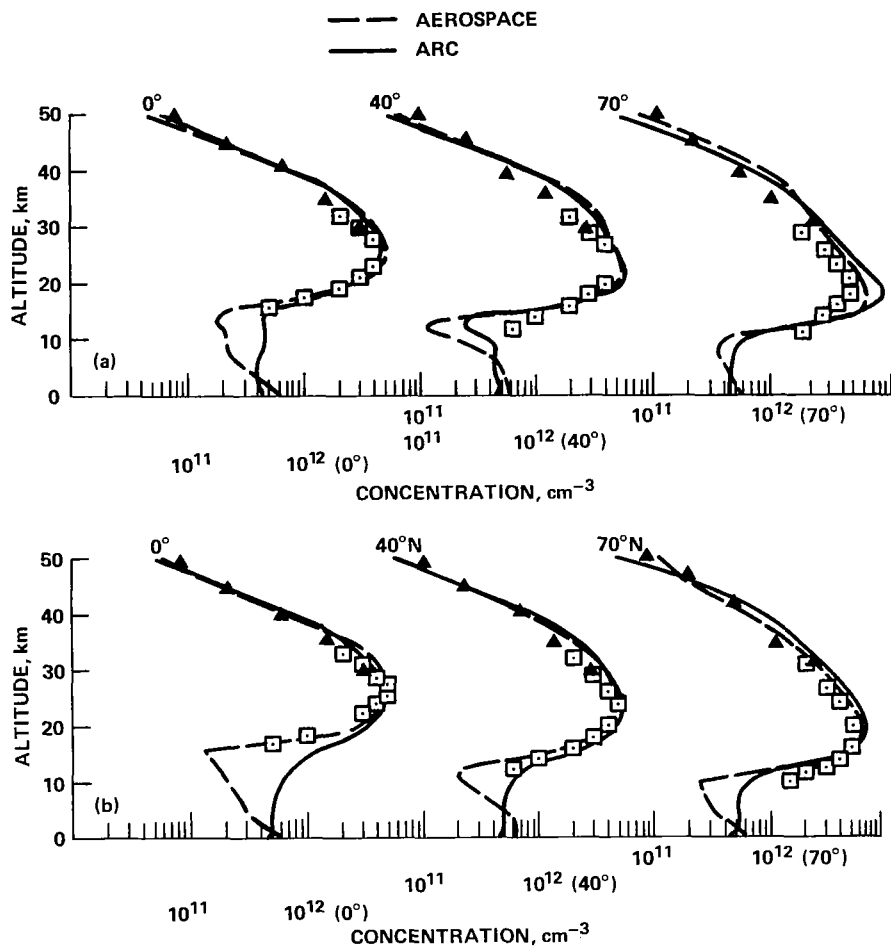
Figure 6.- Comparison of calculated and measured profiles of ozone at three latitudes in the Northern Hemisphere. The squares represent the mean seasonal measured values obtained by Wilcox et al. (1977). The Goddard data (triangles) (Private communication from I. Eberstein, Goddard Space Flight Center [1977]), were obtained from satellite measurements of backscattered solar ultraviolet radiation (Heath et al. 1973). (a) Summer. (b) Autumn.
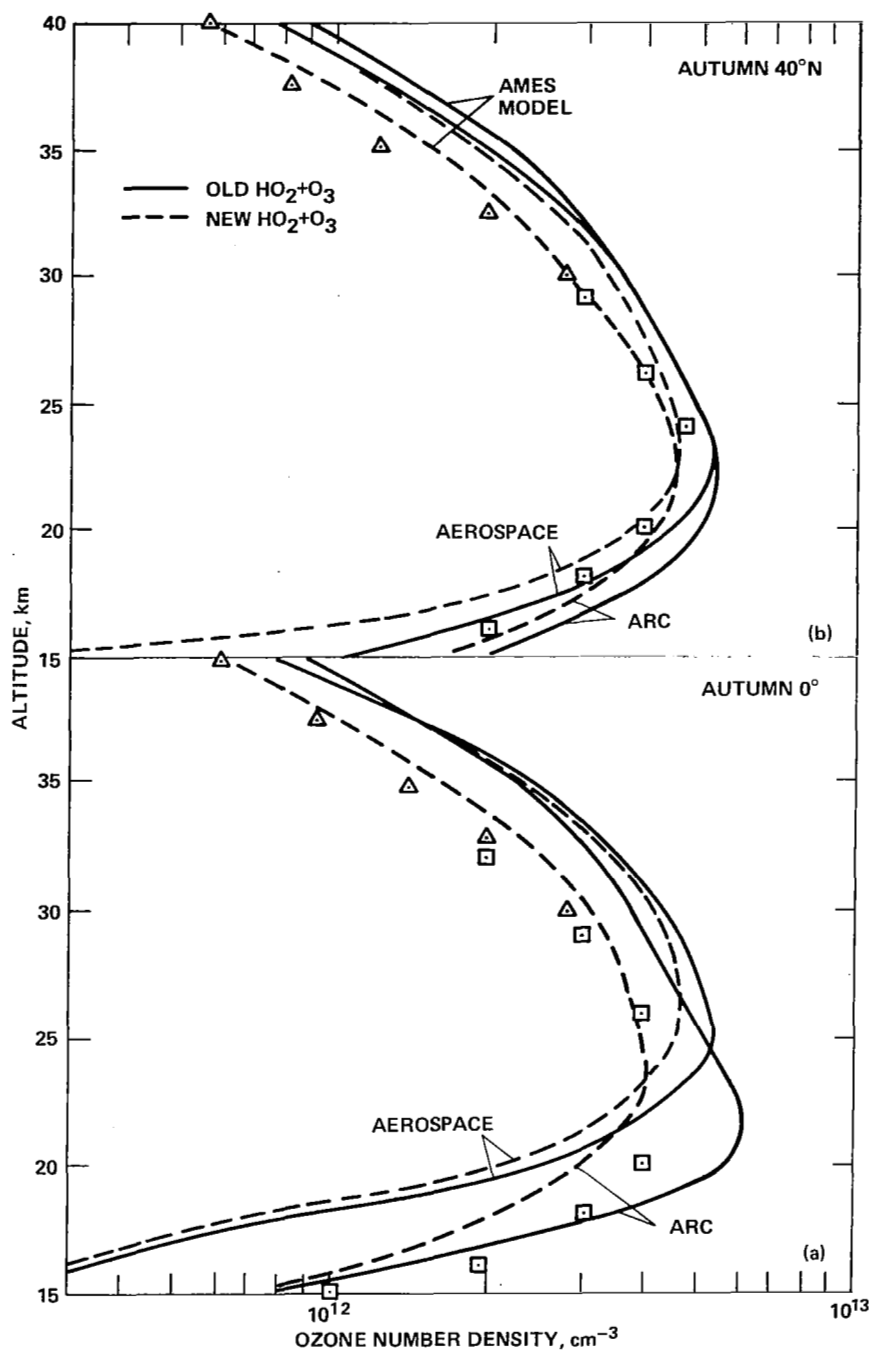
Figure 7.– Computed (using the new value for the rate coefficient of reaction (7)) and measured ozone concentration profiles for autumn in the Northern Hemisphere. The squares represent the mean seasonal measured values obtained by Wilcox et al. (1977). The Goddard data (triangles)(Private communication from I. Eberstein, Goddard Space Flight Center [1977]) were obtained from satellite measurements of backscattered solar ultraviolet radiation (Heath et al., 1973). The solid lines correspond to the older value for the rate coefficient of reaction (9) and the broken lines to the value reported by Zahniser and Howard (1978). The Ames model (broken line) simulated 2.5 ppbv Clx; the Aerospace model simulated no Clx. (a) Equator. (b) Latitude 40° N.
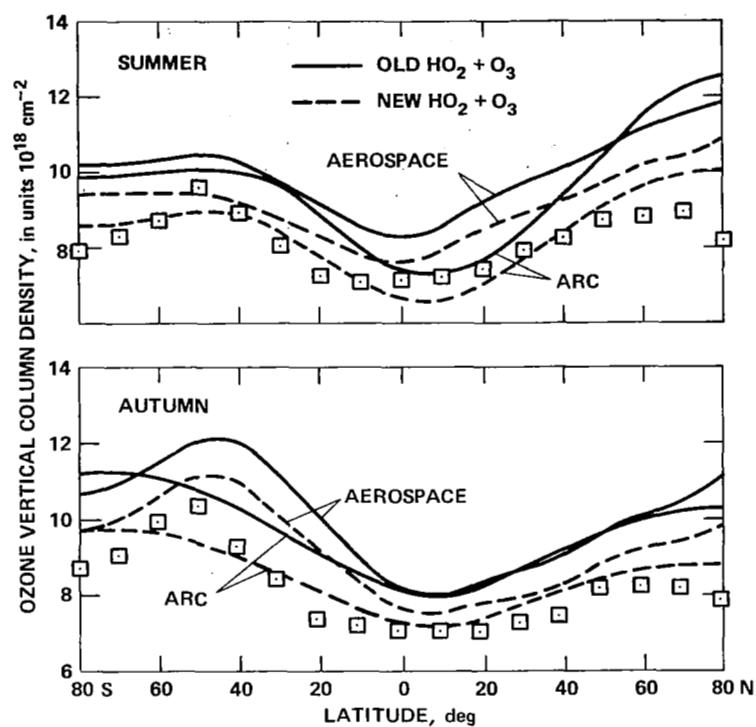
Figure 8. — Total ozone vertical column densities in the Northern Hemisphere. The solid lines represent computed values corresponding to the older value of the rate coefficient of reaction (9). The broken lines represent the computed values that correspond to the value reported by Zahniser and Howard (1978). The squares represent the mean seasonal values obtained by Wilcox et al. (1977). (a) Summer. (b) Autumn.

NO$_y$–SUMMER (NH)
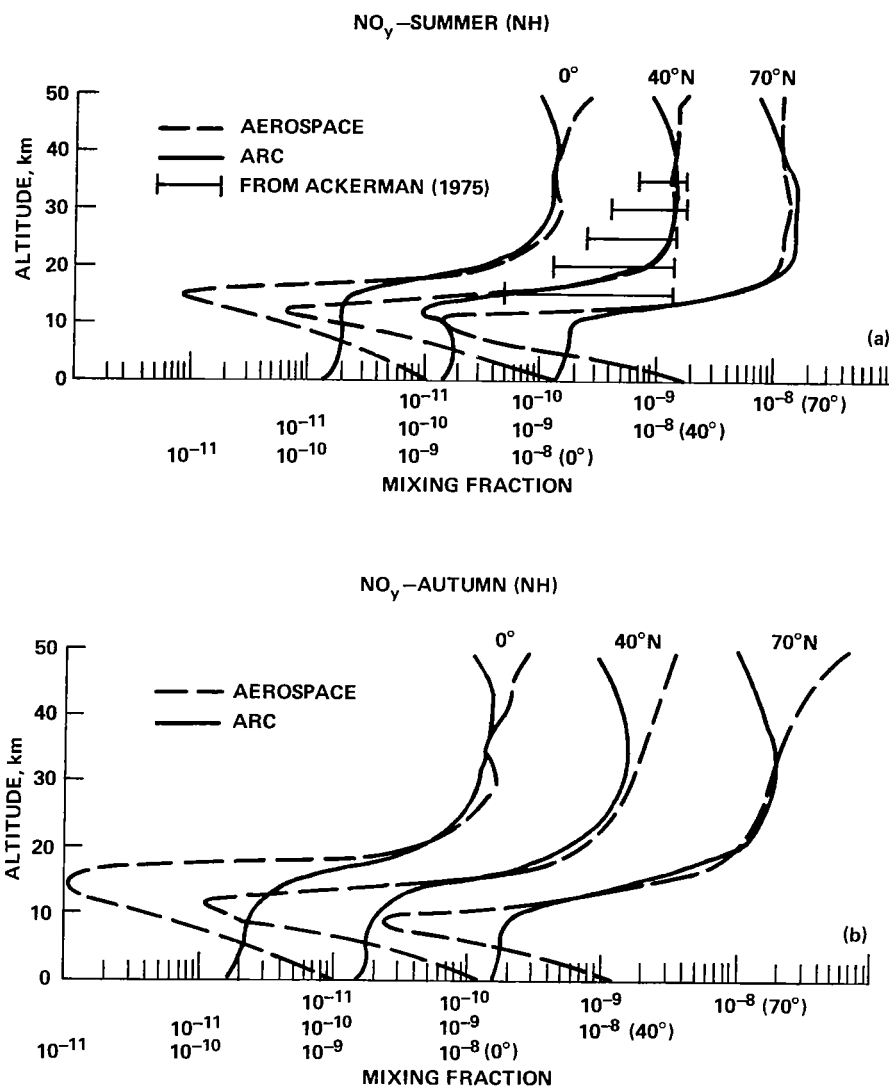
Figure 9. — Computed profiles of odd-nitrogen, NO$_y$, mixing ratios at three latitudes in the Northern Hemisphere. The data points are from a compilation by Ackerman (1976) of various measurements of NO, NO$_2$, and HNO$_3$ mostly at mid-latitudes; they are shown in figure 9 (a) for convenience. (a) Summer. (b) Autumn.

38
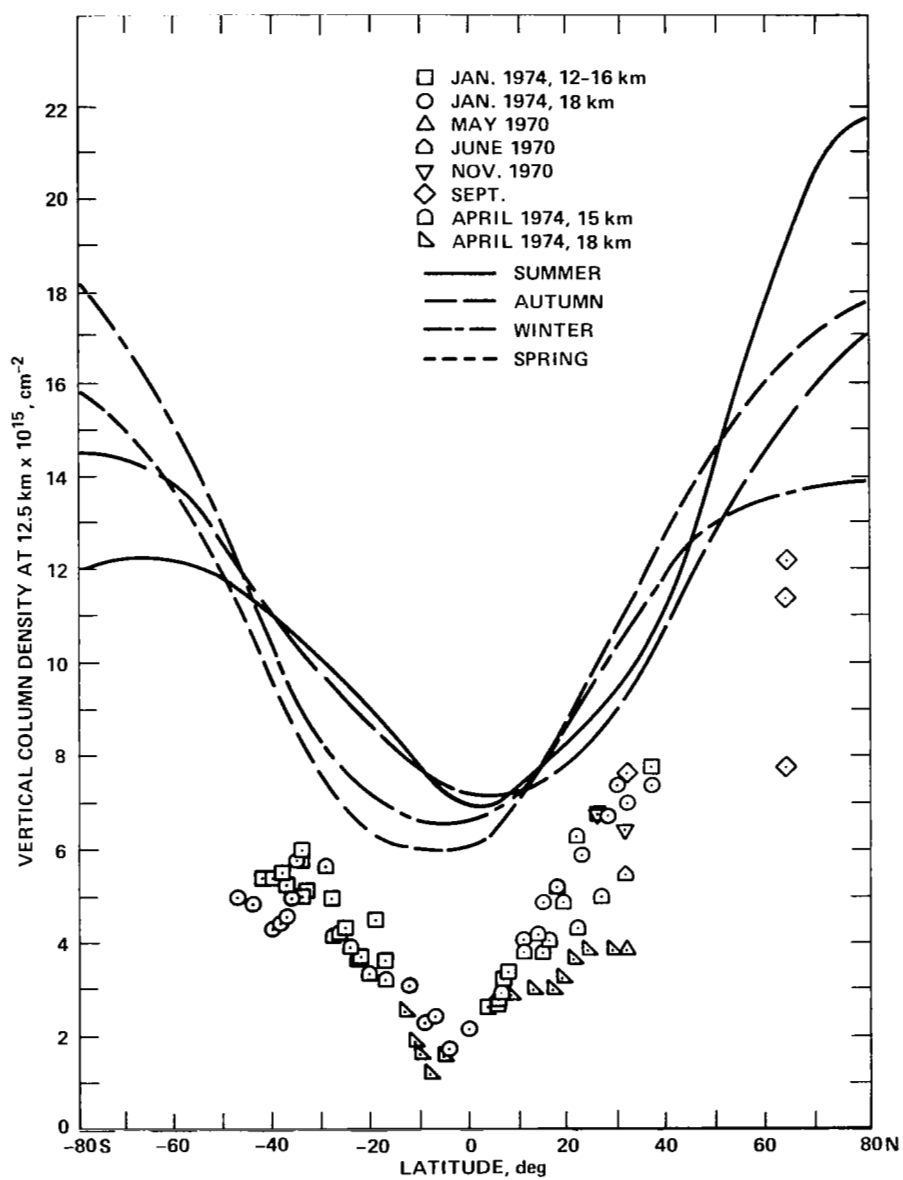
(a) Ames model.

Figure 10.— Nitric acid column densities above 12.5 km as a function of latitude and season; balloon measurements were made in 1970.
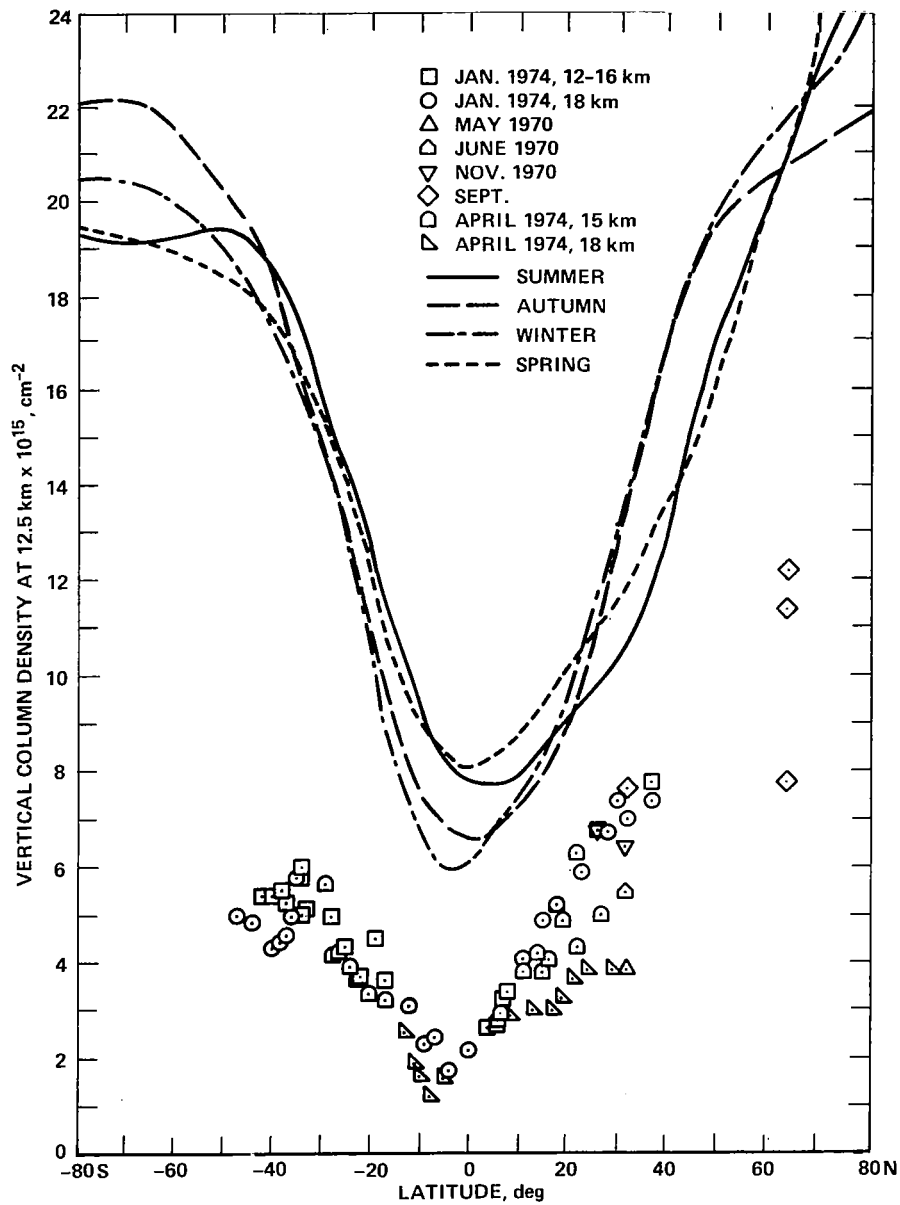
(b) Aerospace model.

Figure 10.– Concluded.
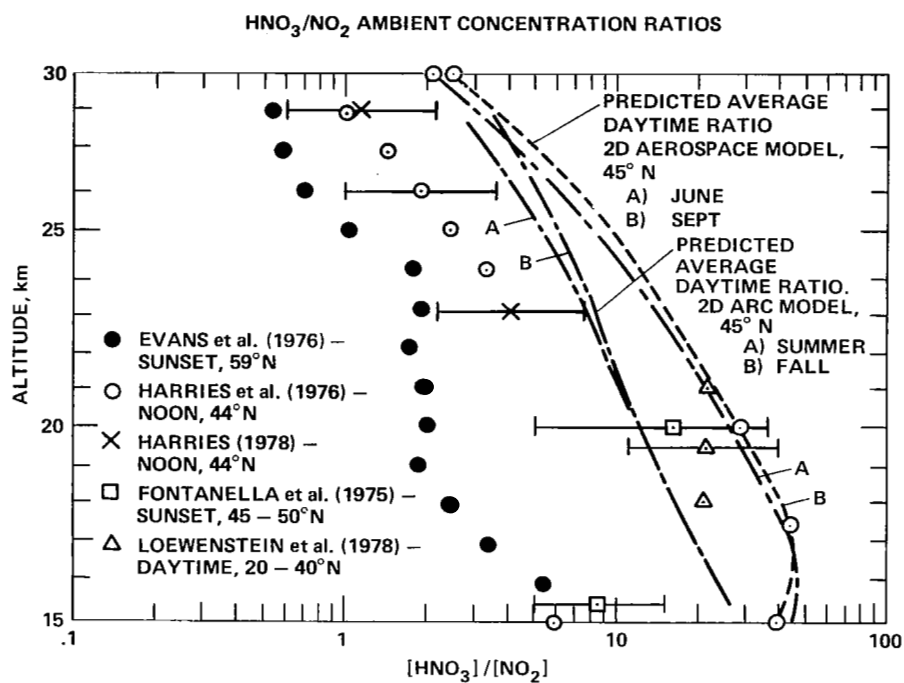
Figure 11. — Comparison of measured and computed values of the HNO_3/NO_2 abundance ratio; the Harries (1978) data are from a re-analysis of the measurements first reported by Harries et al. (1976).

H₂O—SUMMER (NH)

— — AEROSPACE
——— ARC
—·— HARRIES (1976) MEAN DATA
······ HARRIES STD. DEV.

H₂O—AUTUMN (NH)

— — AEROSPACE
——— ARC

MIXING FRACTION
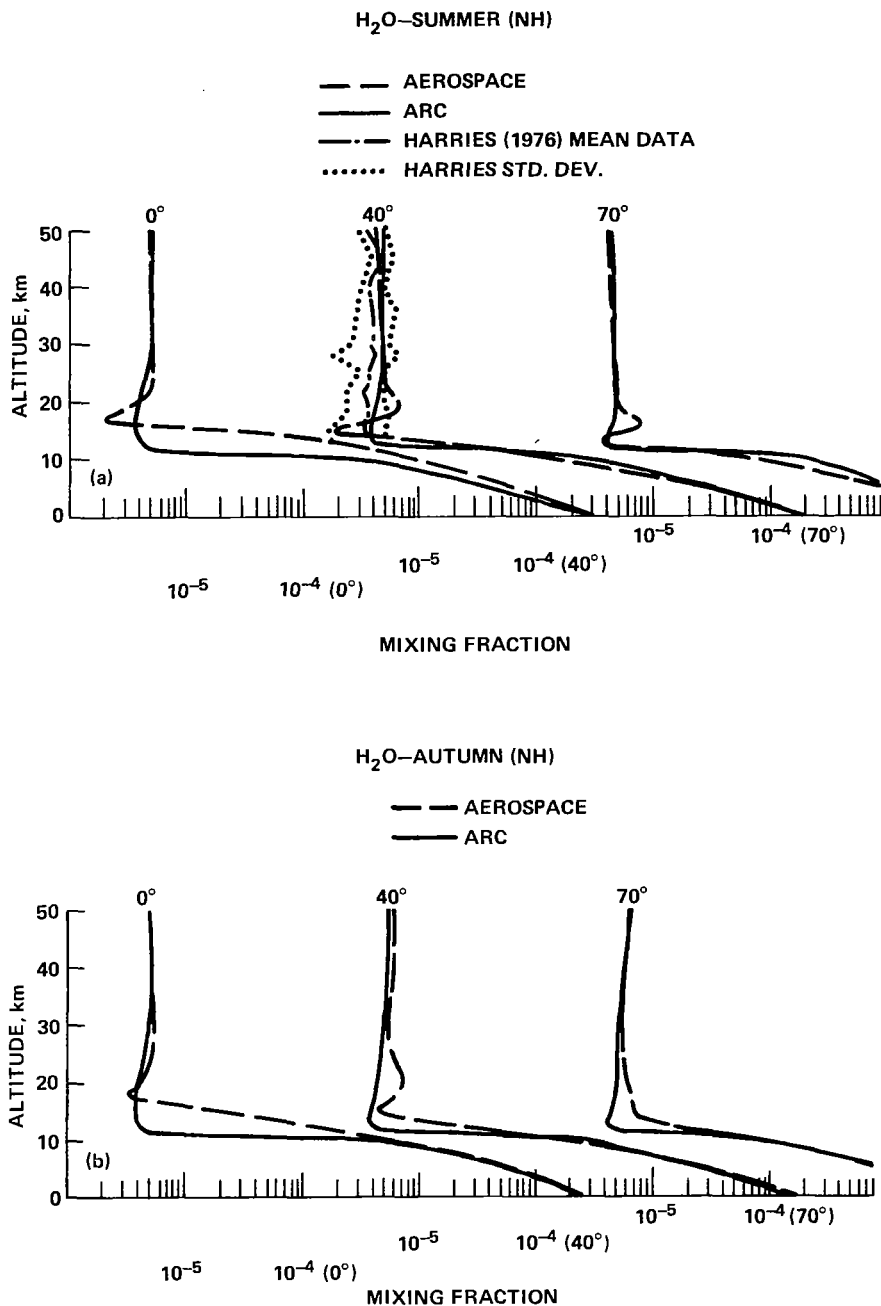
Figure 12. — Computed profiles of water-vapor volume mixing ratios at three latitudes in the Northern Hemisphere. The mean mid-latitude Northern Hemisphere vertical distribution of water vapor derived by Harries (1976) from available data are also shown; the dotted lines represent the rms variance among the individual measurements at each level. The measured data are plotted in figure 12 (a) for convenience, but they include measurements made in all seasons. (a) Summer. (b) Autumn.

OH—SUMMER (NH)

— — — AEROSPACE
———— ARC
├—⊙—┤ ANDERSON (1976)

OH-AUTUMN (NH)

— — — AEROSPACE
———— ARC
├—●—┤ ANDERSON, 1976
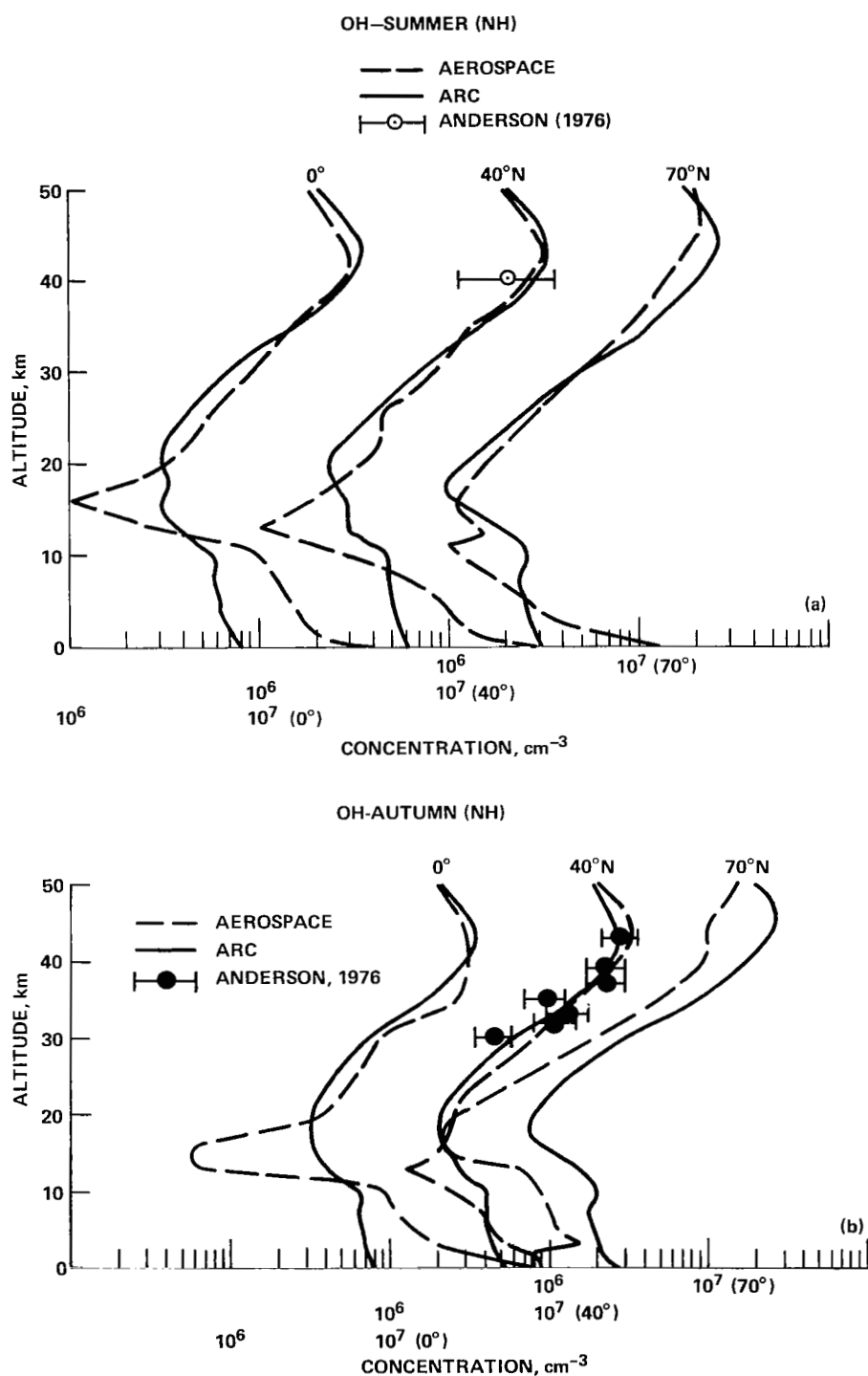
Figure 13. — Comparison of calculated and measured vertical distributions of the hydroxyl radical OH; the measured values were obtained by balloon flights at Palestine Texas, lat. 32°(N.) (a) Summer (measured in July 1975; Anderson, 1976). (b) Autumn (measured in January 1976; Anderson, 1976).

HO$_2$ SUMMER (NH)

- - - AEROSPACE
——— ARC

ALTITUDE, km

CONCENTRATION, cm^{-3}

HO$_2$–AUTUMN (NH)

- - - AEROSPACE
——— ARC

ALTITUDE, km

CONCENTRATION, cm^{-3}
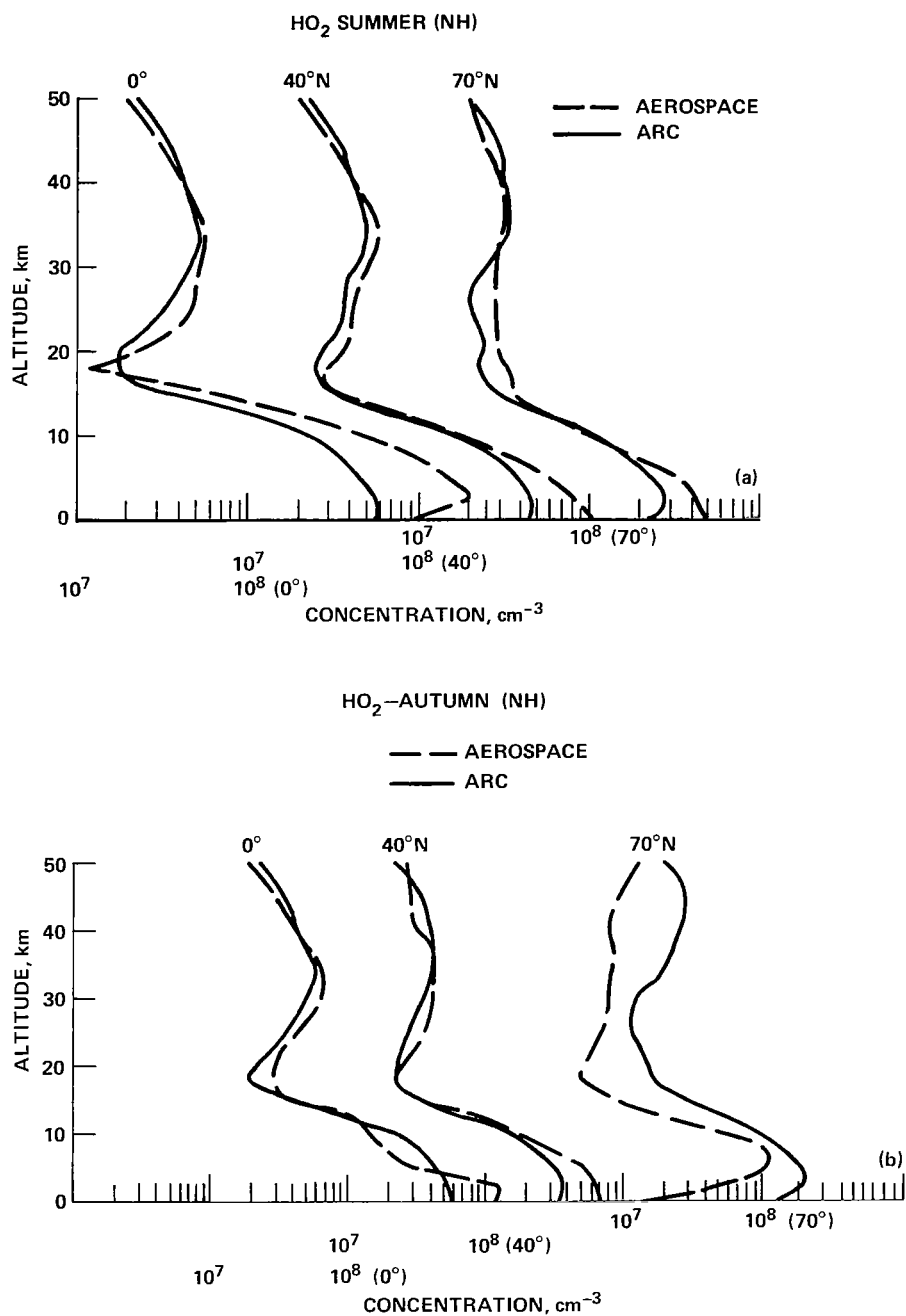
Figure 14. — Comparison of calculated vertical distributions of the hydroperoxyl radical HO$_2$. (a) Summer. (b) Autumn.

CH$_3$O$_2$—SUMMER (NH)

— — AEROSPACE
—— ARC

0°   40°   70°N

ALTITUDE, km

50
40
30
20
10
0

(a)

10^6 10^7 10^8 (70°)
10^6 10^7 10^8 (40°)
10^6 10^7 10^8 (0°)

CONCENTRATION, cm^{-3}

CH$_3$O$_2$—AUTUMN (NH)

0°   40°   70°

ALTITUDE, km

50
40
30
20
10
0

— — AEROSPACE
—— ARC

(b)

10^6 10^7 10^8 (70°)
10^6 10^7 10^8 (40°)
10^6 10^7 10^8 (0°)

CONCENTRATION, cm^{-3}
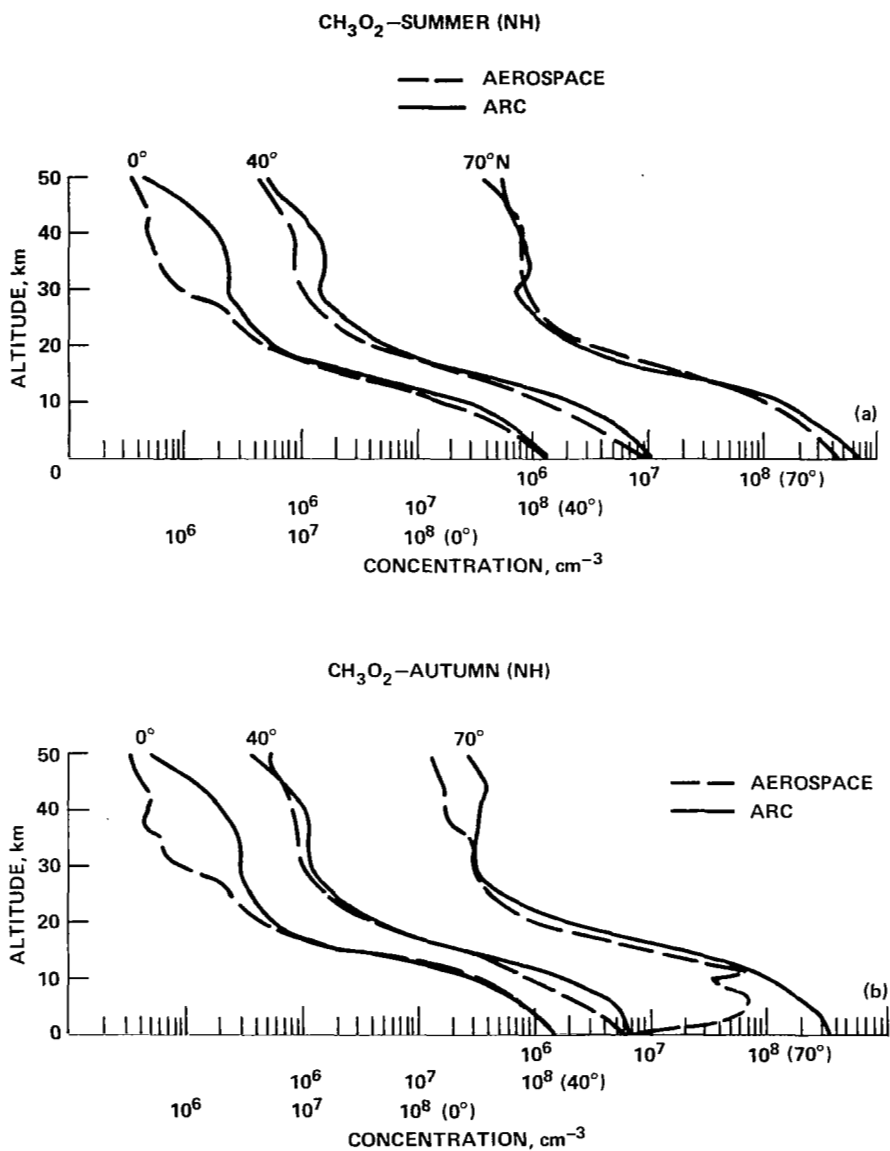
Figure 15. – Comparison of calculated vertical distributions of CH$_3$O$_2$. (a) Summer. (b) Autumn.

45

NO$_x$–SUMMER (NH)

NO$_x$ AUTUMN (NH)
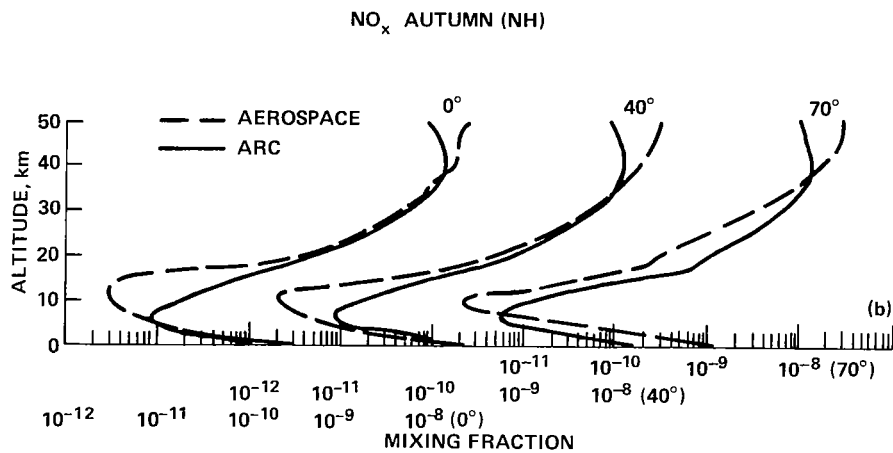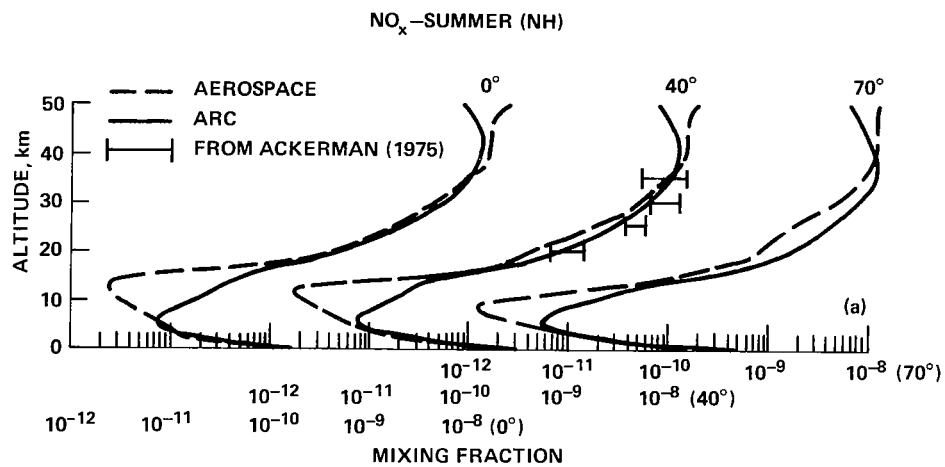
Figure 16. — Comparison of calculated and measured vertical distributions of NO$_x$ (= NO + NO$_2$). The measured values were obtained over Aire sur l'Adour, France (lat. 43°35'N) in May 1974 (Ackerman et al., 1975).
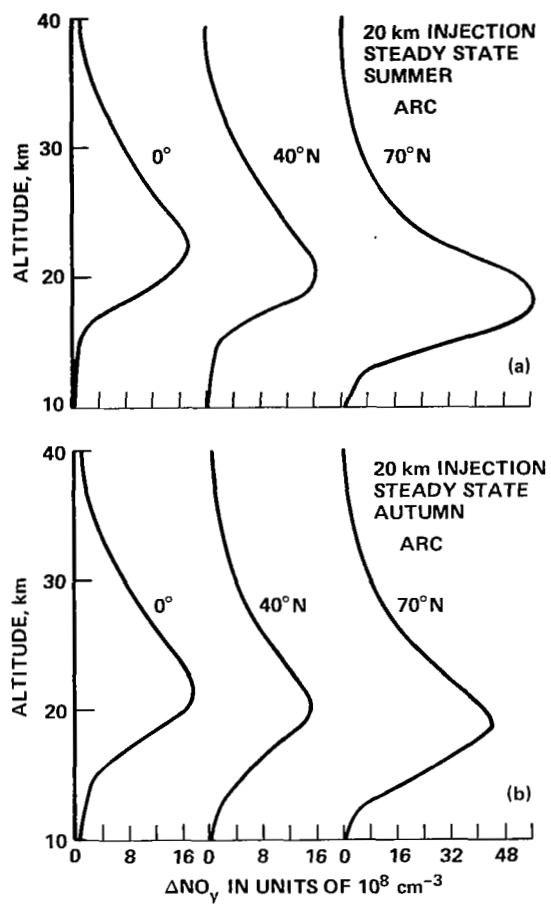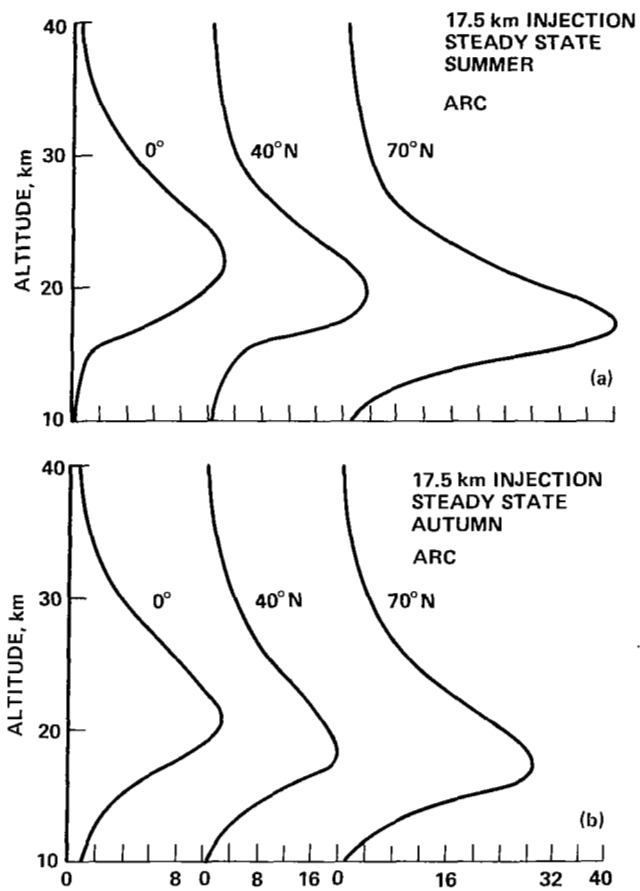(a) Summer. (b) Autumn.

46
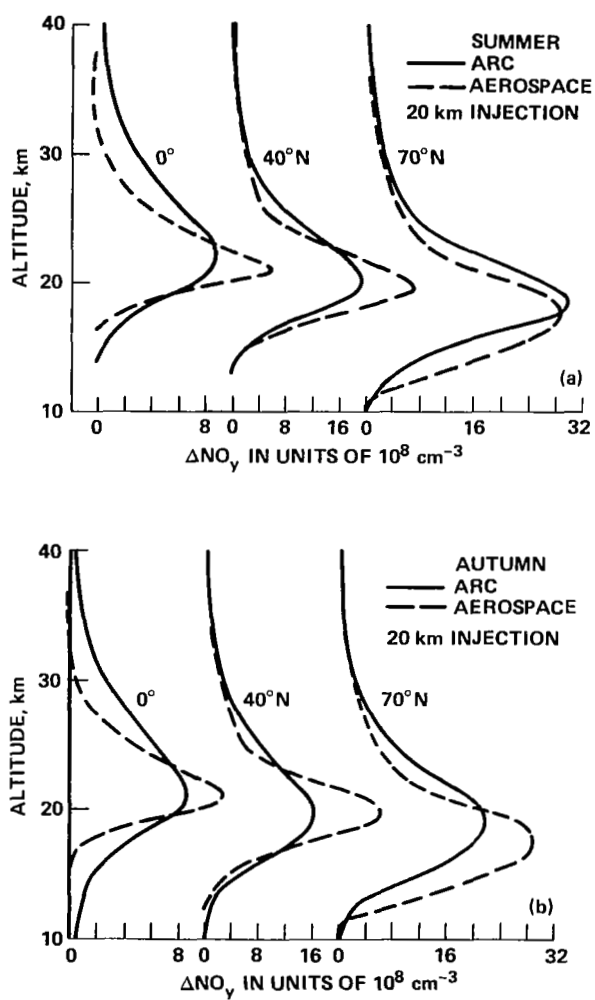
Figure 17. — Odd-nitrogen increments (ΔNO_y) that correspond to scenario (1). (a) Summer. (b) Autumn.
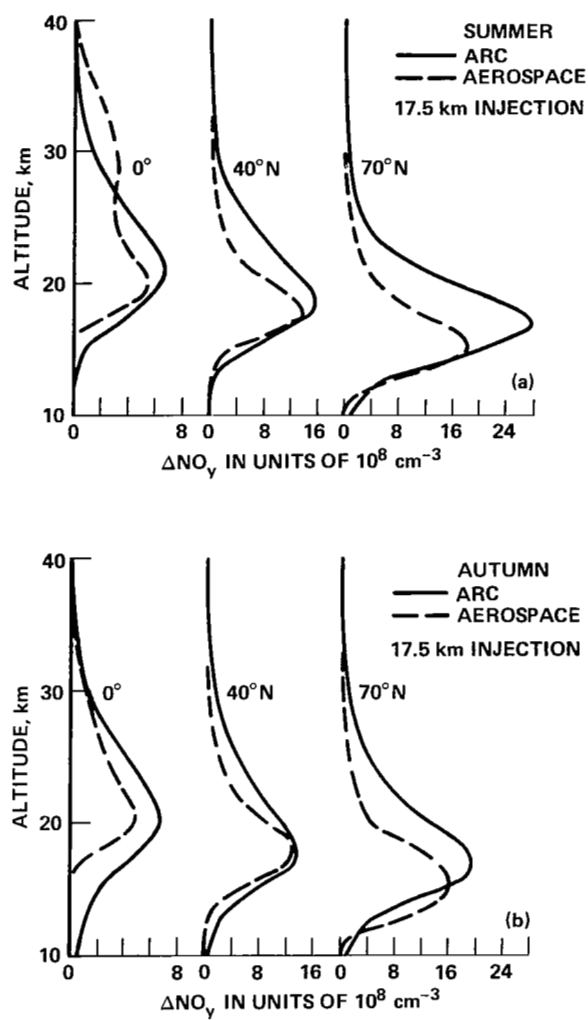
Figure 18. — Odd-nitrogen increments (ΔNO_y) that correspond to scenario (2). (a) Summer. (b) Autumn.
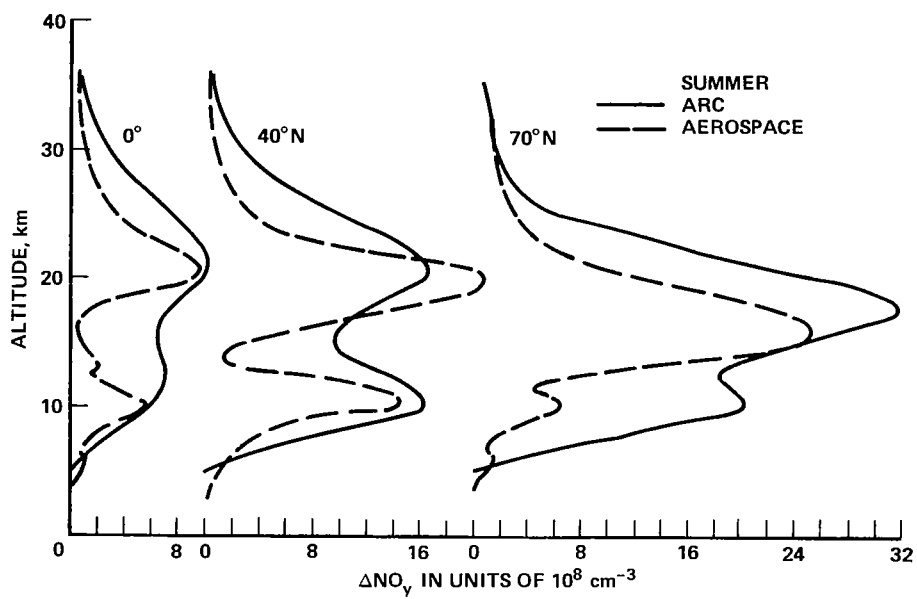
(a) Summer.

Figure 19.— Odd-nitrogen increments (ΔNO_y) that correspond to scenario (3).
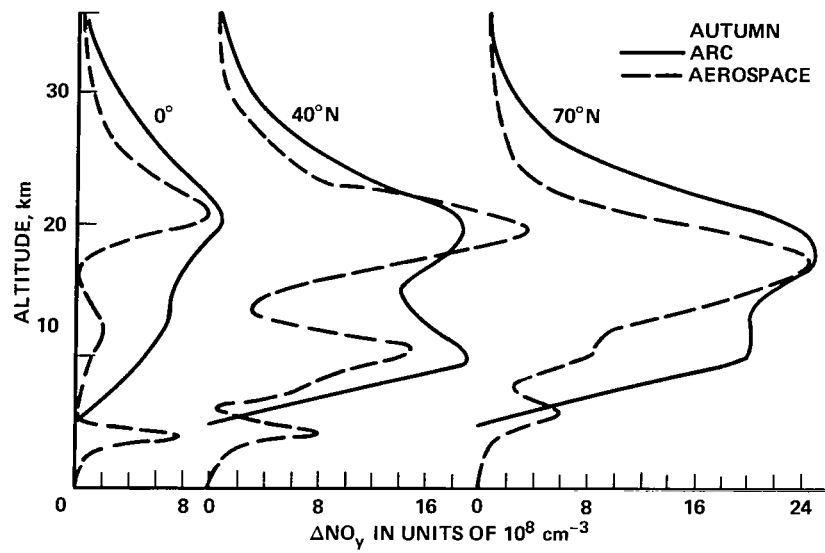
(b) Autumn.

Figure 19.— Concluded.

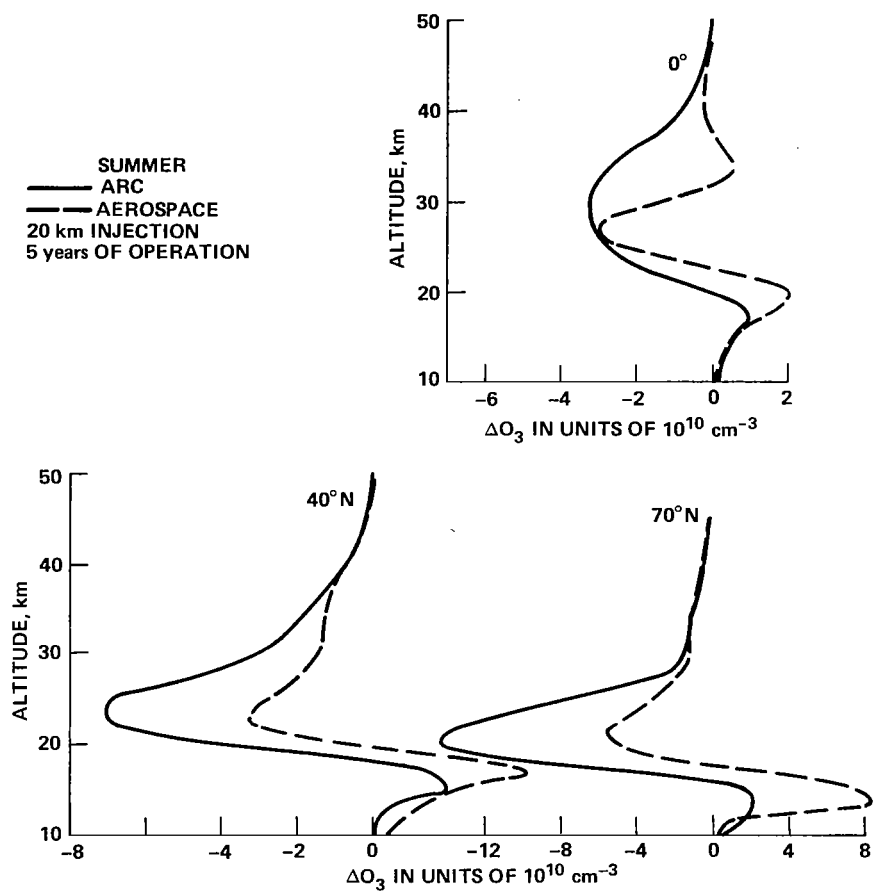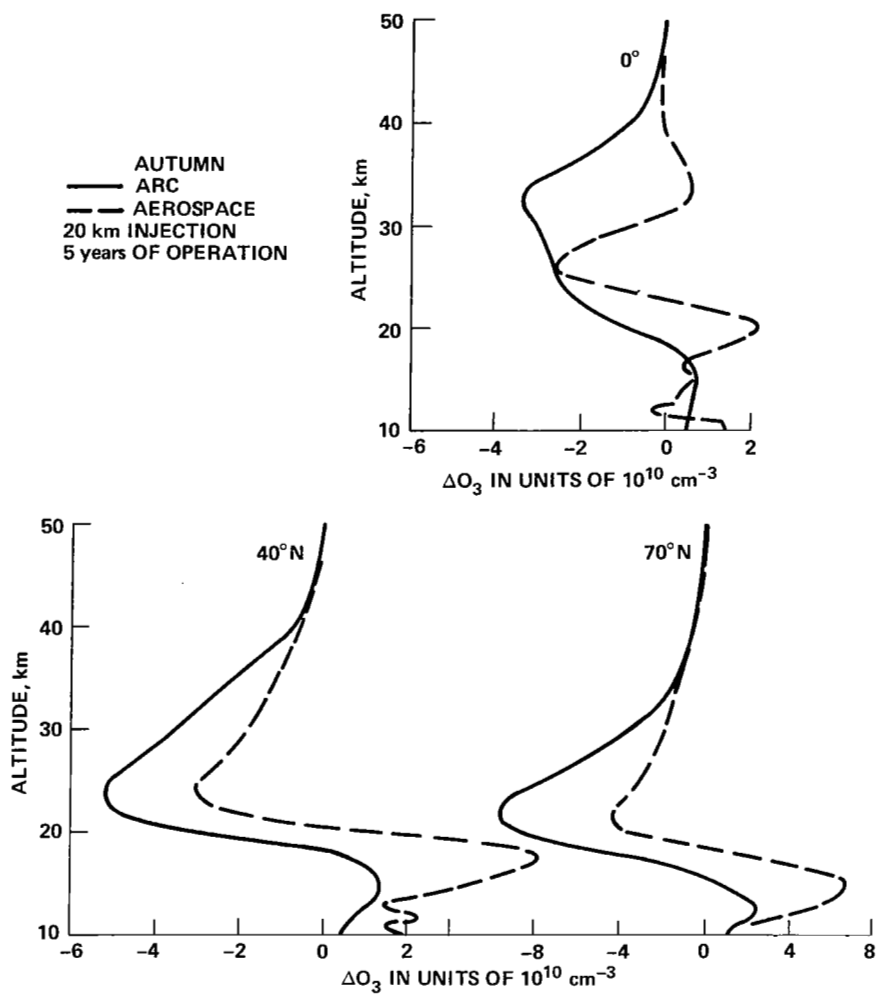Figure 20. – Odd-nitrogen increments (ΔNO_y) that correspond to scenario (4). (a) Summer. (b) Autumn.

Figure 21. — Odd-nitrogen increments (ΔNO_y) that correspond to scenario (5). (a) Summer. (b) Autumn.
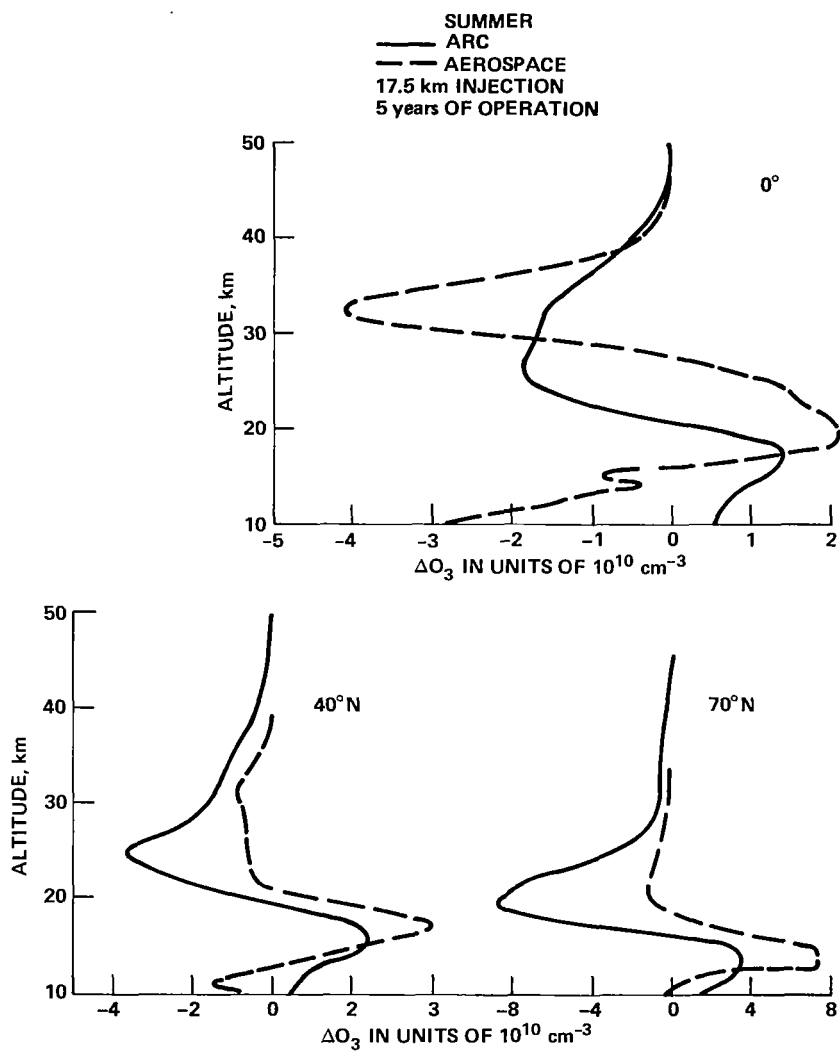
SUMMER
——— ARC
— — —AEROSPACE
20 km INJECTION
5 years OF OPERATION

(a) Summer.

Figure 22.— Absolute ozone changes (ΔO_3) that correspond to scenario (1).

AUTUMN
——— ARC
— — — AEROSPACE
20 km INJECTION
5 years OF OPERATION

(b) Autumn.

Figure 22.– Concluded.

SUMMER
ARC
AEROSPACE
17.5 km INJECTION
5 years OF OPERATION

ALTITUDE, km

ΔO_3 IN UNITS OF 10^{10} cm^{-3}

0°

40° N

70° N

(a) Summer.

Figure 23.— Absolute ozone changes (ΔO_3) that correspond to scenario (2).

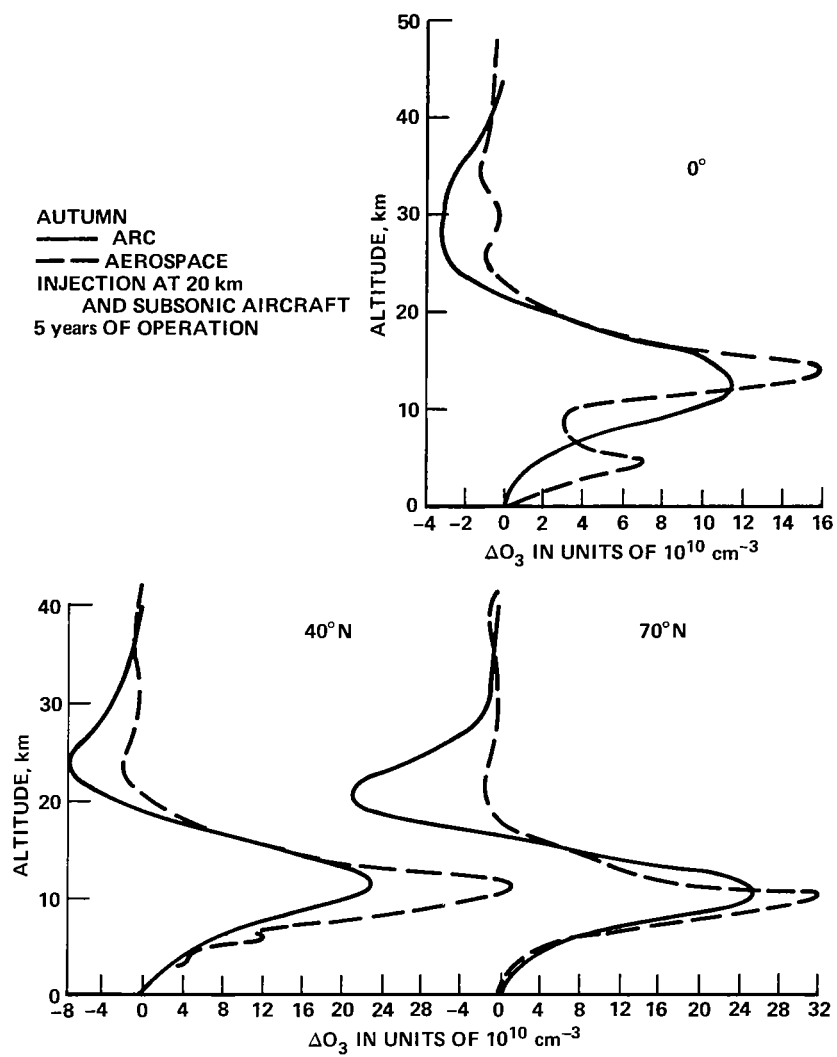AUTUMN
——— ARC
— — AEROSPACE
17.5 km INJECTION
5 years OF OPERATION
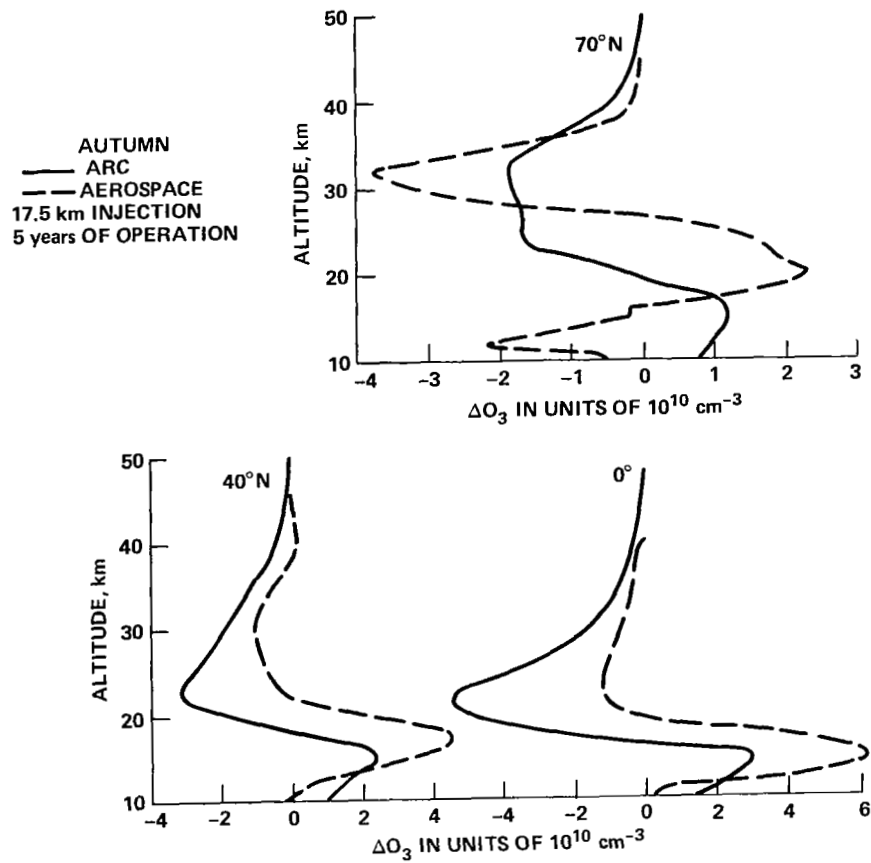
(b) Autumn.

Figure 23.– Concluded.
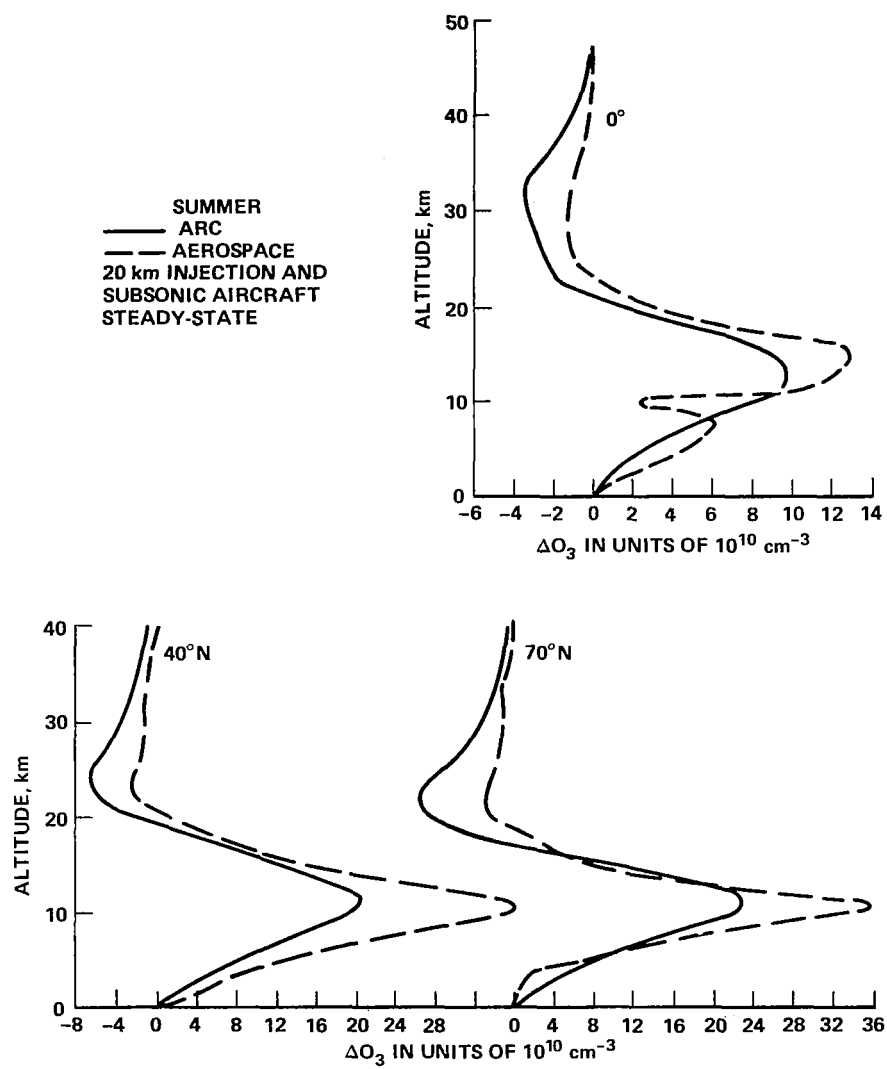
(a) Summer.

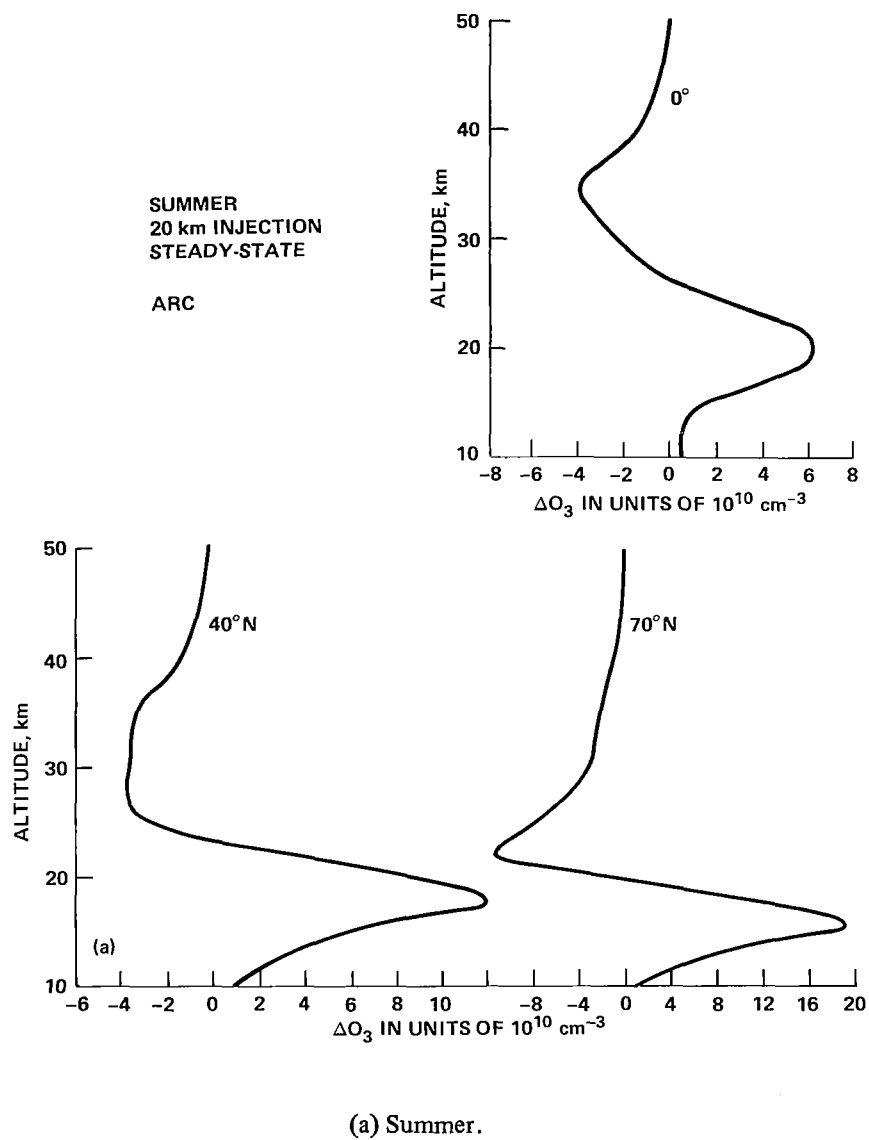Figure 24.— Absolute ozone changes (ΔO_3) that correspond to scenario (3).

AUTUMN
———— ARC
— — AEROSPACE
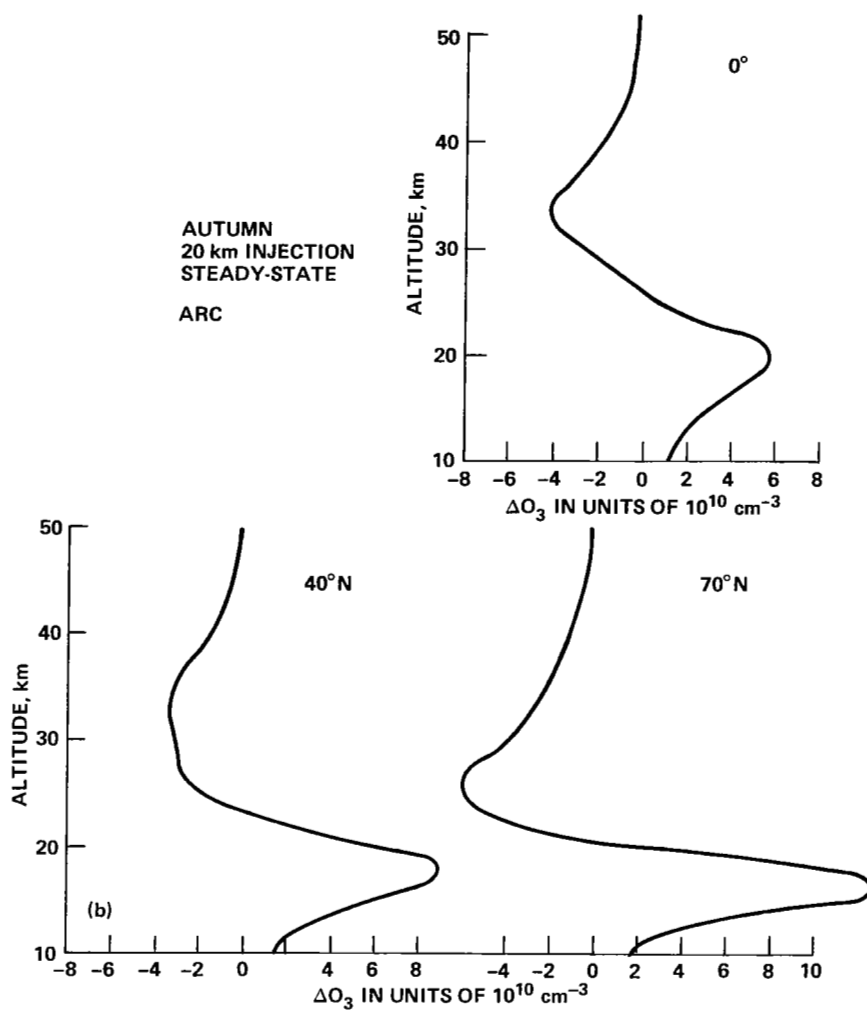INJECTION AT 20 km
AND SUBSONIC AIRCRAFT
5 years OF OPERATION

(b) Autumn.

Figure 24.— Concluded.

SUMMER
20 km INJECTION
STEADY-STATE

ARC

ALTITUDE, km

ΔO_3 IN UNITS OF 10^{10} cm^{-3}

0°

40° N

70° N

(a)

(a) Summer.

Figure 25.— Absolute ozone changes (ΔO_3) that correspond to scenario (4).

AUTUMN
20 km INJECTION
STEADY-STATE

ARC

(b) Autumn.

Figure 25.— Concluded.

SUMMER
17.5 km INJECTION
STEADY-STATE

ARC

0°

ΔO_3 IN UNITS OF 10^{10} cm^{-3}

ALTITUDE, km

40°N

70°N

(a)

ΔO_3 IN UNITS OF 10^{10} cm^{-3}

(a) Summer.
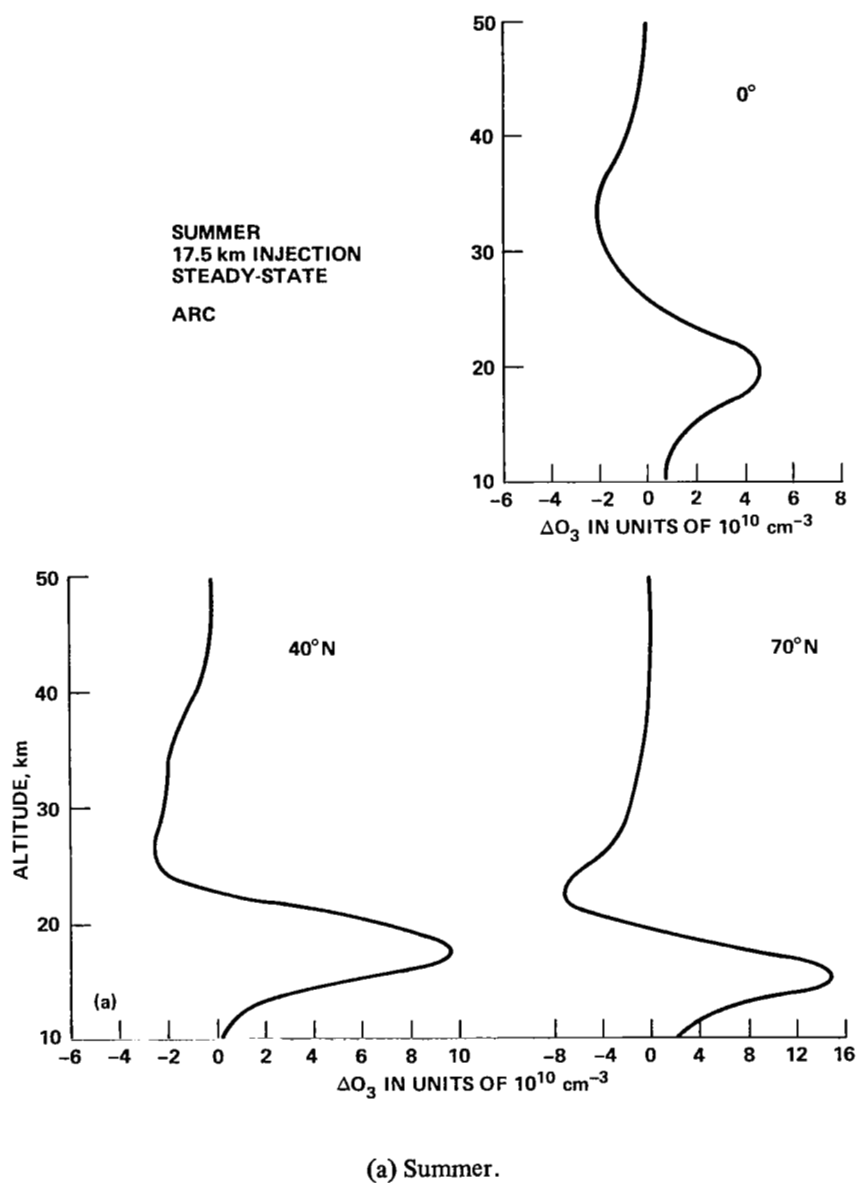
Figure 26.– Absolute ozone changes (ΔO_3) that correspond to scenario (5).

AUTUMN
17.5 km INJECTION
STEADY-STATE

ARC

50
40
30 ALTITUDE, km
20
10

0°

-6 -4 -2 0 2 4 6 8
ΔO_3 IN UNITS OF $10^{10} cm^{-3}$

50
40
30 ALTITUDE, km
20
10

40°N

70°N

(b)

-6 -4 -2 0 2 4 6 8 10   -8 -4 0 4 8 12 16
ΔO_3 IN UNITS OF $10^{10} cm^{-3}$
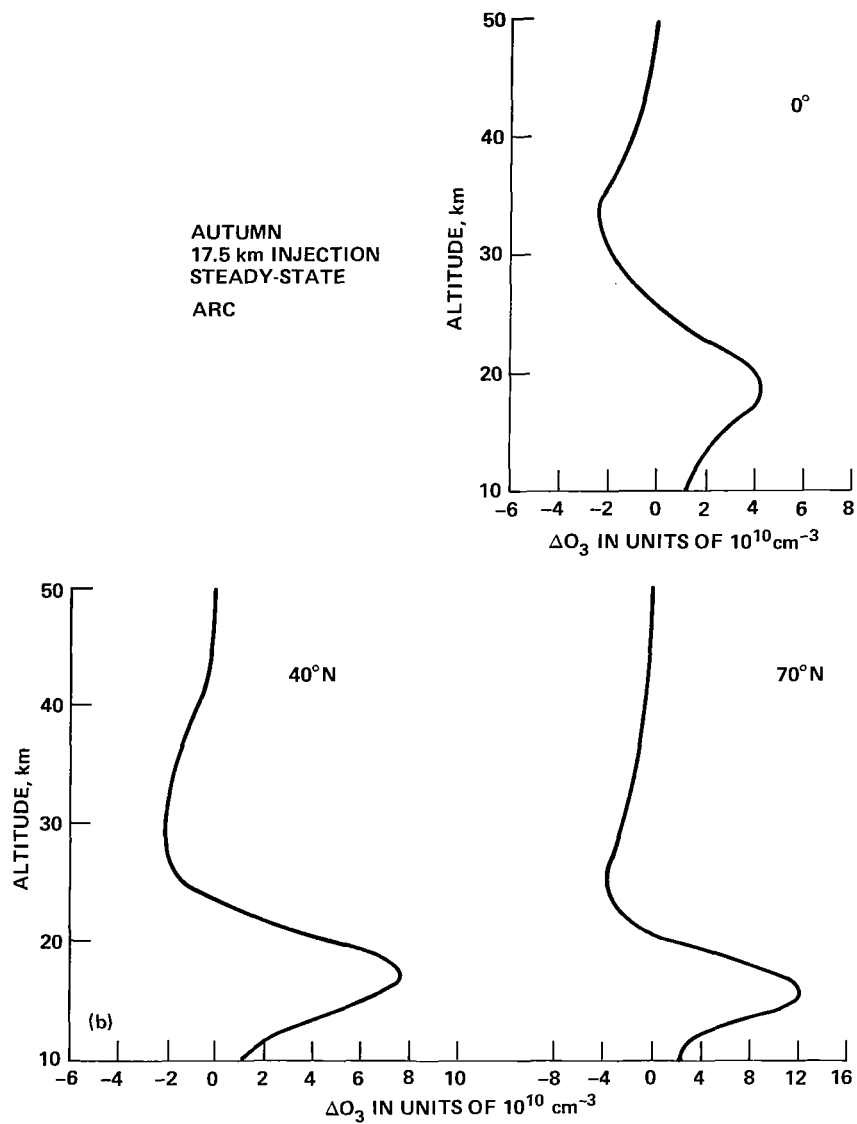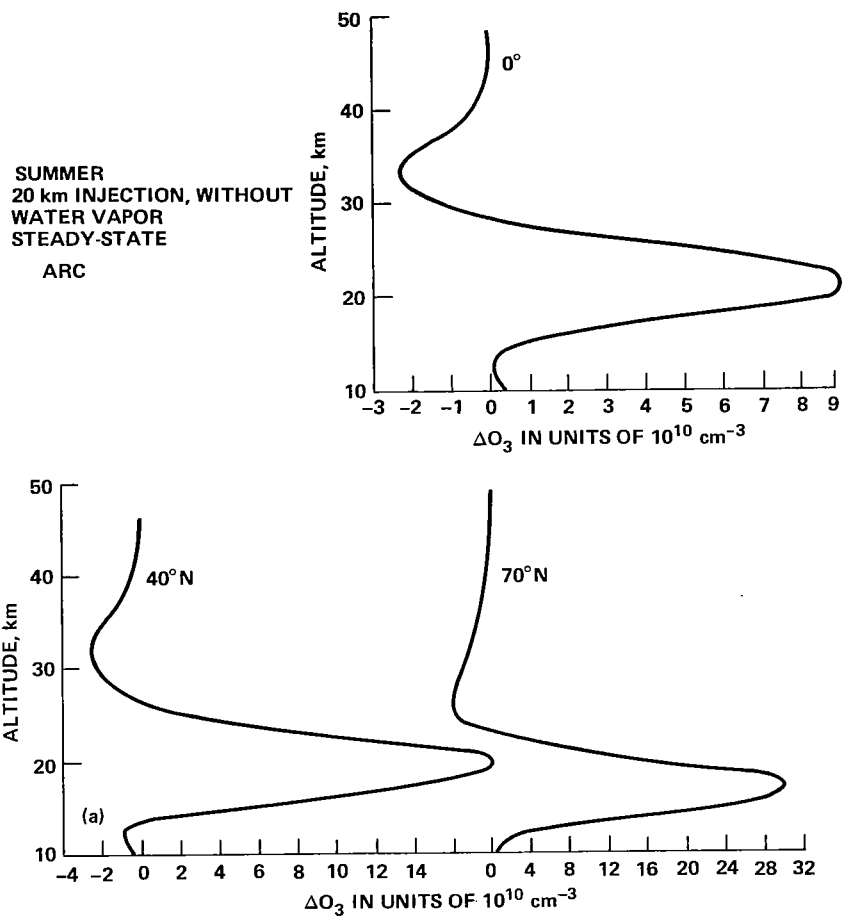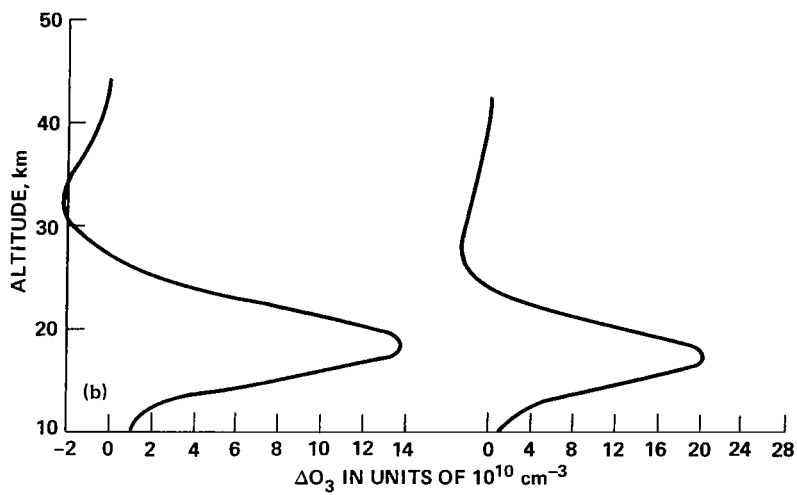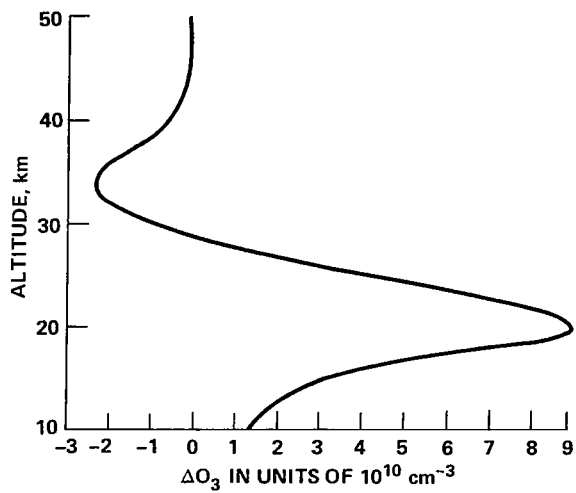
(b) Autumn.

Figure 26.— Concluded.

Figure 27.— Absolute ozone changes (ΔO_3) that correspond to scenario (4), but *without* water-vapor injection.

AUTUMN
20 km INJECTION,
WITHOUT WATER VAPOR
STEADY-STATE

ARC

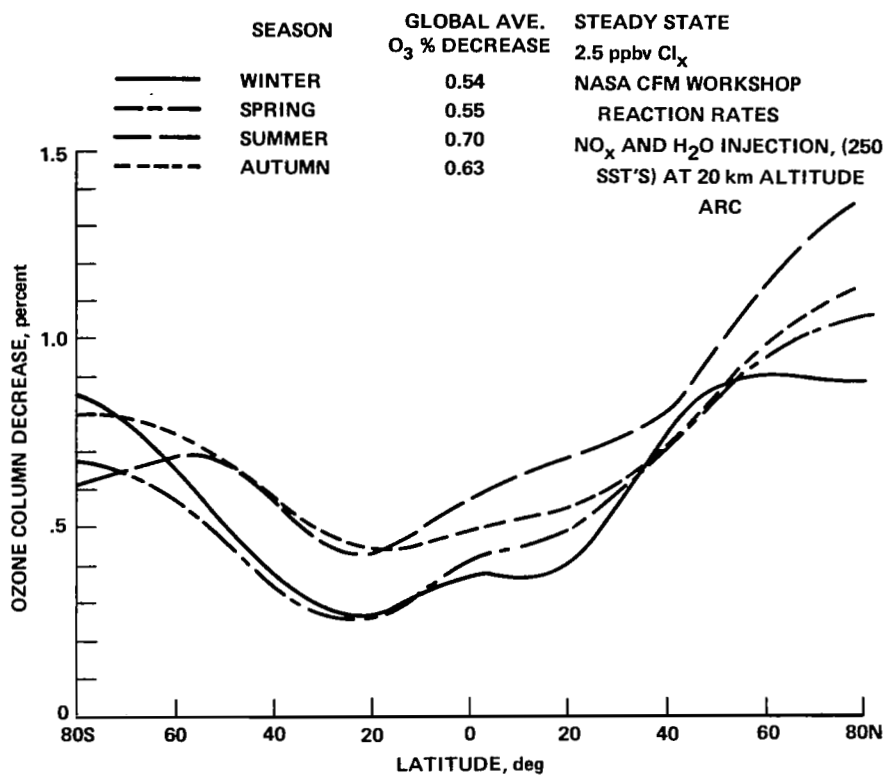(b) Autumn.

Figure 27.– Concluded.

Figure 28. — Predicted ozone column changes as a function of latitude for scenario (4), but with the old value of the rate coefficient for reaction (2).
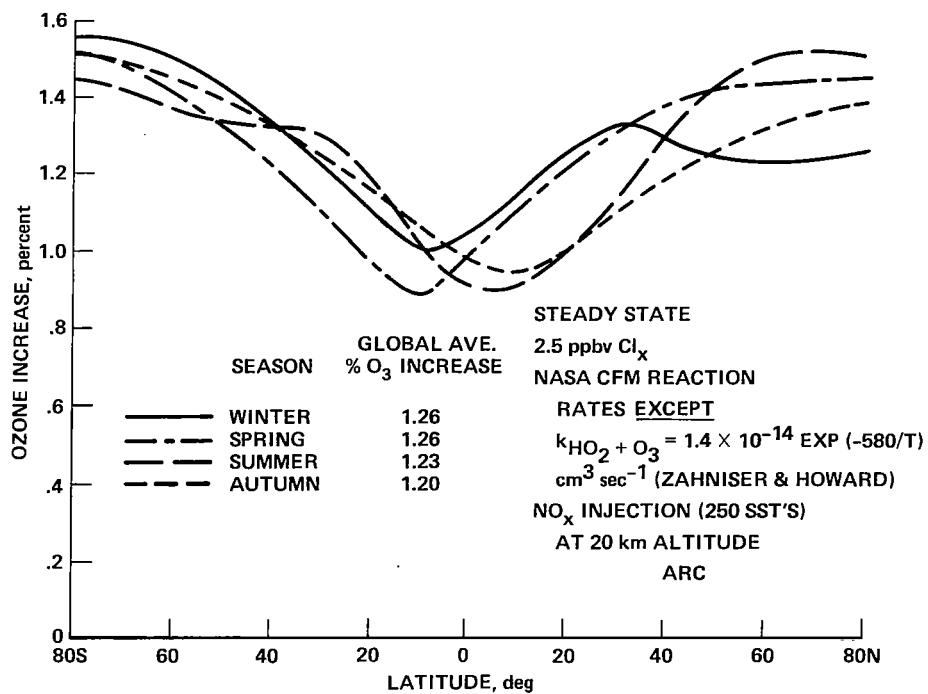
Figure 29.— Predicted ozone column change as a function of latitude for scenario (4), but *without* water-vapor injection.
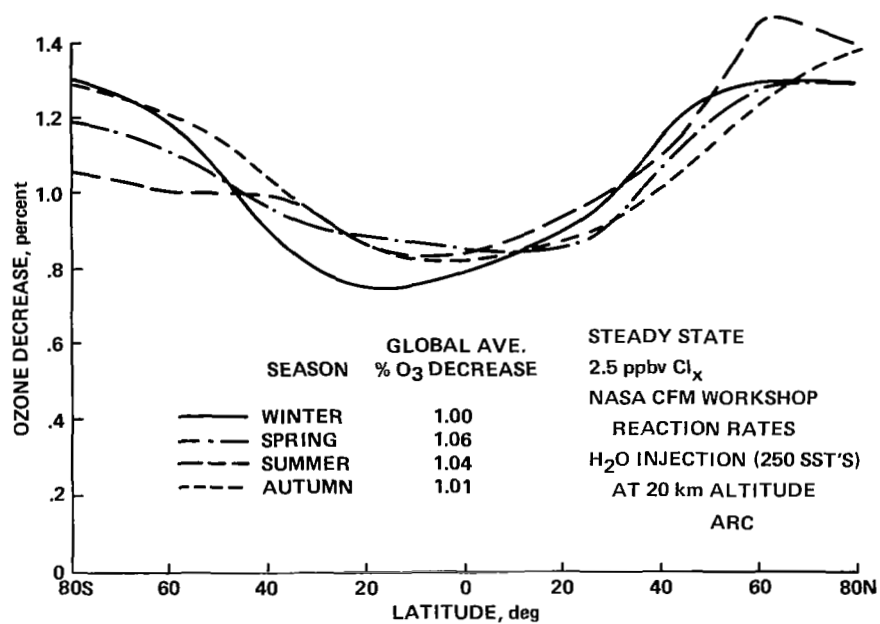
Figure 30. — Predicted ozone column change as a function of latitude for scenario (4), but with water-vapor injection *only*.

SEASON	GLOBAL AVE. % O_3 INCREASE	STEADY STATE 2.5 ppbv Cl_x
WINTER	0.26	NASA CFM WORKSHOP
SPRING	0.20	REACTION RATES EXCEPT
SUMMER	0.19	$k_{HO_2 + O_3} = 1.4 \times 10^{-14}$ EXP $(-580/T)$
AUTUMN	0.19	$cm^3\,sec^{-1}$ (ZAHNISER & HOWARD)

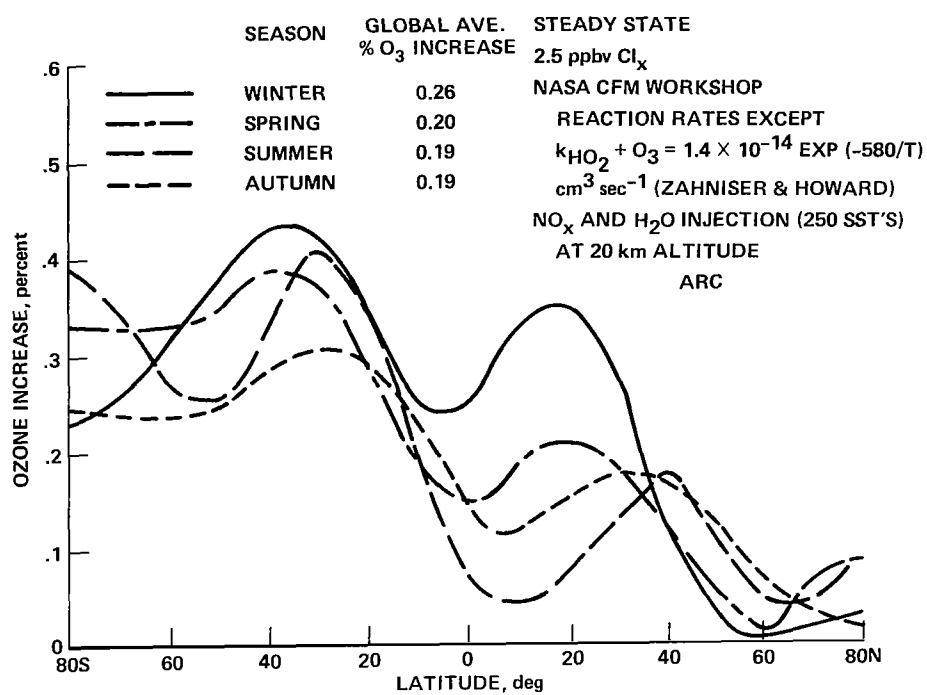NO_x AND H_2O INJECTION (250 SST'S)

AT 20 km ALTITUDE

ARC

Figure 31. — Predicted ozone column change as a function of latitutde for scenario (4) with the new value of the rate coefficient for reaction (2).
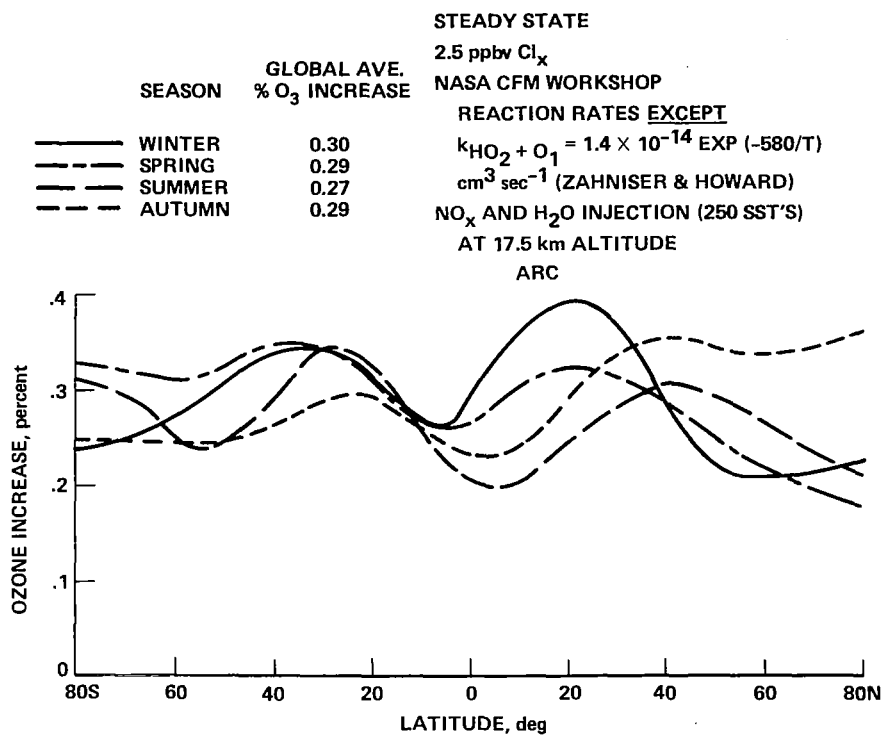
SEASON	GLOBAL AVE. % O_3 INCREASE
WINTER	0.30
SPRING	0.29
SUMMER	0.27
AUTUMN	0.29

STEADY STATE

2.5 ppbv Cl_x

NASA CFM WORKSHOP

REACTION RATES EXCEPT

$k_{HO_2 + O_1} = 1.4 \times 10^{-14}$ EXP (-580/T)

$cm^3 sec^{-1}$ (ZAHNISER & HOWARD)

NO_x AND H_2O INJECTION (250 SST'S)

AT 17.5 km ALTITUDE

ARC

Figure 32. — Predicted ozone column changes as a function of latitude for scenario (5).

1. Report No. NASA RP-1064	2. Government Accession No.	3. Recipient's Catalog No.
4. Title and Subtitle TWO-DIMENSIONAL MODEL STUDIES OF THE EFFECT OF SUPERSONIC AIRCRAFT OPERATIONS ON THE STRATO-SPHERIC OZONE CONTENT		5. Report Date February 1981
		6. Performing Organization Code
7. Author(s) R. C. Whitten, W. J. Borucki, I. G. Poppoff,* L. Glatt, † G. F. Widhopf,† L. A. Capone,‡ and C. A. Reigel‡		8. Performing Organization Report No. A-8270
9. Performing Organization Name and Address Ames Research Center, NASA Moffett Field, Calif. 94035		10. Work Unit No. 154-30-80-01
		11. Contract or Grant No.
12. Sponsoring Agency Name and Address National Aeronautics and Space Administration Washington, D.C. 20546		13. Type of Report and Period Covered Reference Publication
		14. Sponsoring Agency Code

15. Supplementary Notes
*Flick Point Associates, Carnelian Bay, Calif.
†Aerospace Corporation, El Segundo, Calif.
‡San Jose State University, San Jose, Calif.

16. Abstract

An earlier assessment (NASA Reference Publication 1026) of the potential effects of advanced supersonic aircraft on stratospheric ozone employed one-dimensional photochemical models to obtain estimates of globally averaged changes in ozone. The study reported here, an extension of the earlier work, was undertaken to estimate the latitudinal dependence of the ozone perturbation; two two-dimensional photochemical models were used for the purpose. The two SST design concepts assumed in the previous work were also employed for the work reported here.

As predicted in an earlier study, it appears that realistic SST fleet sizes should not cause concern with respect to the reduction of the total ozone overburden. For a fleet of 250 aircraft, the change in the ozone column is predicted to be very close to zero; in fact, the ozone overburden may actually increase as a result of nitrogen oxides deposited at altitudes of 17.5 or 20 km. The calculations performed, using the chemical system described herein (ca. 1978), show that above 25 to 30 km the ozone abundance decreases via catalytic destruction, but at lower heights it increases, mainly as a result of coupling with odd-hydrogen species. Water vapor released in the engine exhaust is predicted to cause ozone decreases; for the hypothetical engines used in the study, the total column ozone changes due to water-vapor emission largely offset the predicted ozone increases due to NO_X emission. The actual effect of water vapor may be less than calculated because present models do not include thermal feedback. "Feedback" refers to the cooling effect of additional water vapor that would tend to slow the HO_X reactions which destroy ozone.

Because it is also appropriate to the study reported here, the reader is referred to the last paragraph of the "Summary" of the earlier work.

17. Key Words (Suggested by Author(s)) Ozone Supersonic aircraft Stratosphere	18. Distribution Statement Unclassified – Unlimited Subject Category 45		
19. Security Classif. (of this report) Unclassified	20. Security Classif. (of this page) Unclassified	21. No. of Pages 71	22. Price A04

THIRD-CLASS BULK RATE

Postage and Fees Paid
National Aeronautics and
Space Administration
NASA-451

U.S.MAIL

6   1 1U, E,   021381 S00903DS
DEPT OF THE AIR FORCE
AF WEAPONS LABORATORY
ATTN: TECHNICAL LIBRARY (SUL)
KIRTLAND AFB NM 87117

NASA

POSTMASTER: **If Undeliverable (Section 158
Postal Manual) Do Not Return**